MASS SPECTROMETRY FOR REACTION MONITORING AND REACTION ACCELERATION

by

Xingshuo Chen

A Dissertation

Submitted to the Faculty of Purdue University

In Partial Fulfillment of the Requirements for the degree of

Doctor of Philosophy

Department of Chemistry

West Lafayette, Indiana

December 2021

THE PURDUE UNIVERSITY GRADUATE SCHOOL

STATEMENT OF COMMITTEE APPROVAL

Dr. R. Graham Cooks, Chair

Department of Chemistry

Dr. Hilkka I. Kenttämaa

Department of Chemistry

Dr. Chengde Mao

Department of Chemistry

Dr. Scott A. McLuckey

Department of Chemistry

Approved by:

Dr. Christine Hrycyna

Dedicated to my parents and my friends

ACKNOWLEDGMENTS

Firstly, I would like to thank my parents for their unconditional love and support throughout my life. They encourage me to face up to challenges in life and not giving up. The time with them in vacations and conversations with them overseas are always fuel for me.

I would like to express my deepest gratitude to my advisor Prof. Graham Cooks, a great scientist, and a great mentor. He is always enthusiastic for new discoveries and encourages me to tackle difficult problem. During my study in graduation school, he is always patient and supportive, and I really cherish the time to work in his group.

My deep appreciation goes to all the members in Aston labs. I am grateful to Dr. Steve Ayrton, my first mentor in conducting a project. I also want to thank deeply Dr. Zhenwei Wei and Dr Honggang Nie, not only for their invaluable mentoring in my research and but also for sharing their life wisdom. I want to give a big thank to Kai-Hung Huang, who is an excellent collaborator, for all the productive works and inspirations. I acknowledge former group members Dr. Valentina, Pirro, Dr. Karen Yannell, Dr. Ryan Bain, Dr. Chris Pulliam, Dr. Xinming Huo, Dr. Adam Hollerbach, Dr. Patrick Fedick, Dr. Dalton Snyder, Dr. Clint Alfaro, Dr. David Logsdon, Dr. Kiran Iyer, and Dr. Fan Pu, Dr. Zhuoer Xie, Zezhen Zhang, Dr. Tianyang Guo, Dr. Jing Yi, Dr. Hong Zhang for all the training and guidance that lead me into the wonderful world of science. A big thank to my lab mates for all the valuable discussion and emotional supports along my life in graduate school: Dr. Robert Schrader, Dr. Tsdale Mehari, Dr. Yangjie Li, Lucas Szalwinski, Hannah Brown, Sangeeta Pandey, Rong Chen, Saquib Rahman, Lingqi Qiu, Edwin Gonzalez, Nicolás Morato Gutiérrez, Yanyang Hu, Kai-Hung Huang, Phoebe Le, and Dylan Holden. I also want to thank our secretaries, Brandy McMasters and Lee Hua Chiang, for making our life enjoyable.

I am grateful to my collaborators from Merck Company, Amgen Company and Prof. Kubis Tillmann's research group, who have contributed a lot to my research. I sincerely thank Prof. Hilkka Kenttämaa, Prof. Chengde Mao, Prof. Scott Mcluckey, for being on my defense committee.

TABLE OF CONTENTS

LIST OF TABLES

LIST OF SCHEMES

LIST OF FIGURES

ABSTRACT

Mass spectrometry-based techniques have been widely used in reaction monitoring due to their high sensitivity and ability to offer structure information by tandem mass spectrometry. We applied nano-electrospray mass spectrometry (nanoESI-MS) to simultaneously monitor pre-catalysts, catalytic intermediates, reagents, and products of palladium catalyzed Suzuki-Miyaura cross-coupling reactions. A set of Pd cluster ions related to the monoligated Pd (0) active catalyst is detected, and its deconvoluted isotopic distribution reveals contributions from two neutral molecules. One is assigned to the generally accepted Pd (0) active catalyst, seen in MS as the protonated molecule, while the other is suggested to correspond to a deactivated form of Pd catalyst. Oxidative stress testing of the synthetic model catalyst XPhos Pd cyclo-octadiene, performed using oxygen and Fe(III), supported this assignment. Thus, the make-up of the monoligated set of Pd (0) ions appears to indicate the oxidation state of the system. The formation and removal of the oxidative addition intermediate during the catalytic cycle was monitored to provide information on the progress of the transmetalation step.

Recently, microdroplets created by ambient ionization source have been used as reaction vessels to accelerate organic reactions. Field desorption mass spectrometry under ambient conditions is applied to study solution-phase organic reactions in micro-volumes. Compared to nanoelectrospray, it is noteworthy that radical cations and formation of radical cation products are observed. Three reactions, the hydrazone formation by phenyl hydrazine and indoline-2,3-dione, the Katritzky reaction between a pyrylium salt and anisidine, and the Hantzsch synthesis of 1,4-dihydropyridine, were investigated by this system and reaction acceleration was observed to different extents. The increase in rate relative to that for the corresponding bulk reactions is attributed to solvent evaporation which increases concentration, and to the increase of surface-to-volume ratio with enhanced interfacial reaction rate constants. Later work in this thesis describes explicit solvent calculations to study the energies and structures of the hydrazone formation reaction from phenylhydrazine and indoline-2,3-dione in acidic methanol with density functional tight binding (DFTB) methods. Additionally, the thesis covers MS based methods for determination of isoaspartate and aspartate in peptide by gas-phase chemistry and detection of S-nitrosoglutathione in exhaled breath condensate sample.

CHAPTER 1. INTRODUCTION

1.1 Electrospray ionization mass spectrometry (ESI-MS)

Mass Spectrometry based methods offer detection and characterization of trace amounts of material in complex mixtures with high sensitivity and specificity. Electrospray ionization mass spectrometry (ESI-MS) is an ideal method for reaction monitoring due to its ability to gently transfer ionic species or ionized forms of neutral species in the condensed phase into the gas phase. During the electrospray process, analytes in solution are transferred through a capillary supplied with an external high voltage, where the cations move toward the counter electrode in the positive mode while the anions move to the metal capillary, to produce a continuous stream of charged droplets.[1] An electrospray ion source can be viewed as an electrolytic cell in which electrochemical reactions produce extra charged species.[2] For example, water is oxidized to produce protons in the positive mode while it undergoes reduction in the negative mode. The protons are attached to neutral molecules which are removed as charged droplets containing positive ions to maintain charge balance. The analyte containing charged droplets undergo solvent evaporation and droplet fission to eventually produce charged forms of the analytes in the gas phase prior to being analyzed by the mass spectrometer. Typically, neutral analytes with basic functional groups will be detected as the protonated forms in the positive mode and those with acidic groups will form deprotonated ions in the negative mode. More rarely, organic molecules can be oxidized or reduced to generate radical ions.

NanoESI is a variant form of ESI, which features greatly reduced flowrates (<1000 nL/min) compared to conventional ESI.[3–5] NanoESI is usually performed with glass capillaries that have a small diameter. NanoESI is superior to conventional ESI for its low sample consumption and greatly improved ionization efficiency due to smaller charged droplets. Further it is reported that ion suppression and matrix effects are reduced in nanoESI, making it appealing for analysis of complex mixtures.[4]

1.2 ESI-MS as an effective tool to study Pd catalyzed coupling reactions

ESI based methods have been used in mechanistic studies of various Pd catalyzed coupling reactions, including the Suzuki-Miyaura, Negishi, Mizoroki-Heck, Sonogashira, Stille and Buchwald-Hartwig reactions[6–12]. The Canary group[13] first utilized offline ESI to study Suzuki coupling of pyridyl(pyr) bromide complexes and phenyl boronic acid with different substituted groups catalyzed by Pd $(PPh_3)_4$. The reaction solutions were sampled and quenched in cold methanol and allowed to reach room temperature before analysis. Intermediate ions related to the oxidative addition product ($[(pyrH)Pd(PPh_3)_2Br]^+$ and $[(pyr)Pd(PPh_3)_2]^+$ and the transmetalation product (the protonated diaryl Pd(II) complex) were detected. Although the study did not provide detailed structural information, it did demonstrate that ESI is an effective tool to "fish" intermediates from complex reaction mixtures.

MS also offers powerful tools to help identify and characterize the intermediates of Pd catalyzed reactions. Analytes in the reaction mixture can be identified by *m/z* value and by the characteristic isotopic distributions of elements such as Pd, Br, Cl. Chemical structures can often be deduced by tandem mass spectrometry because collision induced dissociation gives fragmentation patterns of selected ions with high specificity.

Based on the time resolution chosen and the duration of monitoring,[14] the ESI-MS monitoring technique can be classified as offline monitoring, continuous online monitoring of the reactor or discrete online monitoring of the products of rapidly mixed reagents. Both offline and online ESI analysis have been extensively used in the mechanistic studies. In offline line analysis, the reaction mixture is sampled at a desired time interval decided by the kinetics of the reaction involved. Samples are often diluted and quenched in a solvent that assists in the ESI process and prepared in concentrations that are appropriate to the dynamic range of the mass spectrometer. Offline methods are often preferred due to their simplicity, flexibility with respect to experimental design and the ease with which sample preparation routes can be changed to optimize the analytical results. Online ESI monitoring methods require that the reactor be coupled directly to the MS, to avoid a separate sample preparation step. The most direct coupling method is to use a syringe for sample injection into the ESI; the syringe then functions as a micro reactor and also serves to pump the reaction mixture continuously into the ESI source. The McIndoe group[9,15,16] developed a

pressurized sample infusion (PSI) method which features long-term sampling and analysis of air and moisture sensitive reactions. They utilized 1-5 psi inert gas to push the reaction mixture from the bulk reactor through a capillary to reach the MS interface and so allow continuous monitoring of the components in the reactor and to collect kinetic information under standard reaction conditions. To monitor the chemical reaction at the beginning of the reaction period when it is fastest and to minimize any delay time before analysis. one can prepare the reactants in two syringes and mix them in a tee assembly just before they are transferred into the ESI source. The delay time, which in return represents the reaction time after mixing, can then be varied by changing the dimensions of the capillary connecting the tee and the ESI source,

The reaction mixture for a typical catalytic reaction usually contains reactants, products, bases, metal or other catalyst and transient species, and their concentrations can vary over orders of magnitude. MS methods which allow simultaneous monitoring of various species offer useful information from which to deduce the reaction mechanism. However, since ESI samples preferably ionic spices, the signals associated with the ionization of neutral species may be suppressed. Also, reaction intermediates are often transient species and have much lower concentrations compared to the reactants, products and acids/bases in the system, which again adds to the difficulties of detection. Therefore, it's important to optimize analytical conditions where possible, as well as developing new methods to increase the sensitivity of analytes of interest. Additives, such as acid, are sometimes added to aid the protonation of neutral molecules (especially when the reaction mixture contains base). Another advance is the incorporation of charge tags[16,17] into the reactants or catalyst by direct synthesis to convert the analytes of interests into pre-charged species. Such charge tags should be designed to be surface active and bulky[16] for easily sampling by the ESI but an effect on the coupling reaction cannot always be avoided.

Recently, ionization methods closely related to ESI have been developed and applied in mechanistic studies. Our group developed the inductive ESI (iESI)[18,19] method which features high efficiency and tolerance to salt and matrix effects (ion suppression of signal due to other components). This has been applied to online ESI monitoring of reductive elimination, Negishi cross-coupling, as well as a heterogeneous reaction, Pd/C catalyzed hydrogenolysis.[20] Intermediates involving zinc complexes were captured in the air and water sensitive Negishi

reaction, which suggests the zinc reagent coordination plays a role in the catalytic cycle. Hao Chen's group developed a liquid desorption ESI (DESI)[21] technique which uses a solvent sprayer to extract the analyte from the rapidly mixed reaction mixture emerging from a tee assembly. They captured the Pd(0) active catalyst from the Buchwald G3 precatalyst and successfully detected several intermediates in the Buchwald C-N coupling reaction as well as in the Suzuki coupling reaction.

1.3 Some considerations regarding ESI-MS analysis of solution-phase reactions

Although great success has been achieved by ESI-MS based mechanistic studies, care should be taken when attempting to identify and deduce the role of the intermediates detected by MS.

Firstly, during the ESI process, solvent evaporation from the charged droplet causes significant changes in the reaction environment including in concentration and pH.[22] As has long been known, reaction acceleration can occur in charged microdroplets. Nevertheless, in reaction monitoring using short distances from the sprayer to the MS inlet and using large droplets, non-accelerating conditions can be ensured. Secondly the electrolytic reactions that may occur in ESI-MS as mentioned before, may cause redox-active analytes to undergo unwanted redox reactions. McIndoe's group[17] synthesized negatively charged phosphine ligands so that they could monitor the Pd catalyzed Sonogashira reaction in the negative mode and so study Pd intermediates with low oxidation states. They claim that their method avoids potential oxidation reactions of Pd intermediates in the positive mode. However, this approach is not always applicable as introduction of a charge tag on certain ligands without affecting reactivity is difficult. Researchers thus should consider the possible side reactions when analyzing data. Moreover, solvent clustering is also a common effect in MS. The ligands of the palladium catalyst are important to its reactivity. When a new ligated form of a Pd intermediate is seen in the MS, it is not always easy to tell whether this species forms in the solution phase or in the gas phase. In a study of the Stille reaction by the Eberlin group,[23] the mass spectrum of the catalyst $Pd(PPh_3)_2$ showed the $Pd(PPh_3)_2^{+\cdot}$ radical cation as well as its CH_3CN and water adducts, whereas the researchers proposed the adducts are formed from the di-ligated radical cation during ESI process. In another study of Heck reaction[24] from the same group, solvent molecules ligated to Pd were proposed to be related to the reactivity of the oxidative addition intermediates (details are given in following discussion)

Based on these considerations, researchers need to design experiments to validate their understanding of intermediates. For example, mixing two or more reactants and changing the order of addition is a way to cross-validate the formation of intermediates observed in monitoring the original reaction. Measurement of the time course of evolution of reaction intermediates is also a good way to establish correlations between these intermediates. While accurate quantification in MS relies on internal standards and calibration curves, direct measurement of the ion intensity often serves as an alternative and quick way to get qualitative and semi quantitative information related to the changes undergone by analytes and it is widely used in the study of palladium catalyzed reactions. The absolute ion intensities (total ion chronogram and selective ion chronograms) corresponding to the intermediates help to elucidate the occurrence, development, and consumption of the intermediates. Relative intensity, which is the ratio of the absolute intensities of two ions. is useful to show the evolution from one ion to other and validate their function in the catalytic cycle.

Eberlin[24] use a direct injection ESI to study the mechanism of the Heck reaction with arene diazonium salts. In the oxidative addition step between the arene diazonium salt 4-MeOPh$N_2^+BF_4^-$ and $[Pd_2(dba)_3]$dba, they detected four different cations which correspond to the proposed oxidative addition intermediate but with different ligands (different numbers of dba and solvent molecule acetonitrile) and with a change in the relative abundance of these ions change with time. After 90 min of mixing, the Pd complex with one CH_3CN and one dba dominates. To decide which intermediate reacts most efficiently with the olefin, they mixed the oxidative addition reaction mixture with olefin. Based on the resulting olefin insertion intermediate, the authors proposed the oxidative addition intermediate with one CH_3CN and one dba might be the most reactive intermediate.

In ESI analysis, one can choose to optimize the source conditions so as to assist in declustering of solvent and other loosely bond species from the analyte where there is uncertainty about the form of intermediate in solution and that detected by MS. One example is the detection of the oxidative addition intermediate Pd-Ar-I detected as $[Pd\text{-}Ar\text{-}I]H^+$ and $[Pd\text{-}Ar]^+$ where the latter is believed to be caused by dissociation of Pd-I bond during analysis[13]. Recent studies of the McIndoe group[9] using a positively charged tag on the aryl group show that a oxidative addition intermediate ion

$[Pd\text{-}Ar^{+}]^{+}$ will formed even when the formation of doubly charged species is less favored. They thus proposed $[Pd\text{-}Ar^{+}]^{+}$ is likely to be formed in solution.

1.4 Spectroscopic and electrochemical methods in mechanistic studies of catalytic coupling reactions

While independent synthesis of proposed intermediates and X-ray diffraction analysis gives undoubted structure information on the species of interest, it's still important to monitor the reaction in progress to establish the role of intermediates in the reaction mechanism. Spectroscopic methods have been used in mechanistic studies of coupling reactions. IR and Raman for the monitoring of functional groups and NMR for structural information as well quantification. The most widely used online monitoring technique is standard static tube NMR, but recently rapid injection NMR and stopped flow NMR have shown the existence of short-lived intermediates. Low temperature rapid injection NMR has been used to monitor the trans-metalation pathway and to observe intermediates containing the Pd-O-B subunit via NOE and HMBC experiments.[25,26] NMR monitoring of complex mixtures may suffer from signal overlap which hinders structure assignments. Stoichiometric reaction of partial step of a reaction is often conducted in this type of study to simplify the data interpretation. Computational methods are sometime also used for prediction of putative structures when assignments are unclear. ESI-MS have much higher sensitivity than is commonly available in NMR, allowing detection of species with concentration even down to 10^{-18} M. [27]

Electrochemical techniques have been used in mechanistic studies of metal-catalytical reactions which often involve a series of oxidation and reduction steps in the catalytic cycle connected by redox active intermediates. [28,29] In cyclic voltammetry (CV) experiments, chemical species in solution undergo electrochemical oxidation or reduction reactions in presence of an external potential and form intermediates that can be characterized by their distinctive dependence on redox potential and quantified using the measured current. While the fast scan rate (time scale 10^{-1} to 10^{-6} second) allows study of short lived species,[30] CV provides limited information on the chemical structure of the compound and characterization is difficult especially when authentic sample is not available, thus spectroscopic methods are often needed. Recently Wagschal, Jutand and Grimaud et al [31] used CV and NMR to study the in situ reduction reaction of PdOAc and XPhos and

provided evidence for the formation of the Xphos-ligated Pd(0) species and Pd^{I}-Pd^{I} dimers. The kinetics of oxidative addition can also be derived by following the change of peak current of the Pd-0 complex (which is proportional to concentration). Apart from reaction monitoring, CV also offers information on the electron transfer ability and stability of synthetic catalyst which may help to elucidate the catalytic power of the catalyst.[29] Chronoamperometry with a rotating disk electrode is another constant potential technique which has been established for real time monitoring and rate constant measurement. Amatore and Jutand[32] et al. measured kinetic data of the transmetalation/reductive elimination step of the Suzuki-coupling reaction. Their combined CV and chronoamperometry study provided evident for hydroxide is crucial in promoting those two steps.

It is interesting to consider how much additional information might be accumulating when one combines E-chem with MS. Firstly, MS can serve as a highly sensitive detection tool to couple with EC, which not only captures chemical spices in an electrochemical reaction in real time but also offers structure information. Online EC-MS has been proved useful in a simulation study of the oxidation degradation of fungicide.[33] Secondly, electrochemical reactions have been used to effectively improve the response of analytes that are hard to ionize, either by intrinsic electrochemical reactions in ESI or by targeted derivatization reactions by external electrochemical cell.[34] Recently, Yan's group recently developed a micro-reactor based on a nano-ESI emitter where an accelerated electro-epoxidation reaction in the ion source is used to help discriminate the carbon-carbon double bond positional isomers of lipids.[35]

1.5 **Reaction acceleration in microdroplets**

Organic reaction acceleration has been widely exploited in confined volume systems, including microdroplets generated by various spray-based systems, levitated droplets and thin films. Rates of reactions can be orders of magnitude faster than bulk phase, making it a promising tool for synthesis. Biochemical reactions such as synthesis of ribonucleotides and degradation of enzymes are also accelerated in microdroplets, which offer new possibility for modelling of reactions in biological systems.[36,37]

The mechanism of reaction acceleration still remains to be fully understood and may vary between systems. It is generally believed that the intrinsic rate acceleration is due to the extremely fast interfacial reactions in small droplets with large surface-to-volume ratio. This is explained by the partial solvation effect which depicts interfacial reactions as an intermediate scenario between the reaction in the gas phase (generally six orders of magnitude faster than solution phase counterpart) and in solution. A recent study examined the impact of interfacial area and reaction molarity on reaction acceleration.[38] Reaction acceleration of bimolecular reaction is attributed to its more charged dispersed transition state than reagents, which means that it is less solvated in solution phase, leading to a higher activation barrier and this activation barrier is reduced at the interface when both regents and transition state are partially solvated. This acceleration effect was not attained in monomolecular reactions. Apart from this factor, solvent evaporation, rapid mixing and diffusion in small droplets, molecular ordering effects and high electric field at the surface, have been suggested to contribute to reaction acceleration.[39,40]

Reaction acceleration benefits the study of organic reactions in several ways. Firstly, study of reactions in accelerated fashion greatly shortens the time of reaction and allow data acquisition on reaction intermediates and products. Such a study is readily compared with reaction monitoring of bulk phase for validation. Secondly, fast derivatization techniques based on accelerated reaction allow detection of low ionization efficiency species. For example, analysis of reducing sugars from a single onion cell was established with acceleration derivatization by imine formation in thin films.[35]

1.6 Outline of the thesis

The thesis starts from discussion on mass spectrometry-based methods to study the Suzuki-Miyaura cross-coupling reaction in Chapter 2. Several Pd intermediates including the active form of the Buchwald G3 precatalyst were successfully detected by nano-ESI-MS. The second part of the thesis focuses on reaction acceleration in microdroplets. In Chapter 3 reaction acceleration effects were exploited by a new spray-based technique, ambient field desorption. Chapter 4 offers a discussion on the reaction acceleration mechanism based on quantum mechanics calculations. In Chapter 5, describes a method to distinguished isobaric peptides based on gas phase reactions.

Chapter 6 summarizes the attempts made to develop ambient ionization methods to study the S-nitrosoglutathione in exhaled breath condensate samples.

1.7 References

(1) Cole, R. B. Some Tenets Pertaining to Electrospray Ionization Mass Spectrometry. *J. Mass Spectrom.* **2000**, *35* (7), 763–772.

(2) Kebarle, P.; Verkcerk, U. H. Electrospray: From Ions in Solution to Ions in the Gas Phase, What We Know Now. *Mass Spectrom. Rev.* **2009**, *28* (6), 898–917.

(3) Wilm, M.; Mann, M. Analytical Properties of the Nanoelectrospray Ion Source. *Anal. Chem.* **1996**, *68* (1), 1–8.

(4) Schmidt, A.; Karas, M.; Dülcks, T. Effect of Different Solution Flow Rates on Analyte Ion Signals in Nano-ESI MS, or: When Does ESI Turn into Nano-ESI? *J. Am. Soc. Mass Spectrom.* **2003**, *14* (5), 492–500.

(5) Gibson, G. T. T.; Mugo, S. M.; Oleschuk, R. D. Nanoelectrospray Emitters: Trends and Perspective. *Mass Spectrom. Rev.* **2009**, *28* (6), 918–936.

(6) Roglans, A.; Pla-Quintana, A. *In Reactive Intermediates: MS Investigations in Solution*; Santos, L. S., Ed.; Wiley-VCH: Weinheim, Germany, 2010; Ch.7.

(7) Santos, L. S.; Pavam, C. H.; Almeida, W. P.; Coelho, F.; Eberlin, M. N. Probing the Mechanism of the Baylis–Hillman Reaction by Electrospray Ionization Mass and Tandem Mass Spectrometry. *Angew. Chemie Int. Ed.* **2004**, *43* (33), 4330–4333.

(8) Böck, K.; Feil, J. E.; Karaghiosoff, K.; Koszinowski, K. Catalyst Activation, Deactivation, and Degradation in Palladium-Mediated Negishi Cross-Coupling Reactions. *Chem. - A Eur. J.* **2015**, *21* (14), 5548–5560.

(9) Yunker, L. P. E.; Ahmadi, Z.; Logan, J. R.; Wu, W.; Li, T.; Martindale, A.; Oliver, A. G.; McIndoe, J. S. Real-Time Mass Spectrometric Investigations into the Mechanism of the Suzuki–Miyaura Reaction. *Organometallics* **2018**, *37* (22), 4297–4308.

(10) Schade, M. A.; Fleckenstein, J. E.; Knochel, P.; Koszinowski, K. Charged Tags as Probes for Analyzing Organometallic Intermediates and Monitoring Cross-Coupling Reactions by Electrospray-Ionization Mass Spectrometry. *J. Org. Chem.* **2010**, *75* (20), 6848–6857.

(11) Agrawal, D.; Schröder, D.; Frech, C. M. Observation of Binuclear Palladium Clusters upon ESI-MS Monitoring of the Suzuki–Miyaura Cross-Coupling Catalyzed by a Dichloro-Bis(Aminophosphine) Complex of Palladium. *Organometallics* **2011**, *30* (13), 3579–3587.

(12) Thomas, G. T.; Janusson, E.; Zijlstra, H. S.; McIndoe, J. S. Step-by-Step Real Time Monitoring of a Catalytic Amination Reaction. *Chem. Commun.* **2019**, *55* (78), 11727–11730.

(13) Aliprantis, A. O.; Canary, J. W. Observation of Catalytic Intermediates in the Suzuki Reaction by Electrospray Mass Spectrometry. *J. Am. Chem. Soc.* **1994**, *116* (15), 6985–6986.

(14) Fabris, D. Mass Spectrometric Approaches for the Investigation of Dynamic Processes in Condensed Phase. *Mass Spectrom. Rev.* **2005**, *24* (1), 30–54.

(15) Vikse, K. L.; Woods, M. P.; McIndoe, J. S. Pressurized Sample Infusion for the Continuous Analysis of Air- and Moisture-Sensitive Reactions Using Electrospray Ionization Mass Spectrometry. *Organometallics* **2010**, *29* (23), 6615–6618.

(16) Vikse, K. L.; Ahmadi, Z.; Manning, C. C.; Harrington, D. A.; McIndoe, J. S. Powerful Insight into Catalytic Mechanisms through Simultaneous Monitoring of Reactants, Products, and Intermediates. *Angew. Chemie - Int. Ed.* **2011**, *50* (36), 8304–8306.

(17) Vikse, K. L.; Henderson, M. A.; Oliver, A. G.; McIndoe, J. S. Direct Observation of Key Intermediates by Negative-Ion Electrospray Ionisation Mass Spectrometry in Palladium-Catalysed Cross-Coupling. *Chem. Commun.* **2010**, *46* (39), 7412.

(18) Huang, G.; Li, G.; Cooks, R. G. Induced Nanoelectrospray Ionization for Matrix-Tolerant and High-Throughput Mass Spectrometry. *Angew. Chemie* **2011**, *123* (42), 10081–10084.

(19) Huang, G.; Li, G.; Ducan, J.; Ouyang, Z.; Cooks, R. G. Synchronized Inductive Desorption Electrospray Ionization Mass Spectrometry. *Angew. Chemie* **2011**, *123* (11), 2551–2554.

(20) Yan, X.; Sokol, E.; Li, X.; Li, G.; Xu, S.; Cooks, R. G. On-Line Reaction Monitoring and Mechanistic Studies by Mass Spectrometry: Negishi Cross-Coupling, Hydrogenolysis, and Reductive Amination. *Angew. Chemie* **2014**, *126* (23), 6041–6045.

(21) Zheng, Q.; Liu, Y.; Chen, Q.; Hu, M.; Helmy, R.; Sherer, E. C.; Welch, C. J.; Chen, H. Capture of Reactive Monophosphine-Ligated Palladium(0) Intermediates by Mass Spectrometry. *J. Am. Chem. Soc.* **2015**, *137* (44), 14035–14038.

(22) Schröder, D. Applications of Electrospray Ionization Mass Spectrometry in Mechanistic Studies and Catalysis Research. *Acc. Chem. Res.* **2012**, *45* (9), 1521–1532.

(23) Santos, L. S.; Rosso, G. B.; Pilli, R. A.; Eberlin, M. N. The Mechanism of the Stille Reaction Investigated by Electrospray Ionization Mass Spectrometry. *J. Org. Chem.* **2007**, *72* (15), 5809–5812.

(24) Sabino, A. A.; Machado, A. H. L.; Correia, C. R. D.; Eberlin, M. N. Probing the Mechanism of the Heck Reaction with Arene Diazonium Salts by Electrospray Mass and Tandem Mass Spectrometry. *Angew. Chemie* **2004**, *116* (19), 2568–2572.

(25) Thomas, A. A.; Denmark, S. E. Pre-Transmetalation Intermediates in the Suzuki-Miyaura Reaction Revealed: The Missing Link. *Science (80-.).* **2016**, *352* (6283), 329–332.

(26) Thomas, A. A.; Wang, H.; Zahrt, A. F.; Denmark, S. E. Structural, Kinetic, and Computational Characterization of the Elusive Arylpalladium(II)Boronate Complexes in the Suzuki–Miyaura Reaction. *J. Am. Chem. Soc.* **2017**, *139* (10), 3805–3821.

(27) Tsedilin, A. M.; Fakhrutdinov, A. N.; Eremin, D. B.; Zalesskiy, S. S.; Chizhov, A. O.; Kolotyrkina, N. G.; Ananikov, V. P. How Sensitive and Accurate Are Routine NMR and MS Measurements? *Mendeleev Commun.* **2015**, *25* (6), 454–456.

(28) Amatore, C.; Jutand, A.; M'Barki, M. A. Evidence of the Formation of Zerovalent Palladium from Pd(OAc)2 and Triphenylphosphine. *Organometallics* **1992**, *11* (9), 3009–3013.

(29) Sandford, C.; Edwards, M. A.; Klunder, K. J.; Hickey, D. P.; Li, M.; Barman, K.; Sigman, M. S.; White, H. S.; Minteer, S. D. A Synthetic Chemist's Guide to Electroanalytical Tools for Studying Reaction Mechanisms. *Chem. Sci.* **2019**, *10* (26), 6404–6422.

(30) Jutand, A. Contribution of Electrochemistry to Organometallic Catalysis. *Chem. Rev.* **2008**, *108* (7), 2300–2347.

(31) Wagschal, S.; Perego, L. A.; Simon, A.; Franco-Espejo, A.; Tocqueville, C.; Albaneze-Walker, J.; Jutand, A.; Grimaud, L. Formation of XPhos-Ligated Palladium(0) Complexes and Reactivity in Oxidative Additions. *Chem. – A Eur. J.* **2019**, *25* (28), 6980–6987.

(32) Amatore, C.; Jutand, A.; Le Duc, G. Kinetic Data for the Transmetalation/Reductive Elimination in Palladium-Catalyzed Suzuki-Miyaura Reactions: Unexpected Triple Role of Hydroxide Ions Used as Base. *Chem. - A Eur. J.* **2011**, *17* (8), 2492–2503.

(33) Temgoua, R. C. T.; Bussy, U.; Alvarez-Dorta, D.; Galland, N.; Hémez, J.; Thobie-Gautier, C.; Tonlé, I. K.; Boujtita, M. Using Electrochemistry Coupled to High Resolution Mass Spectrometry for the Simulation of the Environmental Degradation of the Recalcitrant Fungicide Carbendazim. *Talanta* **2021**, *221* (April 2020).

(34) Yuill, E. M.; Baker, L. A. Electrochemical Aspects of Mass Spectrometry: Atmospheric Pressure Ionization and Ambient Ionization for Bioanalysis. *ChemElectroChem* **2017**, *4* (4), 806–821.

(35) Tang, S.; Cheng, H.; Yan, X. On-Demand Electrochemical Epoxidation in Nano-Electrospray Ionization Mass Spectrometry to Locate Carbon–Carbon Double Bonds. *Angew. Chemie - Int. Ed.* **2020**, *59* (1), 209–214.

(36) Nam, I.; Nam, H. G.; Zare, R. N. Abiotic Synthesis of Purine and Pyrimidine Ribonucleosides in Aqueous Microdroplets. *Proc. Natl. Acad. Sci. U. S. A.* **2018**, *115* (1), 36–40.

(37) Zhong, X.; Chen, H.; Zare, R. N. Ultrafast Enzymatic Digestion of Proteins by Microdroplet Mass Spectrometry. *Nat. Commun.* **2020**, *11* (1), 1–9.

(38) Qiu, L.; Wei, Z.; Nie, H.; Cooks, R. G. Reaction Acceleration Promoted by Partial Solvation at the Gas/Solution Interface. *Chempluschem* **2021**, 1–5.

(39) Wei, Z.; Li, Y.; Cooks, R. G.; Yan, X. Accelerated Reaction Kinetics in Microdroplets: Overview and Recent Developments. *Annu. Rev. Phys. Chem.* **2020**, *71* (1), 31–51.

(40) Xiong, H.; Lee, J. K.; Zare, R. N.; Min, W. Strong Electric Field Observed at the Interface of Aqueous Microdroplets. *J. Phys. Chem. Lett.* **2020**, *11* (17), 7423–7428.

CHAPTER 2. REACTION INTERMEDIATES IN SUZUKI-MIYAURA CROSS-COUPLING USING MONOLIGATED PD ACTIVE CATALYSTS AS CHARACTERIZED BY MASS SPECTROMETRY

2.1 Introduction

The Suzuki-Miyaura (SM) cross-coupling reaction between aryl halides and organoboron compounds is an important tool for carbon-carbon bond formation and has been used broadly in total synthesis of natural products as well as in the preparation of pharmaceuticals and fine chemicals.[1, 2]This is because the reaction is operationally simple, proceeds under mild reaction conditions, tolerates a wide variety of polar functional groups, and has a broad substrate scope.[3-5]

Various palladium complexes have been used as catalysts in SM cross-coupling reactions, and the accepted mechanism is typically composed of four steps: 1) catalyst activation or generation of coordinatively unsaturated $L_nPd(0)$ species (n: number of ligands) 2) oxidative addition of an aryl halide 3) transmetalation with an organoboron reagent and 4) reductive elimination to yield the final product accompanied by regeneration of $L_nPd(0)$. Crucial to the success of these reactions is efficient and reproducible catalyst activation; different palladium sources undergo activation through different mechanisms and can form different active species depending on what precatalyst and reaction conditions are used. For example, $Pd(PPh_3)_4$ with zero valent Pd is proposed to undergo ligand dissociation to form $L_2Pd(0)$ before reaction with aryl halides.[6] In the case of using Pd(II) precursors with high air-stability such as $Pd(OAc)_2$, $L_nPd(0)$ complexes are formed in situ through reduction via sacrificial oxidation of the ligand.[7] The advent of palladium catalysts that are supported by electron-rich and bulky phosphine or carbene ligands has greatly expanded the scope and applications of both the SM and other cross-coupling reactions.[8] Additionally, use of palladacyclic precatalysts, in particular those developed by the Buchwald group, has increased the reliability and operational simplicity of cross-coupling reactions as these precatalyst complexes are air-stable, well characterized, and are activated at or near room temperature via deprotonation.[9-13] After activation, highly active monoligated Pd(0) species are proposed to be key to the efficient Buchwald catalytic reactions of the system.

Despite general acceptance that $L_nPd(0)$ complexes are active in catalysis, the mechanism of formation of the Pd(0) active species and their exact structures appear to vary with the choice of precatalyst, as well as the reaction conditions. The nature of the active form of Pd, has continued to arouse interest and remains to be fully understood in many systems.[14-19] For example, a study of Miyaura borylation catalyzed by $Pd(OAc)_2$ and PCy_3, showed that two forms of catalyst, monophosphine and diphosphine Pd (0) complexes, are formed via two Pd(II) reduction pathways.[15] A combined electrochemical and NMR study[17] of the catalytic system of $Pd(OAc)_2$ and PPh_3, suggested that instead of the usually proposed di-coordinated neutral complex $L_2Pd(0)$, an anionic complex $Pd(0)L_2(OAc)^-$ is the active form of the catalyst which undergoes oxidative addition. The study of catalyst activation and the active form of Pd, not only provide mechanistic insights into SM coupling reactions, but also have implications for the design of improved precatalysts. On the other hand, understanding catalyst deactivation also has potential to impact the performance of catalysts and is an important consideration when optimizing for reaction efficiency. Cyclometallation, P-C bond cleavage and P-oxidation are common deactivation pathways for organometallic complexes with phosphine ligands and irreversible oxidation or reduction of the active metal center in catalytic processes may influence catalytic activity.[20]

Detecting and characterizing active forms of the catalyst (as well as resting states and/or any deactivated forms) and identifying the subsequent reaction intermediates is important for understanding the mechanism of coupling reactions. While independent synthesis and characterization by x-ray diffraction and NMR spectroscopy provide detailed structural information on putative, stable organometallic species, detection and identification of proposed intermediates during the catalytic reaction provides the most relevant evidence as to what species are generated under catalytic conditions. Spectroscopic techniques such as IR and Raman can be used to identify certain functional groups in the analyte and thus provide some chemical information. NMR spectroscopic analysis of reaction mixtures offers both structural information and quantification of chemical species and is widely applied in online and offline monitoring. However structural assignments of analytes by NMR in complex systems may be hindered by signal overlap and peak-broadening caused by fast exchange of species and/or limited solubility of reaction components. Electrochemical methods have been applied to study short-lived

intermediates in coupling reactions involving redox processes although structural characterization by these methods is difficult without comparison to authentic compounds.[21]

Mass spectrometry (MS)-based methods of reaction monitoring have become increasingly effective tools for mechanistic studies[22-27] due to the high sensitivity of MS and the ability to directly analyze various species in complex mixtures without isotopic labeling. Tandem mass spectrometry (MS/MS) is an additional capability that offers structural information on particular mass-selected ions and, by implication, on the corresponding neutral species. Electrospray ionization MS (ESI-MS) is often preferred over other ionization methods as it is a soft (gentle) ionization technique which transfers molecular entities from solution to the gas phase as ions, usually without causing fragmentation. The key to detection of low intensity analytes in complex mixtures is to develop MS methods that have high sensitivity and use this method in conjunction with MS/MS.

The Canary group[28] first utilized offline ESI-MS to study SM coupling of pyridyl bromide complexes and phenyl boronic acid with different substituents catalyzed by $Pd(PPh_3)_4$. Intermediate ions related to the oxidative addition and transmetalation steps were "fished" from the complex reaction mixtures and characterized by measurement of *m/z* ratios and by their isotopic distributions. Since then, extensive mechanistic studies of Pd mediated coupling reactions including the SM, Negishi, Mizoroki-Heck, Sonogashira, Stille, and Buchwald-Hartwig reactions have been conducted by ESI-MS[24, 29-34]. Recently, several closely related ionization methods, specifically extractive ESI (EESI), desorption electrospray ionization (DESI) and inductive ESI have been found useful in monitoring rapid solution-phase processes with high sensitivity[35-37]. Hao Chen's group[36] developed a liquid DESI technique to study activation of Buchwald precatalysts (Aphos Pd G3 and SPhos Pd G2). The sodiated ion of the monoligated Pd(0) was captured and several intermediates in the Buchwald-Hartwig coupling and SM coupling were observed.

Here, we describe a nanoESI-MS based method which facilitates mechanistic studies of the SM reaction. Nanoelectrospray ionization (nanoESI) is a variant of ESI which is known for high sensitivity. Compared to DESI and ESI, which were explored in the preliminary stages of this work (see Supplemental Information, sec. 2.5.3), nanoESI features low sample consumption and improved ionization efficiency due to the small-sized droplets created by the emitter. It was chosen

for these properties and for the fact that it minimizes ion suppression and matrix effects.[38] The ease of performing nanoESI-MS experiments allowed us to monitor reactions at various time points and under various reaction conditions. By simultaneously monitoring reagents and reaction products, while also observing changes in the levels of key Pd species, we seek to understand the evolution of catalytically-relevant Pd intermediates throughout the time course of a typical SM reaction.

2.2 Experimental

The SM cross-coupling reaction of 3-Br-5-Ph-pyridine and phenylboronic acid with XPhos Pd G3 precatalyst and NaOEt as base in EtOH was chosen as the model reaction. We conducted two types of reaction monitoring 1) a simple one-pot reaction to capture the Pd containing intermediates. 2) A sequential addition experiment where we mix 3-Br-5-Ph-pyridine with XPhos Pd G3 precatalyst and NaOEt (as base) in EtOH to start the oxidative addition reaction and run it for 10 min before subsequently adding phenylboronic acid and continuing reaction monitoring for 10 min more. We made relative quantitative measurements of the intermediates using an internal standard (tetradodecylammonium nitrate) and correlated these values with the signal due to the oxidative addition intermediate and the product. The sequential addition experiment provides information on the Pd-compound flow in the reaction system.

2.2.1 Chemicals and Reagents

All reagents and solvents were used directly as received without further purification. Phenylboronic acid, XPhos Pd G3, BrettPhos Pd G3 sodium ethoxide, K_3PO_4, $FeCl_3$, formic acid and THF were purchased from Sigma-Aldrich (St. Louis, MO, USA). Ethanol (EtOH) was purchased from Decon Labs, Inc. (King of Prussia, PA, USA). 3-Br-5-phenyl pyridine, 2-(1H-pyrazol-1-yl)-5-(4,4,5,5-tetramethyl-1,3,2-dioxaborolan-2-yl) pyridine and 4-methoxy phenylboronic acid, were received from Merck Company. Water was purified and deionized by a Milli-Q system (Millipore, Bedford, MA, USA).

2.2.2 Synthesis of the XPhos-Pd-COD

Our college from Merck, Mycah Uheling, synthesized the XPhos-Pd-COD compound.

2.2.3 Suzuki coupling reaction of phenylboronic acid and 3-Br-5-Phenyl pyridine

The Suzuki reaction was performed using 1 eq. of 3 mM 3-Br-5-phenyl pyridine, 1.3 eq. of phenylboronic acid, 2 eq. of NaOEt as base and 0.1 eq. XPhos G3 as catalyst. Reagent solutions were freshly prepared in ethanol, mixed to give the required stoichiometry in a 1.5 mL Eppendorf tube and gently vortexed for the desired amount of time. For sequential addition reactions, the XPhos Pd G3, NaOEt and 3-Br-5-phenyl pyridine were mixed for the desired amounts of time before phenylboronic acid solution was added into the mixture and reaction continued. The Suzuki reaction in THF solvent shared the same procedure and used the same concentration, except 2 eq. K_3PO_4 (80 mM aqueous solution) was used as base.

2.2.4 Oxidative stress test of XPhos-Pd-COD

Stock solution of XPhos-Pd-COD was prepared in ethanol at a concentration of 4 mM. The Xphos-Pd-COD solution was sonicated until dissolved. For the $FeCl_3$ test, 80 µL of 100 mM FeCl3 solution was added to 1 mL of 0.4 mM XPhos-Pd-COD solution while an equal volume of water was used in the control experiment. For the oxygen test, oxygen gas (5 psi, transferred via 1/16-inch peek tubing) was bubbled through the reaction solution for 1 min. The treated solution was then analyzed by MS. The Suzuki reaction was performed using the same reagents as in sec 2.2.3.

2.2.5 Analysis method

NanoESI emitters were prepared using a micropipette tip puller (Sutter instruments, Novato, CA) using borosilicate glass without filament (B150-86-10) (Sutter Instruments). For analysis, aliquots of reaction mixture were diluted ten-fold in EtOH (containing 0.1% formic acid to facilitate MS detection of both reaction intermediates and product) to quench the reaction. Tetradodecylammonium nitrate (1 µM) was added to the diluted solution as internal standard to quantify the Pd-containing intermediates in the reaction mixture. For the oxidative test experiment, the quenched solution was further diluted by a factor of 10 in EtOH (1% formic acid) to allow better measurement of reagent conversion to product ("conversion ratio", product over sum of product and reagent signals).

A linear ion trap mass spectrometer (LTQ, Thermo Fisher Scientific, San Jose, CA, USA) was used to record mass spectra. Typical MS parameters were as follows: average of 3 microscans, 100 ms injection time, 275°C capillary temperature and 1.6 kV nanoESI voltage. Mass spectra were recorded in a mass range from *m/z* 50-2000. Tandem mass spectrometry (MS/MS) using collision-induced dissociation (CID) was carried out for identification of ion structure. The standard CID conditions include: 1 Th (mass/charge unit) isolation window, normalized collision energy of 20-30 unit (manufacturer's unit). Typically tube lens 140 V was used for reaction intermediate characterization in the higher mass range and tube lens 65 V for conversion ratio (Product/(Product + Reagent)) calculation in the lower mass range.

2.2.6 Ionization efficiency correction for measurement of the conversion ratio in the oxidation stress experiment

For accurate measurement of the reaction conversion in the oxidation stress experiment, we corrected the ionization efficiency of the reagent and product ions of the Suzuki reaction based on a method given in a previous report[39]. The definition of ionization efficiency correction factor is given below. After 40 min reaction at room temperature, the reaction mixture was quenched and analyzed by MS. We recorded the ratio of the product peak intensity over reagent peak intensity as S_1. After spiking an equimolar reagent into the quench solution, we recorded the ratio of product peak intensity over reagent peak intensity as S_2. Using the equation below for the ionization correction factor f in terms of S_1 and S_2, we get an average value of f from five replicate determinations (Table 2.1).

$$f = \frac{I_P/I_R}{[P]/[R]}$$

$$f \cdot \frac{[P]}{[R]} = S_1$$

$$f \cdot \frac{[P]}{[R]+[R]+[P]} = f \cdot \frac{[P]}{2[R]+[P]} = S_2.$$

$$f = \frac{S_1 S_2}{S_1 - 2S_2}$$

Table 2.1 Measured S1 and S2 values and calculated ionization correction factor f

	1	2	3	4	5
S1	3.04	3.15	4.49	3.35	3.75
S2	0.82	0.78	0.82	0.84	0.89
f	1.8	1.5	1.3	1.7	1.7
Avg *f*	1.6 +/- 0.2				

2.2.7 Least squares algorithm to deconvolute Pd cluster ions (centered at *m/z* 583)

The algorithm to calculate percentages of the three ionic forms *m/z* 583, *m/z* 582 and *m/z* 581 in the ion cluster is based on this procedure:

1. Record the absolute peak intensities of the isotopes from *m/z* 577 to *m/z* 590 and normalize this data to the highest intensity peak and this is stored as **vector 1**.

2. Recursively assign the percentages of the three ionic forms *m/z* 583, *m/z* 582 and *m/z* 581 to a, b, 1-a-b (start from 100% ,0%, 0% to 0%,0% ,100%, step size set to 1%) and calculate isotopic peak intensities in item 1 by summing the theoretical distributions (https://www.sisweb.com/mstools/isotope.htm) of the proposed three ionic forms and storing this as **vector 2**. Calculate the square of the error of the **vector 1** and **2**. Find the best fit value with the least error.

2.3 Results and Discussion

2.3.1 Monitoring of SM reaction

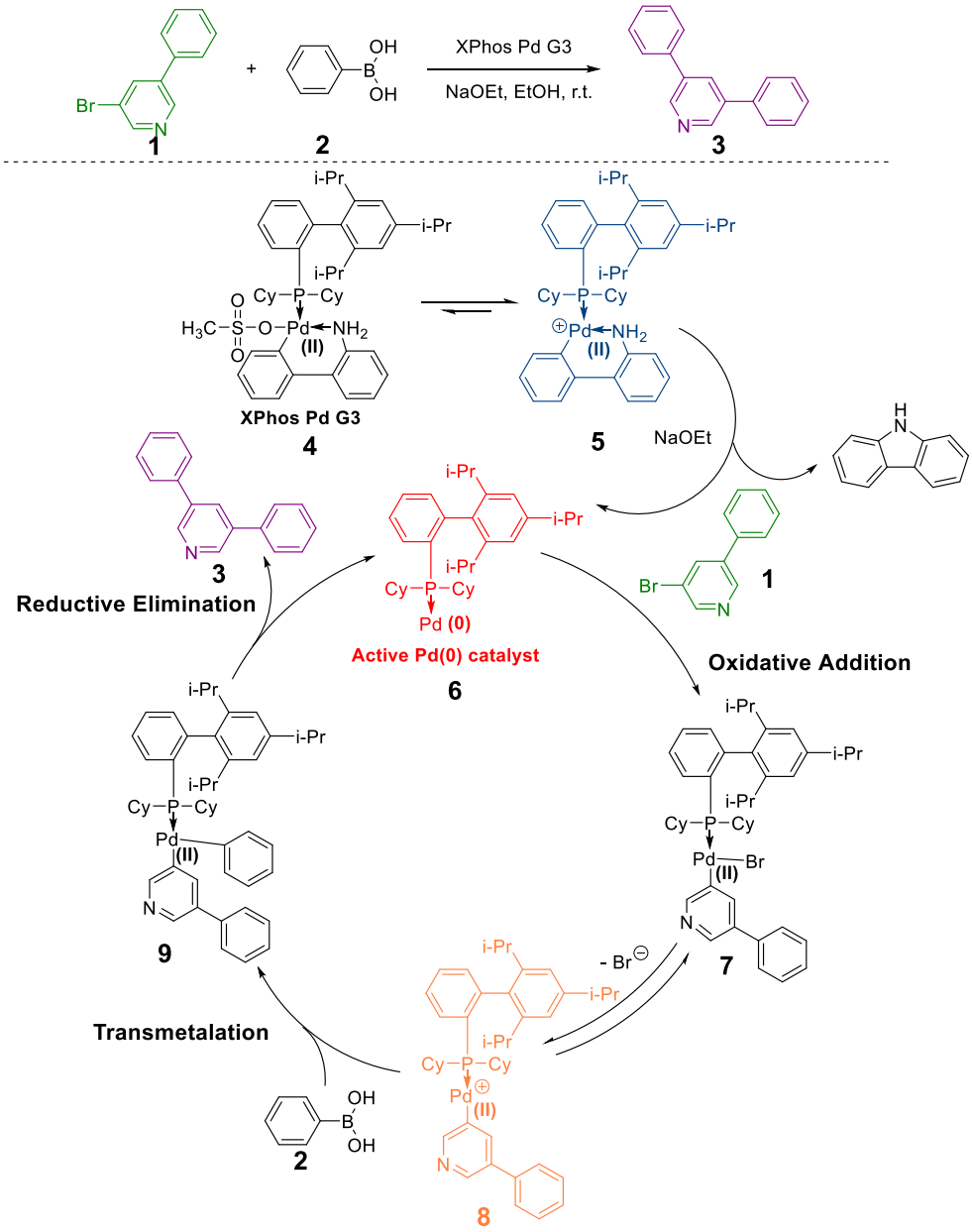

Scheme 2.1 Mechanism of the SM coupling reaction of aryl halide **1** with arylboronic acid **2** to form product **3** showing forms of the catalyst (**4** - **6**) and proposed intermediates (**7**, **8** and **9**). Note that **8** is not always considered in representations of the mechanism but it is included here because it appears in the mass spectra of the reaction mixture.

We studied the SM cross-coupling reaction of 3-Br-5-Ph-pyridine and phenylboronic acid with XPhos Pd G3 precatalyst while using NaOEt as base in EtOH. According to the accepted mechanism of the SM cross-coupling reaction (Scheme 2.1), the precatalyst is expected to undergo base-mediated reductive elimination of carbazole to form the monoligated Pd(0) active catalyst **6**. The active catalyst enters the catalytic cycle and undergoes oxidative addition of the aryl bromide to give **8**, possibly via reaction intermediate **7)**, followed by transmetalation with phenylboronic acid (or its ester or "ate" complex) to form the Pd(II) di-aryl complex **9**, which subsequently yields the coupling product through reductive elimination with regeneration of the active catalyst.

For our experiments, we mixed all reagents for 2 min at room temperature in air, and then analyzed the reaction mixture using nanoESI ionization after quenching with ethanol containing 0.1% formic acid and an internal standard, tetradodecylammonium nitrate (details are provided in Experimental Section). As shown in Figure 2.1(a), We detected a doublet peak at *m/z* 234 and 236 corresponding to the aryl bromide reagent **1**, and the desired coupling product **3,** at *m/z* 232 (Figure 2.1(b)), as well as peaks corresponding to various Pd intermediates which are discussed below.

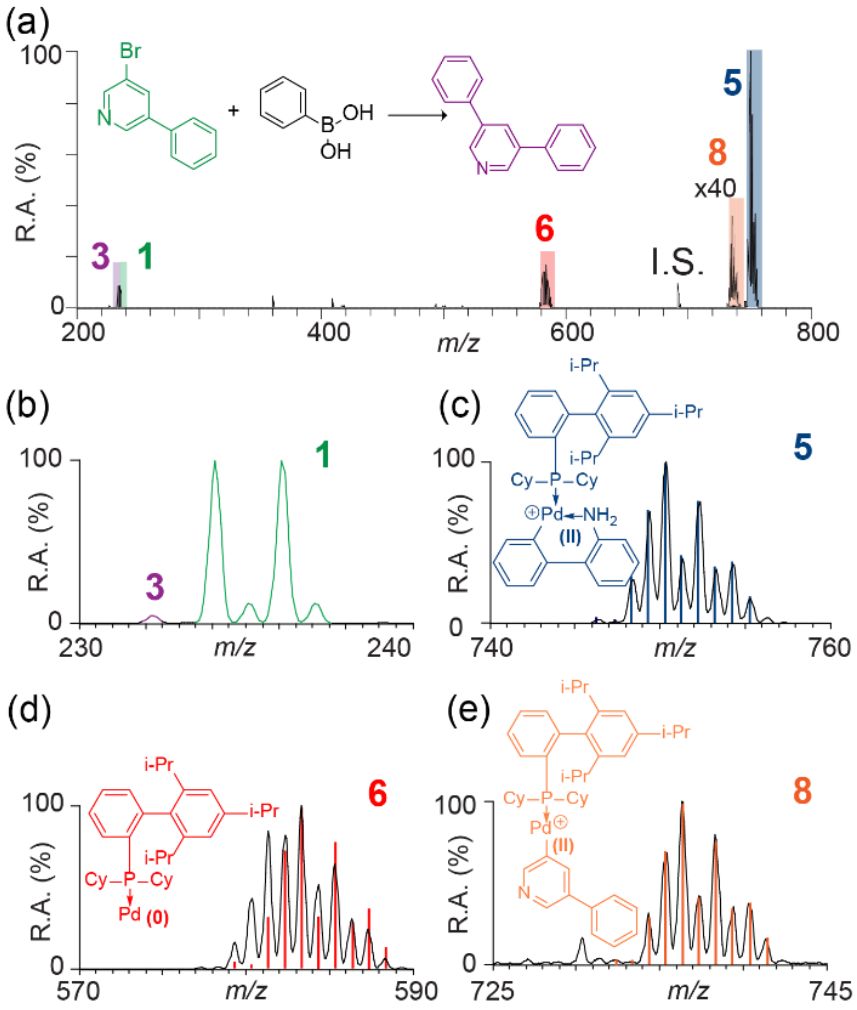

Figure 2.1 Mass spectra of (a) reaction mixture of 3-Br-5-Ph-pyridine (1 eq 3mM) with phenylboronic acid (1.3 eq) with XPhos Pd G3 precatalyst (0.1 eq) and NaOEt (2 eq) as base in EtOH after 2 min reaction in air, (b) zoomed-in region of spectrum showing product **3** (*m/z* 232) and reactant **1** (*m/z* 234,236). (c)-(e) Zoomed-in spectra of precatalyst **5** (ca. *m/z* 750), intermediate **6** (ca. *m/z* 582) and intermediate **8** (ca. *m/z* 736) and their theoretical isotopic peak distributions, respectively. All intermediate structures are notional. The internal standard (I.S.) is tetradodecylammonium nitrate.

The base peak in the nanoESI MS (Fig. 1(a)) is represented by a set of isotopic peaks around *m/z* 750 which appear to correspond to **5**, generated from the intact XPhos Pd G3 precatalyst **4** after loss of the methanesulfonate anion. Among other ions corresponding to reaction intermediates is a set of peaks, centered around *m/z* 736, which corresponds to the cationic Pd-aryl complex **8**, generated by loss of bromide anion from the oxidative addition intermediate **7**. It is an open question as to whether the species **8** occurs in solution or only as the gas phase ion. Figures 2.1(c) and 1(e) show the measured versus predicted isotopic distributions of the *m/z* 750 and *m/z* 736

species, respectively. They show good agreement with the displayed empirical formulae for species **5** and **8.** (Note that the precatalyst **4** shows small contributions of an ion m/z 736 when examined by nanoESI in solution, see sec. 2.5.5 for further discussion.) In contrast to these results, the isotopic distribution for the putative activated XPhos Pd(0) form of the catalyst **6** shows poor agreement (Figure 2.1(d)) with the calculated isotopic distribution for the molecular formula of the protonated molecule ($C_{33}H_{50}PPd^+$). This result can be accommodated by proposing contributions from a set of ions with this formula plus others with one and two fewer hydrogen atoms (vide infra).

Figure 2.2(a) displays a magnified view of the set of peaks in the range of *m/z* 583 in Figure 2.1(a). The most obvious product of ionization of the intact activated Pd(0) catalyst **6** is its protonated form $[M+H]^+$, shown in Figure 2.2(b) where M represents **6**. Comparison of the isotopic distribution calculated for the $[M+H]^+$ ion with the experimental distribution clearly shows contributions from other ions. To account for this, we considered closely related forms of the ion with one and two more or fewer hydrogen atoms and developed an algorithm (see sec. 2.2.7) to numerically determine the ratios of the three contributions that best fit the experimental isotopic distribution of the target peak set. The best fit (Figure 2.2(a)) to the experimental isotopic distribution for the cluster of ions centered on *m/z* 583 shows similar contributions by each of the three ions which are formally the result of (i) Pd insertion into a ligand C-H bond (with H atom and electron loss to give $[M - H]^+$); (ii) electron loss from the Pd(0) complex (to give $[M]^{+\bullet}$), and (iii) proton addition to the Pd(0) complex (to give $[M+H]^+$) (Figure 2.2(b)). Collision-induced dissociation (CID) of the mass-selected ions *m/z* 581, *m/z* 582 and *m/z* 583 showed strong resemblances between the resulting product ions (because of isotopes the structures are not fully separated by mass alone) as indicated by the common losses of cyclohexene (once or twice, neutral loss 82 and 164) and in combination with cyclohexane loss (neutral loss 166). The common loss of the isopropyl radical (neutral loss 43) is consistent with the presence of isopropyl substituents in the aryl rings. While the MS/MS data does not prove the three ion structures, the least squares fitting does show that species with these three molecular compositions are the only contributors to the isotopic envelope in the mass spectrum.

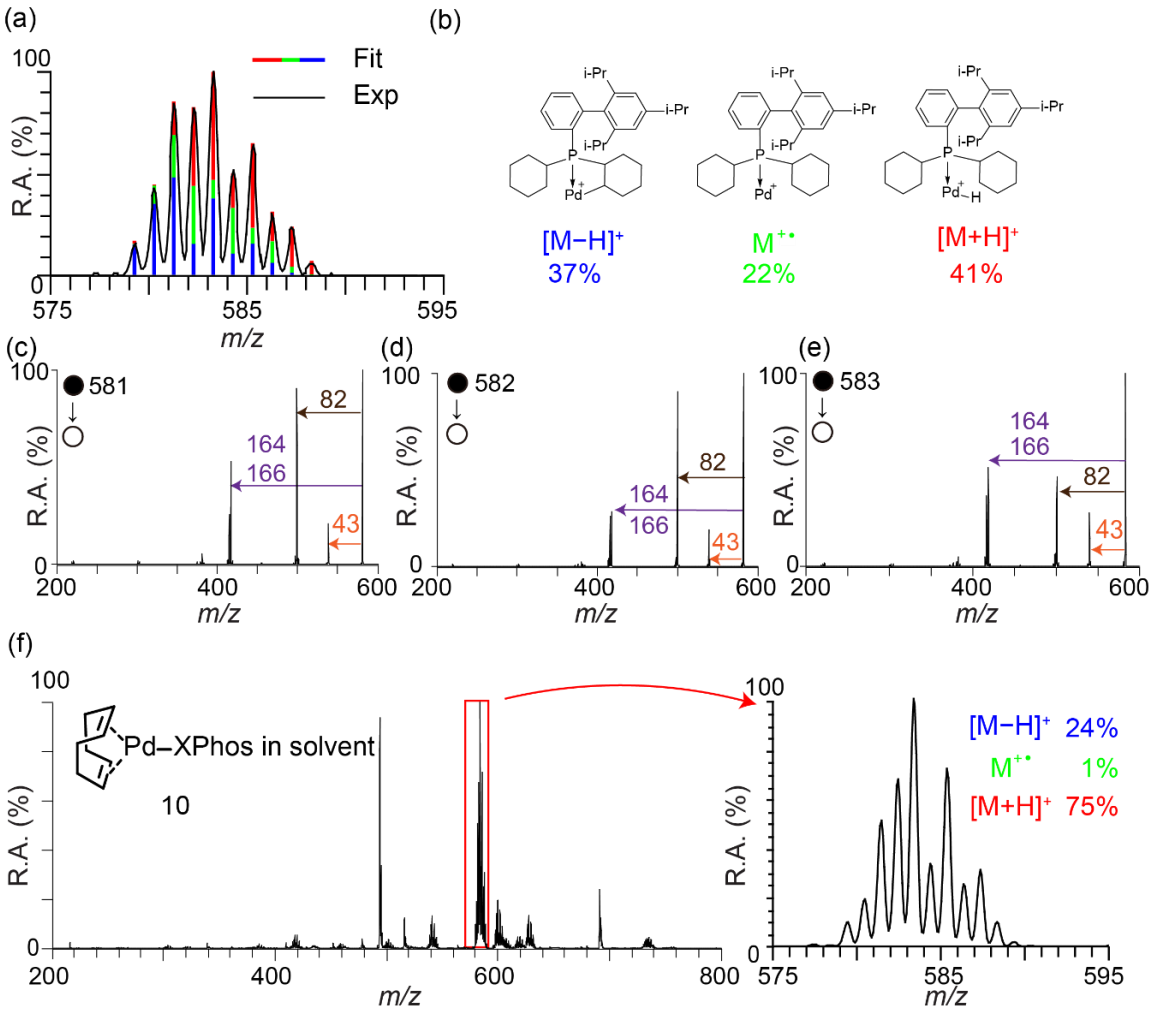

Figure 2.2 (a)-(b) Deconvolution of the Pd(0) isotopic peak distribution into three ionic forms of the Pd(0) intermediate and tentatively suggested structures of the three ions. (c)-(e) MS/MS showing collision induced dissociation of m/z 581, 582 and 583, respectively. (f) MS of an authentic Pd(0) compound with expanded view of the region around m/z 581 – 583 and the result of deconvolution into $[M-H]^+$, $[M]^{+\bullet}$ and $[M + H]^+$.

It is important to recognize that MS gives information on ions in the gas phase but does not directly inform on the species present in solution. The connection between these two regimes is not necessarily simple. Two important questions are (i) whether we can unambiguously relate the observed ions in the gas phase and the catalyst species present in solution and (ii) whether we can suggest reasonable structures for the solution phase species based on this relation and information obtained on the structures in the gas phase. The answer to both questions is affirmative, as we demonstrated in this study.

To address these questions, we synthesized the COD-Pd-XPhos complex **10** which is assumed to lose the COD ligand easily in solution to form the monoligated phosphine-Pd(0) complex (**6**), presumably the same complex that is proposed to be active in the catalytic cycle. We analyzed complex **10** in solution using the same conditions as were used for the XPhos Pd G3 catalyst, and it showed a similar envelope of peaks centered at *m/z* 583 (Figure 2.2(e). The spectrum is discussed in detail in the sec. 2.5.1). The difference between the set of peaks arising from **10** and those arising from precatalyst **4** under catalytic reaction conditions, however, is that the MS of **10** displays two rather than three forms of the activated complex as ions, viz. the nominal $[M - H]^+$ ion at *m/z* 581 and $[M+H]^+$ at *m/z* 583. This was not due to the choice of base or other reagents in the reaction solution, as the radical cation $[M]^{+\bullet}$ was still missing when these were added (see sec 2.5.4 for these results). Thus, we tentatively conclude that $[M]^{+\bullet}$ is generated by oxidation in an electron transfer reaction that is specific to the species in the reaction mixture in XPhos Pd G3. We also conclude that the ions we are designating as $[M - H]^+$ and $[M+H]^+$ are ionic representatives of two forms of the COD Pd(0) catalyst. Furthermore, given the similarities in reactivity[40] of the COD and G3 catalysts, these ions are candidates to be surrogates for the active and deactivated forms of the catalyst. Evidence is provided for this by monitoring their abundances while the reaction proceeds as will now be shown.

An experiment was done by studying stoichiometric oxidative addition (Figure 2.3). After mixing the 3-Br-5-Ph-pyridine with XPhos Pd G3 precatalyst and NaOEt in EtOH, we took aliquots of the reaction mixture to monitor the Pd containing intermediates over a 10 min reaction time. The $[M+H]^+$ and $[M]^{+\bullet}$ signals tracked each other, consistent with their simply being different ionized forms coming from the same solution phase species; both varied inversely with the formation of the oxidative addition intermediate **8** (centered at *m/z* 736). By contrast, $[M - H]^+$ tracked roughly with the oxidative addition reaction intermediate **8**. These results indicate that the active catalyst was being consumed while deactivated forms of the catalyst increased (Figure 2.3b) as the oxidative addition reaction proceeded, and that these processes can be tracked in the XPhos Pd G3 system using the ions $[M+H]^+$ and $[M - H]^+$, respectively. In this interpretation, the radical cation $[M]^{+\bullet}$ is simply a special ionized version of the active catalyst.

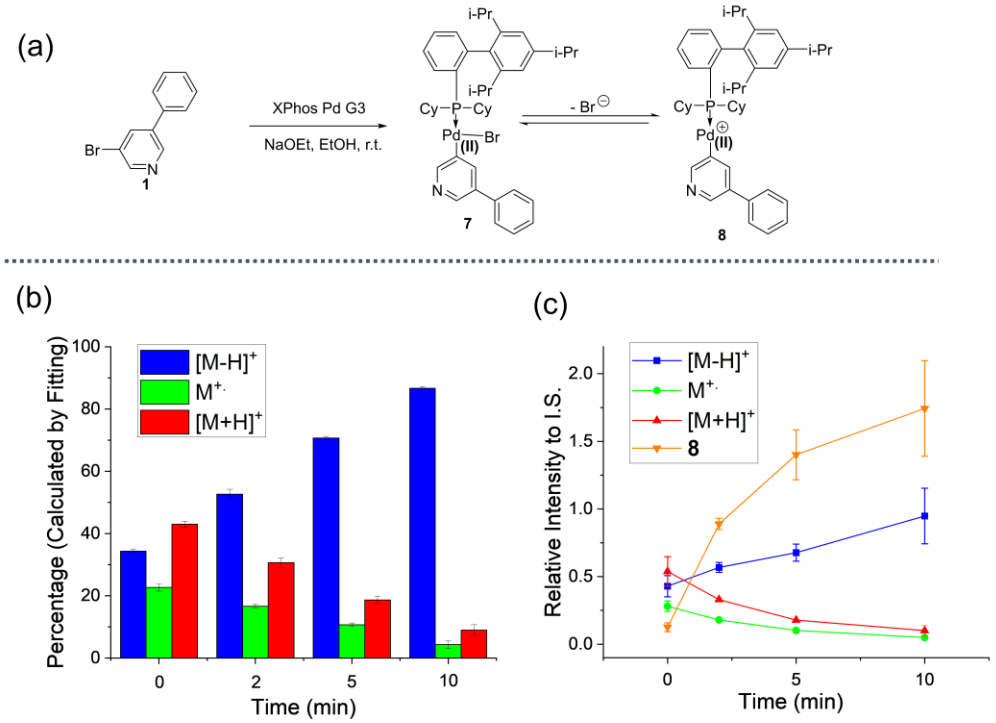

Figure 2.3 Analysis of changes in contributions of the three ionic forms of catalyst (a) Reaction scheme of the stoichiometric oxidative addition of 3-Br-5-Ph-pyridine with XPhos Pd G3 precatalyst and NaOEt as base in EtOH. (b) Variation in relative contributions of the three ionic forms during reaction. c) Variation in intensity of the three ionic forms of the Pd(0) species and the oxidative addition intermediate **8** (Pd(II)-Ar^+) all expressed relative to the internal standard during reaction.

To further investigate the impact of oxidation on the three ionic forms of the Pd catalyst, we performed oxidation stress experiments with the synthetic XPhos-Pd-COD complex. We first tested the effect of oxygen by bubbling pure oxygen into the catalyst solution (in EtOH) for 1 min (Figure 2.4). These conditions did not change the minor amount of radical cation, $[M]^{+\bullet}$. Moreover, there was no change in the percentage of the $[M - H]^+$ and $[M+H]^+$ ions in the catalyst solution and the reaction proceeded exactly the same as it did without the oxygen treatment. This result is in accord with the common observation that the SM cross coupling reaction is not particularly air sensitive. It is also consistent with the suggestion that there are two neutral forms that give rise to the $[M - H]^+$ and $[M+H]^+$ ions. Next, we tested another oxidant by adding 80 µL $FeCl_3$(aq) (20 eq

per equivalent of catalyst) to the 1 mL catalyst solution (in EtOH) while adding the same amount of water (80 µL) to another aliquot of catalyst solution as control (Figure 2.5). A significant drop of the $[M+H]^+$ percentage was observed, accompanied by almost complete suppression of the reaction when the treated catalyst solution was mixed with SM reagents. It seems that the relative intensities of the $[M - H]^+$ and $[M+H]^+$ ions in the catalyst solution can serve as indicators of the oxidation state of the catalyst and that more equivalents of oxidant cause the reaction to slow down.

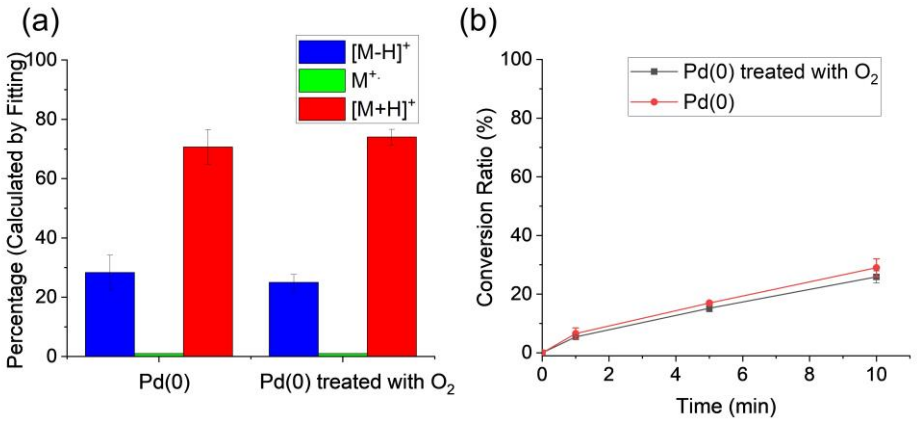

Figure 2.4 Oxygen stress test on XPhos-Pd-COD. (a) Percentage of ions in the *m/z* 583 cluster. (b) Reaction conversion ratio with time.

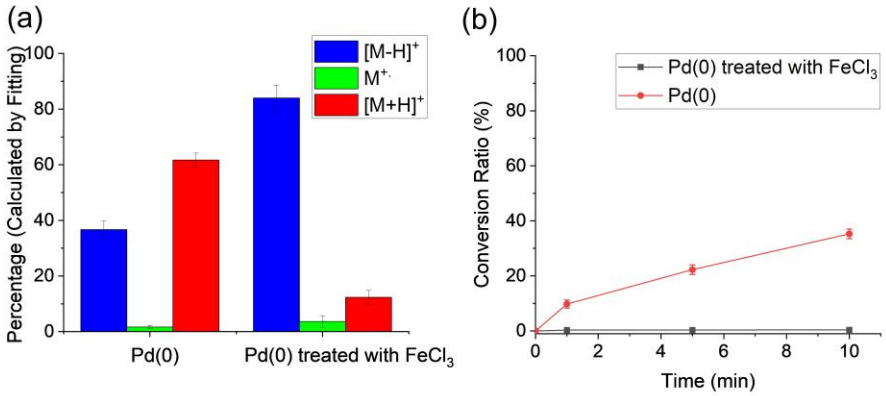

Figure 2.5 $FeCl_3$ stress test on XPhos-Pd-COD. (a) The percentage of ions in the *m/z* 583 cluster. (b) Reaction conversion ratio with time.

2.3.2 Structures of the gas phase ions

Because ionization by nanoESI typically involves protonation in the positive mode, the ion centered at *m/z* 583 is simply assigned as the protonated form of a molecule M, which is the active catalyst. We suggest that this molecule is the commonly assumed Pd(0) active catalyst, but do not know whether it is protonated at Pd or at P. In an earlier report[33] of a Pd dichloro-bis(aminophosphine) complex as precatalyst for SM cross coupling reaction monitored by ESI-MS, $[PdL_2H]^+$ (L is phosphine ligand) was detected when the precatalyst was dissolved in CH_3CN and was assigned as the protonated form of the active species PdL_2.

The species with its main isotope at *m/z* 581 is best considered as the gas-phase oxidation product of the solution phase Pd (0) species after ligand C-H activation, viz. the neutral [M – H]. This species undergoes electron loss to form the ion $[M - H]^+$, the surrogate ion for the deactivated catalyst which we propose has a cyclic structure although the details are not known. Palladacycles formed by activation of aryl C-H bonds to form five-membered rings are observed and proposed to be favored[41], but that would not be possible with Pd-XPhos complexes. Cyclometalation via alkyl C-H activation generally requires bulky and basic ligands and the four member ring palladacycles have been observed in some systems when Pd(II) precursors reacted with P*t*Bu$_3$.[41,42] The question of the structure of the ion *m/z* 581 is taken up below.

We propose that the active catalyst formed a palladcyclic structure by activation of C-H bond on the phosphine ligand to give the $[M-H]^+$. One possible route is that Pd react with the aryl-H to form a five-membered ring palladacycle. To test this hypothesis, we monitored the Suzuki reaction as list in sec 2.2.3 with the precatalyst Brettphos Pd G3 which share similar structure of the XPhos Pd G3, except the ortho and para positions of the aryl are is substituted by -OCH3.We examine the isotopic distribution of the active catalyst Pd(0) and it again suggests more than one gaseous ion,. After deconvolution the set of peaks with the algorithm in sec 2.2.7. We observed that $[M-H]^+$ still formed in considerable amount though the five-member ring structure is unlikely to form with Brettphos. Thus, we proposed the $[M-H]^+$ is formed via C-H activation on the cyclohexyl.

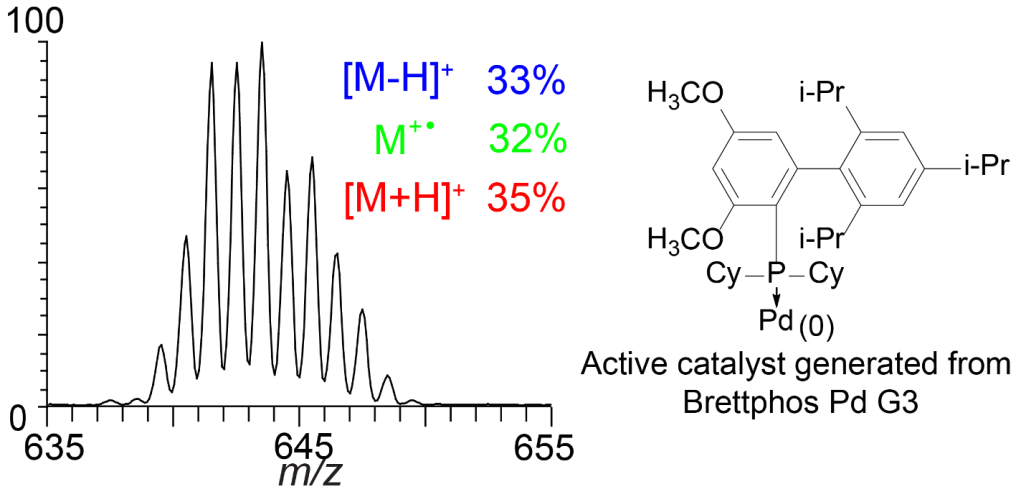

Figure 2.6 Proposed structure of the active catalyst Pd(0) generated from the Brettphos Pd G3 and deconvolution of the Pd(0) isotopic peak distribution into three ionic forms of the Pd(0) intermediate. Tubelens 170 V used after re-optimized the instrument parameter.

The ion at *m/z* 582 must be an odd-electron ion and as such is simply the gas phase oxidation product ($M^{+\bullet}$) of the active catalyst. There is no evidence that the radical cation plays any role in the reaction in solution and its formation as a gas phase ion is likely to be strongly dependent on exact redox conditions of the solution. In a related report of an ESI-MS study of a Stille reaction catalyzed by $Pd(OAc)_2$ and PPh_3, the radical cation $[Pd(PPh_3)_2]^{+\bullet}$ was detected: the neutral form is the proposed active catalyst formed in solution.[43]

2.3.3 Transmetalation step in SM cross coupling reactions

While the investigation into the monoligated Pd complexes has implications for the state of the active catalyst in the system, another important intermediate, the oxidative addition intermediate (centered at *m/z* 736) helped us to track the Pd mass flow in the catalytic cycle and to evaluate the progress of the coupling reaction. A previous MS study[19] of SM coupling of aryl iodides identified a $L_nPd(II)$-aryl intermediate as possibly being on the pathway to transmetalation. In order to examine the transmetalation step, we broke the reaction cycle into two parts and monitored the oxidative addition and transmetalation/reductive elimination steps separately by sequential addition of the appropriate reagents (see Experimental section). Observation of the products of a mixture of XPhos Pd G3 precatalyst **4**, aryl bromide **1** and NaOEt base for 10 min showed a steady decrease in MS signals arising from the precatalyst **5** and Pd(0) species **6** and concomitant

formation of the oxidative addition complex **8** (Figure 2.6(a)). After 10 minutes and upon adding phenylboronic acid to the reaction mixture, the relative intensity of the oxidative addition intermediate **8** was seen to drop precipitously, and product formation (indicated by the ratio of product ion (**3**) to reagent ion (**1**) plus product (**3)** intensities) was observed to increase over the next 10 min (see Figure 2.6(b)).

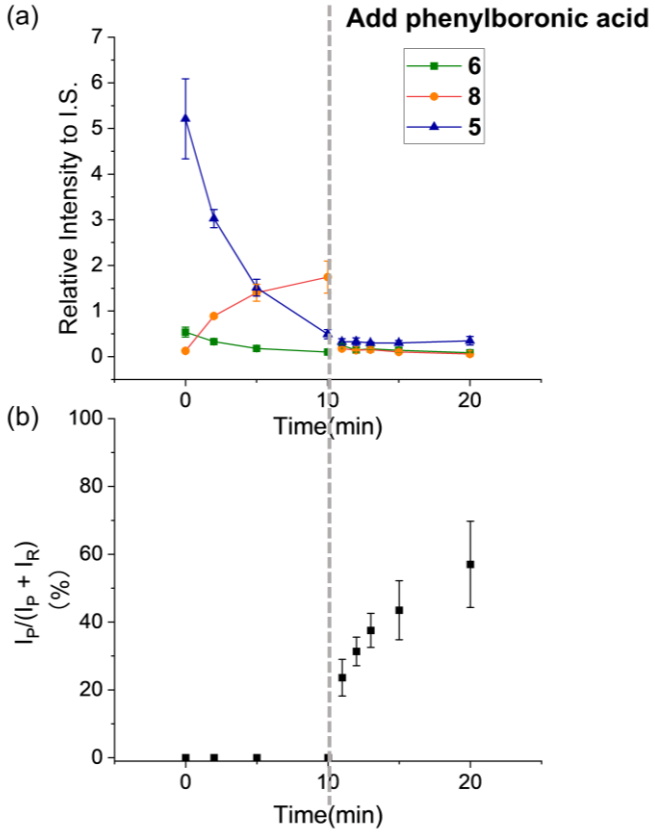

Figure 2.7 Monitoring changes in (a) the oxidation reaction intermediate **8** (LPd(II)-Ar), the intermediate **5** (Precatalyst) and **6** (LPd(0), protonated active catalyst) during the oxidative addition step and the transmetalation step of the SM reaction and (b) the product conversion represented by the Ion intensity of product **(3**) divided by the sum of ion intensity of product **(3**) and reagent (**1**) The grey dashed bar indicates the timepoint of addition of the boronic acid.

We then set out to explore the value of this approach in evaluating the transmetalation step in two different SM cross-coupling reaction systems (Figure 2.7). We conducted a sequential addition experiment on the 5 min time scale for the SM reaction in THF using 3-Br-5-Ph-pyridine with two boron derivatives: 4-methoxy phenylboronic acid (**11a**) and 2-(1H-pyrazol-1-yl)-5-(4,4,5,5-

tetramethyl-1,3,2-dioxaborolan-2-yl) pyridine (**11b**). After addition of the 4-methoxyphenylboronic acid **11a**, the oxidative addition intermediate was observed to drop by 63% in one minute accompanied by fast product formation (indicated by the ratio of product ion intensity and reagent ion intensities, Fig. 7d). In the case of the boronic ester **11b**, the decrease of oxidative addition intermediate and product conversion is much slower, Fig 7e. We attribute the slow product formation of the reaction with the boronic ester vs. the boronic acid to be due to the relatively slow transmetalation step in the former case. Thus, MS analysis of the oxidative addition intermediate may help to characterize the speed of the transmetalation step in a reaction under study.

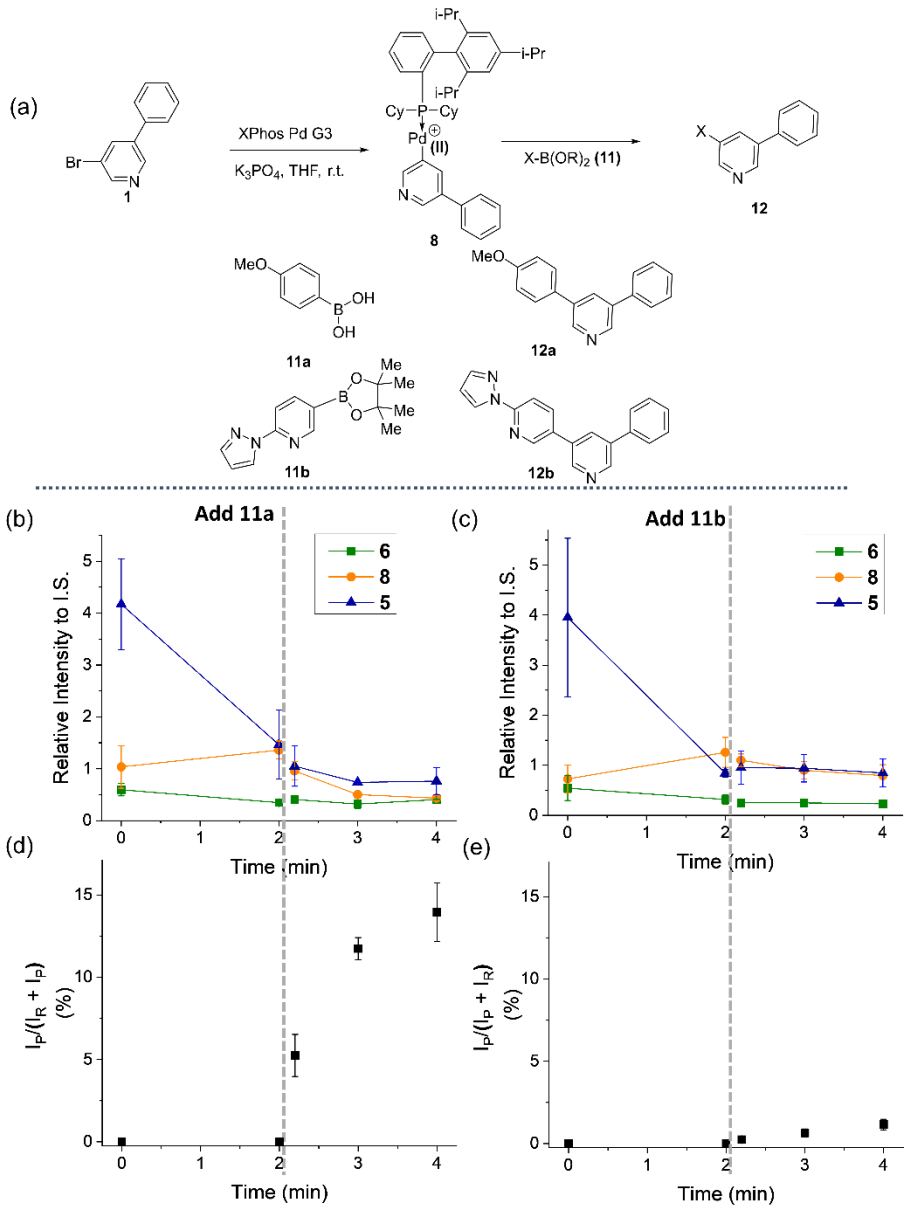

Figure 2.8 Monitoring the SM reaction of the aryl bromide Br-Ph-Py with boronic acid and ester. a) Scheme of sequential addition experiment b) Intermediate ion intensity relative to I.S. for reaction with 4-methoxyphenylboronic acid c) Intermediate ion intensity relative to I.S. for reaction with 2-(1H-pyrazol-1-yl)-5-(4,4,5,5-tetramethyl-1,3,2-dioxaborolan-2-yl) pyridine. d) Ion intensity of reagent (**1**) vs. reagent plus product (**12a**) (e) Ion intensity of reagent (**11b**) vs. reagent plus product (**12b**). Intensity of reagent (**11b**) was used since the ionization efficiency is similar to that of the product based on structural similarity. The grey dashed lines indicate the timepoint of addition of the boronic acid/ester.

2.4 Conclusions

Nano ESI-MS methodology was implemented to detect multiple intermediates in Suzuki-Miyaura (SM) coupling including the active and a deactivated form of the Pd(0) catalyst, as well as multiple other catalytically relevant intermediates, all in one reaction time course. A key difficulty in the interpretation of the mass spectra of organometallic compounds is the relationship between the molecular entity in solution and the form(s) into which it is converted during ionization and desolvation. We have drawn specific conclusions regarding this relationship by observing correlations between oxidation conditions and the corresponding changes in the Pd(0) derived ions.

We captured a set of monoligated catalyst Pd(0) ions, the nature of which varied with the oxidative state of the reaction system (e.g., presence of various oxidizing agents). This cluster contained three ionic forms *m/z* 583, *m/z* 582 and *m/z* 581 and we used a least-squares-based algorithm to deconvolute the cluster spectra and measure the relative ratios of the three ionic components. We interpret these three ions as being related to just two forms of the catalyst (the active catalyst and an oxidized form of catalyst). Their ratios, when considered in conjunction with data on product formation, provide information on the extent of catalyst oxidation and consequently how much of the catalyst is in a low valent state at a point in time.

In more detail, the active catalyst was assigned as the protonated form of the Pd(0) structure, *m/z* 583, while the deactivated catalyst was assigned to a cyclic structure, giving ion *m/z* 581. The third ion, *m/z* 582, is due to electron transfer occurring in competition with protonation but only under particular redox conditions which makes it of less general interest. The connection between the observed ions (Figs. 4 and 5) and the corresponding solution species was made by correlating the extent of reaction with the active/deactivated forms of the catalyst. Note that the structure of the protonated active catalyst–whether it be P-protonated or Pd-protonated–is not known. The structure of the ion that represents spent catalyst is also uncertain: we illustrate it as the product of hydride elimination from the cyclohexyl ring with palladacyclization, but the corresponding solution-phase species is unknown. Apart from the above assignment, we also acknowledge that there is a possibility that $[M - H]^+$ and $[M+H]^+$ result from the same solution species, a possibility which is not otherwise discussed in this paper.

2.5 Supplemental information

2.5.1 Discussion of the mass spectrum of the XPhos-Pd-COD

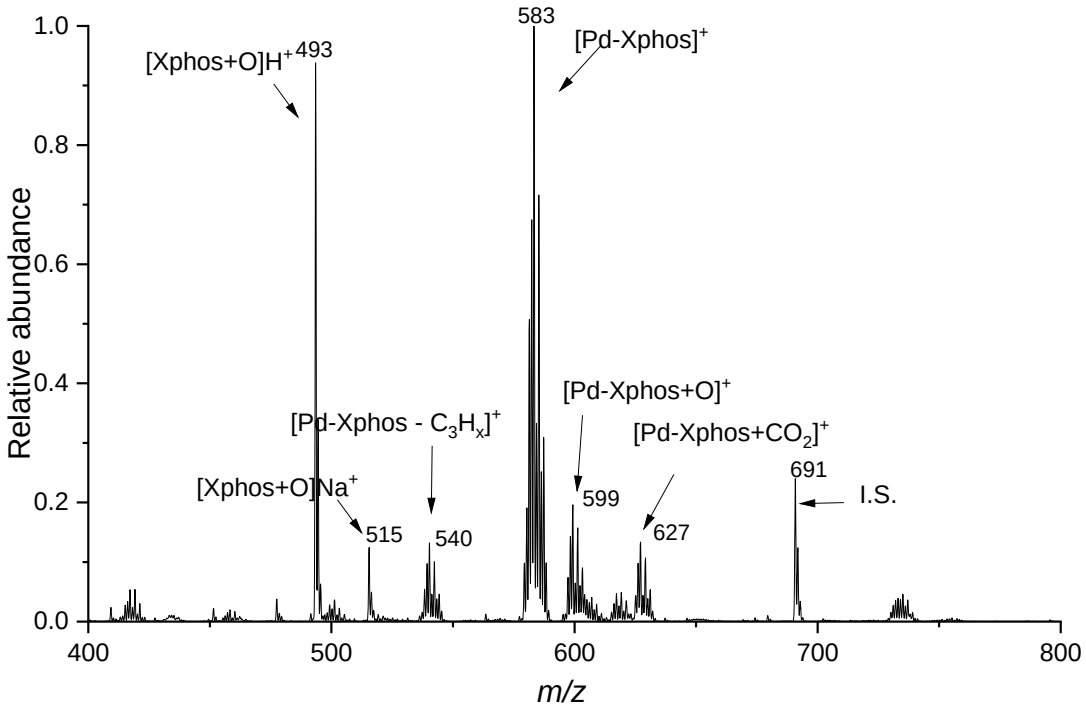

Figure 2.9. NanoESI mass spectrum of authentic XPhos-Pd-COD in ethanol/0.1% formic acid

MS of the XPhos-Pd-COD in ethanol/0.1% formic acid was shown in Figure 2.9

Protonated XPhos-Pd-COD should have isotopic distribution centered at *m/z* 691 but is not seen. The *m/z* 691 peak in the MS is the internal standard (tetradodecylammonium ion). We note the following:

m/z 627 can be assigned as the dehydrogenated adduct of the active Pd(0) catalyst with addition of formic acid.

m/z 599 can be assigned as the protonated form of active Pd (0) catalyst with addition of O (or the dehydrogenated form of active catalyst with addition of H_2O, or the adduct of radical cation of active Pd(0) with OH radical).

m/z 540 can be assigned as the protonated form of active Pd(0) catalyst with loss of isopropyl radical (and/or propene, propane)

m/z 493 515 can be assigned to the oxidized ligand XPhos+O

2.5.2 MS/MS of precatalyst and oxidative addition intermediate

The fragmentation of the protonated form of the precatalyst, *m/z* 750, was elucidated by tandem mass spectrometry (Fig. 2.10) The observed loss of carbazole and further loss of H_2 is consistent with the assigned structure.

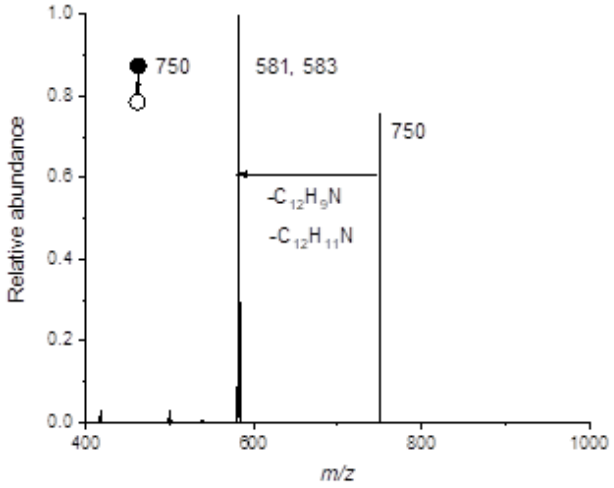

Figure 2.10 MS/MS product ion spectrum of precatalyst (*m/z* 750) recorded by collision induced dissociation; the major fragments correspond to loss of carbazole and carbazole + H_2

The fragmentation of the protonated form of the putative oxidative addition intermediate, *m/z* 736, was elucidated by tandem mass spectrometry (Fig. 2.11). The complex fragmentation behavior is consistent with the suggested structure, as explained in Scheme 2.2.

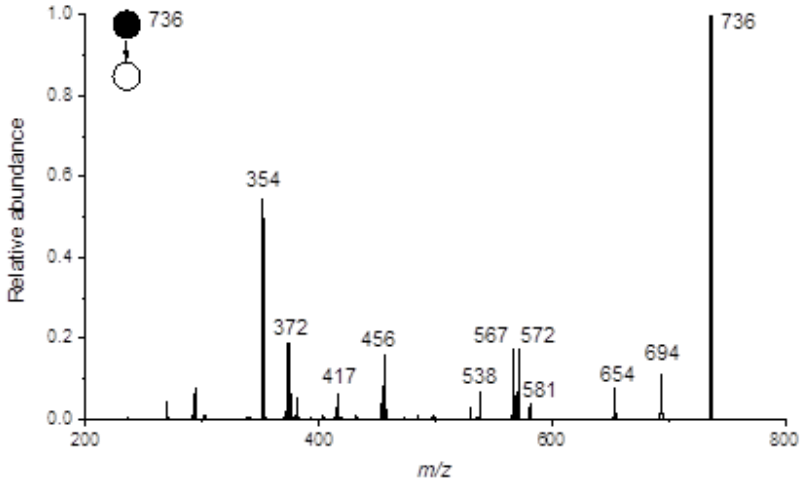

Figure 2.11 MS/MS of oxidative addition intermediate, *m/z* 736 recorded by collision induced dissociation suggested structures of the fragments and fragmentation pathways are show in Scheme 2.2

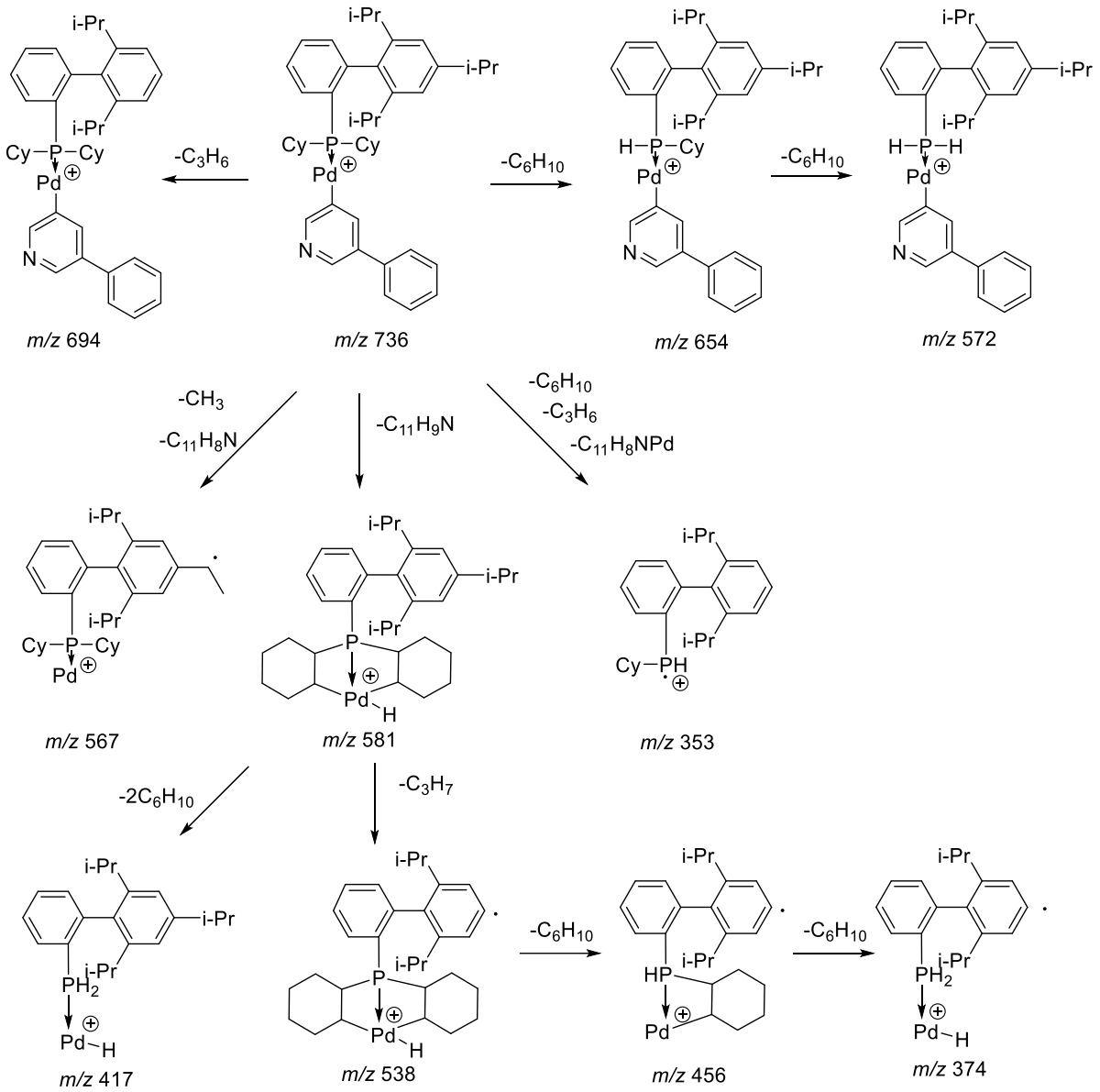

Scheme 2.2 Suggested structures of fragments from MS/MS spectrum of oxidative intermediate, *m/z* 736, Figure 2.11. The first line shows fragments of the oxidative intermediate, *m/z* 736 via losses of isoprene, isohexene and two molecules of cyclohexene; the second line suggests fragments of the proposed palladacycle *m/z* 581 losing isopropyl radical and then undergoing further loss of one or two molecules of cyclohexenes and then additional fragmentations.

2.5.3 Preliminary studies of online monitoring of the Suzuki reaction

We started this study by investigating several methods to monitor the Suzuki coupling reaction. 1) Direct ESI coupled with batch reactor. This allowed continuous online monitoring of reaction mixtures in a batch reactor for long periods (above 20 min). Precatalyst (*m/z* 750) was detected in

the positive mode. However, detection of reagents and product could not be achieved simultaneously because the reagent could not be seen in the positive mode mass spectrum due to the presence of base in the reaction mixture.

2) DESI: We utilized DESI as the ionization method to examine the course of the reaction over time. The reagents were delivered using air-tight syringes and mixed in a tee and reacted for about 10 seconds in a fused silica capillary before analysis by DESI. The nebulizing gas (N_2) from the DESI sprayer served to protect the species in the plume from oxidation in air. The reaction time was varied by changing the flow rate of the sample solution and the length of the capillary. The Suzuki coupling reaction of 2-iodo-pyridine with phenylboronic acid using XPhos Pd G3 precatalyst with NaOEt base in ethanol solvent was examined using this apparatus. Although reaction intermediates and reagents were detected, the ion intensities were not stable. The fact that we could not achieve long periods of monitoring using this method made it less attractive than nanoESI.

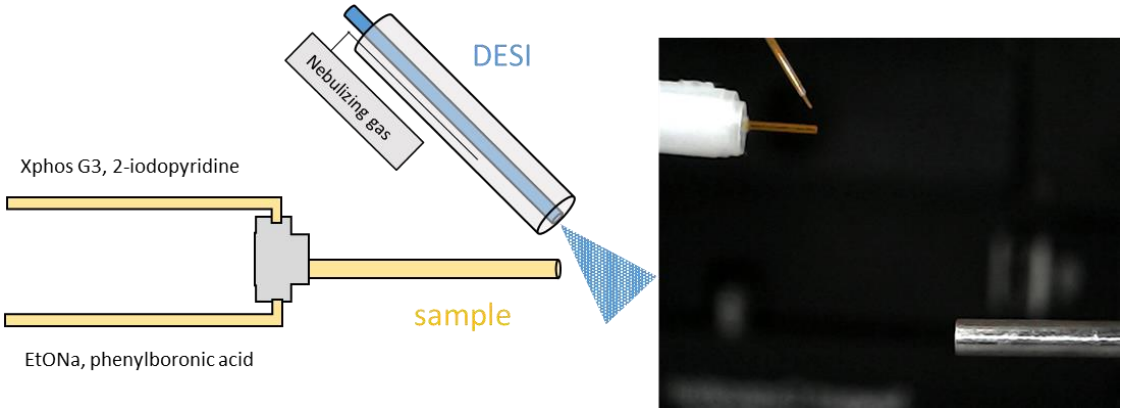

Figure 2.12 Experimental setup of the DESI online monitoring experiment

2.5.4 The contribution of the radical cation $M^{+\cdot}$ (*m/z* 582) in the set of ions.

We observe two rather than three forms of the ion, $[M-H]^+$ ion at *m/z* 581 and $[M+H]^+$ at *m/z* 583 in the MS of XPhos-Pd-COD. The amount of radical cation $[M]^{+\cdot}$ is neglectable. When we mix XPhos-Pd-COD, NaOEt and other reagents in the reaction solution and allow for 1 min of reaction, we deconvoluted the set of peaks we find to three ion forms using algorithm of sec 3, with intensities 59% $[M-H]^+$, 3% $[M]^{+\cdot}$, and 38% $[M+H]^+$.

2.5.5 Contribution to the signal at *m/z* 736 in the mass spectrum

We observed in the XPhos Pd G3 ethanol solution that there is small signal at *m/z* 736 present in the MS (0.4% relative to the *m/z* 750 which is the ionic form of precatalyst). This may be due to impurity in the precatalyst. We also observed that after 2 min and 5 min reaction, the signal at *m/z* 736 increased to 0.6%, 1.8% (relative to the signal at *m/z* 750). Thus, we conclude that the oxidative addition intermediate was indeed formed during the one-pot Suzuki coupling reaction.

2.6 References

(1) Nicolaou, K. C.; Bulger, P. G.; Sarlah, D. Palladium-catalyzed cross-coupling reactions in total synthesis. *Angew. Chem. Int. Ed. Engl.* **2005**, *44* (29), 4442-4489.

(2) Torborg, C.; Beller, M. Recent Applications of Palladium-Catalyzed Coupling Reactions in the Pharmaceutical, Agrochemical, and Fine Chemical Industries. *Adv. Synth. Catal.* **2009**, *351* (18), 3027-3043.

(3) Miyaura, N.; Suzuki, A. Stereoselective Synthesis of Arylated (E)-Alkenes by the Reaction of Alk-1-Enylboranes with Aryl Halides in the Presence of Palladium Catalyst. *Journal of the Chemical Society-Chemical Communications* **1979**, (19), 866-867.

(4) Miyaura, N.; Yamada, K.; Suzuki, A. New Stereospecific Cross-Coupling by the Palladium- Reaction of 1-Alkenylboranes with 1-Alkenyl or 1-Alkynyl Halides. *Tetrahedron Lett.* **1979**, *20* (36), 3437-3440.

(5) Miyaura, N.; Suzuki, A. Palladium-Catalyzed Cross-Coupling Reactions of Organoboron Compounds. *Chem. Rev.* **1995**, *95* (7), 2457-2483.

(6) Fauvarque, J.-F.; Pflüger, F.; Troupel, M. Kinetics of oxidative addition of zerovalent palladium to aromatic iodides. *J. Organomet. Chem.* **1981**, *208* (3), 419-427.

(7) Wagschal, S.; Perego, L. A.; Simon, A.; Franco-Espejo, A.; Tocqueville, C.; Albaneze-Walker, J.; Jutand, A.; Grimaud, L. Formation of XPhos-Ligated Palladium(0) Complexes and Reactivity in Oxidative Additions. *Chem. Euro. J.* **2019**, *25* (28), 6980-6987.

(8) Christmann, U.; Vilar, R. Monoligated palladium species as catalysts in cross-coupling reactions. *Angew. Chem. Int. Ed. Engl.* **2005**, *44* (3), 366-374.

(9) Biscoe, M. R.; Fors, B. P.; Buchwald, S. L. A new class of easily activated palladium precatalysts for facile C-N cross-coupling reactions and the low temperature oxidative addition of aryl chlorides. *J. Am. Chem. Soc.* **2008**, *130* (21), 6686-6687.

(10) Kinzel, T.; Zhang, Y.; Buchwald, S. L. A new palladium precatalyst allows for the fast Suzuki-Miyaura coupling reactions of unstable polyfluorophenyl and 2-heteroaryl boronic acids. *J. Am. Chem. Soc.* **2010**, *132* (40), 14073-14075.

(11) Bruno, N. C.; Tudge, M. T.; Buchwald, S. L. Design and Preparation of New Palladium Precatalysts for C-C and C-N Cross-Coupling Reactions. *Chem Sci* **2013**, *4*, 916-920.

(12) Li, H. B.; Seechurn, C. C. C. J.; Colacot, T. J. Development of Preformed Pd Catalysts for Cross-Coupling Reactions, Beyond the 2010 Nobel Prize. *Acs Catalysis* **2012**, *2* (6), 1147-1164.

(13) Bruneau, A.; Roche, M.; Alami, M.; Messaoudi, S. 2-Aminobiphenyl Palladacycles: The "Most Powerful" Precatalysts in C-C and C-Heteroatom Cross-Couplings. *Acs Catalysis* **2015**, *5* (2), 1386-1396.

(14) Kim, S. T.; Baik, M. H. Reductive activation of Pd(II)-precatalysts via decarboxylation of pivalate in direct C-H arylation reactions. *Chem Commun (Camb)* **2020**, *56* (89), 13868-13871.

(15) Wei, C. S.; Davies, G. H.; Soltani, O.; Albrecht, J.; Gao, Q.; Pathirana, C.; Hsiao, Y.; Tummala, S.; Eastgate, M. D. The impact of palladium(II) reduction pathways on the structure and activity of palladium(0) catalysts. *Angew. Chem. Int. Ed. Engl.* **2013**, *52* (22), 5822-5826.

(16) Proutiere, F.; Aufiero, M.; Schoenebeck, F. Reactivity and stability of dinuclear Pd(I) complexes: studies on the active catalytic species, insights into precatalyst activation and deactivation, and application in highly selective cross-coupling reactions. *J. Am. Chem. Soc.* **2012**, *134* (1), 606-612.

(17) Amatore, C.; Jutand, A. Anionic Pd(0) and Pd(II) intermediates in palladium-catalyzed Heck and cross-coupling reactions. *Acc. Chem. Res.* **2000**, *33* (5), 314-321.

(18) Johansson Seechurn, C. C. C.; Sperger, T.; Scrase, T. G.; Schoenebeck, F.; Colacot, T. J. Understanding the Unusual Reduction Mechanism of Pd(II) to Pd(I): Uncovering Hidden Species and Implications in Catalytic Cross-Coupling Reactions. *J. Am. Chem. Soc.* **2017**, *139* (14), 5194-5200.

(19) Melvin, P. R.; Balcells, D.; Hazari, N.; Nova, A. Understanding Precatalyst Activation in Cross-Coupling Reactions: Alcohol Facilitated Reduction from Pd(II) to Pd(0) in Precatalysts of the Type (η3-allyl)Pd(L)(Cl) and (η3-indenyl)Pd(L)(Cl). *ACS Catalysis* **2015**, *5* (9), 5596-5606.

(20) Crabtree, R. H. Deactivation in homogeneous transition metal catalysis: causes, avoidance, and cure. *Chem Rev* **2015**, *115* (1), 127-150.

(21) Jutand, A. Contribution of electrochemistry to organometallic catalysis. *Chem Rev* **2008**, *108* (7), 2300-2347.

(22) Sun, J.; Yin, Y.; Li, W.; Jin, O.; Na, N. Chemical Reaction Monitoring by Ambient Mass Spectrometry. *Mass Spectrom. Rev.* **2020**, *41* (1), 70–99.

(23) Santos, L. S.; Pavam, C. H.; Almeida, W. P.; Coelho, F.; Eberlin, M. N. Probing the mechanism of the Baylis-Hillman reaction by electrospray ionization mass and tandem mass spectrometry. *Angew. Chem. Int. Ed. Engl.* **2004**, *43* (33), 4330-4333.

(24) Sabino, A. A.; Machado, A. H.; Correia, C. R.; Eberlin, M. N. Probing the mechanism of the Heck reaction with arene diazonium salts by electrospray mass and tandem mass spectrometry. *Angew. Chem. Int. Ed. Engl.* **2004**, *43* (19), 2514-2518.

(25) Wilson, S. R.; Perez, J.; Pasternak, A. Esi-Ms Detection of Ionic Intermediates in Phosphine-Mediated Reactions. *Journal of the American Chemical Society* **1993**, *115* (5), 1994-1997.

(26) Schroder, D. Applications of electrospray ionization mass spectrometry in mechanistic studies and catalysis research. *Acc. Chem. Res.* **2012**, *45* (9), 1521-1532.

(27) Heck, A. J.; Van Den Heuvel, R. H. Investigation of intact protein complexes by mass spectrometry. *Mass Spectrom. Rev.* **2004**, *23* (5), 368-389.

(28) Aliprantis, A. O.; Canary, J. W. Observation of Catalytic Intermediates in the Suzuki Reaction by Electrospray Mass-Spectrometry. *Journal of the American Chemical Society* **1994**, *116* (15), 6985-6986.

(29) Roglans, A.; Pla-Quintana, A. *In Reactive Intermediates: MS Investigations in Solution*; Santos, L. S., Ed.; Wiley-VCH: Weinheim, Germany, 2010; Ch.7.

(30) Bock, K.; Feil, J. E.; Karaghiosoff, K.; Koszinowski, K. Catalyst activation, deactivation, and degradation in palladium-mediated Negishi cross-coupling reactions. *Chem. - A Eur. J.* **2015**, *21* (14), 5548-5560.

(31) Yunker, L. P. E.; Ahmadi, Z.; Logan, J. R.; Wu, W. Z.; Li, T. F.; Martindale, A.; Oliver, A. G.; McIndoe, J. S. Real-Time Mass Spectrometric Investigations into the Mechanism of the Suzuki-Miyaura Reaction. *Organometallics* **2018**, *37* (22), 4297-4308.

(32) Schade, M. A.; Fleckenstein, J. E.; Knochel, P.; Koszinowski, K. Charged tags as probes for analyzing organometallic intermediates and monitoring cross-coupling reactions by electrospray-ionization mass spectrometry. *J. Org. Chem.* **2010**, *75* (20), 6848-6857.

(33) Agrawal, D.; Schroder, D.; Frech, C. M. Observation of Binuclear Palladium Clusters upon ESI-MS Monitoring of the Suzuki-Miyaura Cross-Coupling Catalyzed by a Dichloro-bis(aminophosphine) Complex of Palladium. *Organometallics* **2011**, *30* (13), 3579-3587.

(34) Thomas, G. T.; Janusson, E.; Zijlstra, H. S.; McIndoe, J. S. Step-by-step real time monitoring of a catalytic amination reaction. *Chem Commun (Camb)* **2019**, *55* (78), 11727-11730.

(35) Marquez, C. A.; Wang, H.; Fabbretti, F.; Metzger, J. O. Electron-transfer-catalyzed dimerization of trans-anethole: detection of the distonic tetramethylene radical cation intermediate by extractive electrospray ionization mass spectrometry. *J. Am. Chem. Soc.* **2008**, *130* (51), 17208-17209.

(36) Zheng, Q.; Liu, Y.; Chen, Q.; Hu, M.; Helmy, R.; Sherer, E. C.; Welch, C. J.; Chen, H. Capture of reactive monophosphine-ligated palladium(0) intermediates by mass spectrometry. *J. Am. Chem. Soc.* **2015**, *137* (44), 14035-14038.

(37) Yan, X.; Sokol, E.; Li, X.; Li, G.; Xu, S.; Cooks, R. G. On-line reaction monitoring and mechanistic studies by mass spectrometry: Negishi cross-coupling, hydrogenolysis, and reductive amination. *Angew. Chem. Int. Ed. Engl.* **2014**, *53* (23), 5931-5935.

(38) Gibson, G. T.; Mugo, S. M.; Oleschuk, R. D. Nanoelectrospray emitters: trends and perspective. *Mass Spectrom. Rev.* **2009**, *28* (6), 918-936.

(39) Nie, H.; Wei, Z.; Qiu, L.; Chen, X.; Holden, D. T.; Cooks, R. G. High-yield gram-scale organic synthesis using accelerated microdroplet/thin film reactions with solvent recycling. *Chem Sci* **2020**, *11* (9), 2356-2361.

(40) Lee, H. G.; Milner, P. J.; Colvin, M. T.; Andreas, L.; Buchwald, S. L. Structure and Reactivity of [(L*Pd)n*(1,5-cyclooctadiene)] (n=1-2) Complexes Bearing Biaryl Phosphine Ligands. *Inorganica Chim Acta* **2014**, *422*, 188-192.

(41) Albrecht, M. Cyclometalation using d-block transition metals: fundamental aspects and recent trends. *Chem Rev* **2010**, *110* (2), 576-623.

(42) Goel, R. G.; Montemayor, R. Reactions of tri-tert-butylphosphine with platinum(II) and palladium(II). Facile intramolecular metalation of tri-tert-butylphosphine. *Inorg. Chem.* **2002**, *16* (9), 2183-2186.

(43) Santos, L. S.; Rosso, G. B.; Pilli, R. A.; Eberlin, M. N. The mechanism of the Stille reaction investigated by electrospray ionization mass spectrometry. *J. Org. Chem.* **2007**, *72* (15), 5809-5812.

CHAPTER 3. ACCELERATED REACTIONS IN FIELD DESORPTION MASS SPECTROMETRY

Portions of this chapter have been published in the journal: Journal of Mass Spectrometry as article "**Chen, X.**; Cooks, R. G. Accelerated Reactions in Field Desorption Mass Spectrometry. *J. Mass Spectrom.* **2018**, 53 (10), 942–946."

3.1 Introduction

Over the past decade, the fact that ordinary solution-phase reactions can be greatly accelerated in microdroplets and thin film has become well known.[1-8] These reactions in confined volumes can be orders of magnitude faster than bulk-phase reactions[5] with larger droplets showing smaller effects.[7] Accelerated reactions have been studied by various spray-based ionization methods in conjunction with on-line mass analysis[9] or off-line product collection [10] as well as by droplet levitation.[11] There is evidence that these reactions occur on the mass spectrometry (MS) time scale as in reactive desorption electrospray ionization (DESI), an experiment in which the reagent is supplied with the solvent and reaction occurs in splashed secondary droplets formed upon primary droplet impact with the condensed-phase analyte. An early study showed that the acid-catalyzed reaction of Girard T reagent with ketosteroids is accelerated in the secondary microdroplets generated either by spraying the reaction mixture onto an inert surface or by spraying Girard T reagent onto a surface bearing the ketosteroid.[12] Acceleration has been observed in droplets generated by electrospray ionization (ESI), electrosonic spray ionization (ESSI) and nanoESI.[12-14] In some cases of volatile solvents, the degree of reaction acceleration, judged by product ion abundance relative to reagent ion abundance, increases upon extending the distance from the ionization source to the mass inlet. This is accounted for by increased evaporation of the solvent leading to smaller droplets with relatively higher surface concentrations of analyte.[13] Acceleration is thought to be driven by the decreased energy required for desolvation of reagents located at the surface compared those in the bulk [5]. Apart from droplets, confined volume solutions in the form of thin films generated by drop casting of a solution onto a surface also show accelerated reactions. For example, the Claisen-Schmidt reaction, the Katritzky reaction and the haloform reaction have been accelerated in a paper spray ionization experiment in which the reaction mixture evaporates from the paper to form thin reactive films. [15-17]

Field ionization is a vacuum ionization technique in which an electron is removed from gas phase analyte molecules under the influence of a high electric field.[18] Electrons tunnel from the analyte through a potential barrier to create gas-phase radical cations which are then immediately accelerated in the high electric field and mass analyzed. The method is particularly useful for samples that are volatile but difficult to analyze using other ionization methods, including hydrocarbons and some organometallics. Field emitters are designed to achieve ultra-high electric field strengths with only modest applied potentials by relying on small radius of curvature microstructures; typically, they are composed of a thin tungsten wire with thousands of graphitic or metallic microdendrites in the nanometer size range. The unique structure of the emitter allows it to be wet with an analyte solution and this mode evolved into the related experiment known as field desorption in which heat and the high electric field are combined to create ions in vacuum from a sample supplied in the solution-phase. This method was one of the very first to be used successfully to record mass spectra of non-volatile compounds.[19, 20]

In this study we examine whether this method of applying a high electric field to a field emitter loaded with small amounts of analyte solution, might represent an alternative method of ambient ionization causing reaction acceleration. Wicking of solution towards the sharp ends of the dendrites would expose it to very high fields from which ion emission could occur. This appears indeed to be the case, so we were also interested in the relative advantages of this approach, the nature of the ionic species observed and the degree to which representative reactions were accelerated. Note that the restricted sample volume might be just as important to reaction acceleration reaction as the electric field, a fact suggested by observations using thin uncharged thin films[21] and levitated Leidenfrost droplets.[22] Three reactions were chosen for investigation: i) hydrazone formation from indoline-2,3-dione and phenyl hydrazine which has previously been reported to be accelerated in charged microdroplets generated by ESI;[23] ii) Katritzky transamination of pyrylium ions with functionalized amines, which is known to be accelerated in thin films,[15] and iii) Hantzsch synthesis of symmetric 1,4-dihydropyrdinine, which also known to be accelerated in microdroplets generated by nanospray.[13]

3.2 Experimental

3.2.1 Instrument

Field emitters were purchased from Linden CMS GmbH (Weyhe, Germany). They were constructed on a 13-micron diameter central tungsten wire onto which thousands of micro-graphite whiskers were grown electrolytically. Reaction mixtures were transferred to the emitter by dipping the emitter into a solution of reaction mixture so that a thin layer of solution covered the emitter. The emitter was positioned so as to align with the inlet to the mass spectrometer and placed 3-15 mm from its entrance aperture. A voltage of between 4 and 5 kV was applied to the solution-covered emitter to generate ions in air. Mass analysis was conducted using a linear ion trap and exact masses were measured with an Orbitrap (LTQ-Orbitrap XL, Thermo Scientific, San Jose, CA) instrument. The capillary temperature was 200°C, the capillary voltage was 15 V and the tube lens voltage 65 V. Product ion spectra were recorded using a precursor ion isolation window of 1 Th and a collision energy of 25 arbitrary units. Attempts to visualize droplets made by illumination with a laser pointer were not successful.

3.2.2 Chemicals

All chemicals were purchased from Sigma Aldrich (Milwaukee, Wisconsin). Reaction mixtures for hydrazone formation were prepared by adding 10 µL of phenyl hydrazine to 1 mL of 3 mM indoline-2,3-dione in methanol and 1µL of 1 M methanolic HCl. Mixtures for the radical capture experiments were prepared by adding 10 µL of phenyl hydrazine to 1 mL of 1 mM 2,2,6,6-tetramethylpiperidine-1-oxyl (free radical) (TEMPO) in methanol. Katritzky reaction mixtures were prepared by adding 0.5 mL of 10 mM 3,4,5-triphenylpyrylium tetraborate in acetonitrile to 0.5 mL of 10 mM of p-anisidine in acetonitrile. The Hantzsch reaction mixture was prepared by mixing together 0.5 mL of three reagents, 100 mM benzaldehyde, 200 mM ethyl acetoacetate and 400 mM ammonium acetate.

3.2.3 Calculations

The proton affinity of phenyl hydrazine was estimated from known NIST Webbook values of analogs[24]: hydrazine 853.3 kJ/mol, methyl hydrazine 898.9 kJ/mol, ammonia 853.6 kJ/mol, methylamine 899.0 kJ/mol and phenyl amine 882.5 kJ/mol. Note that methylation of hydrazine

and ammonia both result in an increase of ca. 45 kJ/mol in proton affinity. It is reasonable that phenyl substitution would cause similar shifts in proton affinity and the increase of 29 kJ/mol seen for ammonia → phenyl amine is applied to hydrazine. Thus, we estimate the proton affinity of phenyl hydrazine to be 882 kJ/mol.

3.3 Results and Discussion

3.3.1 Hydrazone formation

Phenyl hydrazine in methanol solution was added to a commercial field emitter to explore the ionization of this reagent in air under a high electric field. An unusual feature of the field desorption (FD) method of ionization is that radical cations can be observed. That was the case here, with phenyl hydrazine being observed as both the radical cation ($M^{+\cdot}$), *m/z* 108 and as the protonated molecule $(M + H)^+$, *m/z* 109. The relative abundance of the two ions changes with distance of the field emitter from the grounded MS inlet, possibly due to the decrease in field strength with distance. Field desorption in air is simple to perform and as these and later experiments show, it gives spectra characteristic of molecular structure.

TEMPO (M = 156 Da), a stable free radical, was added to the phenyl hydrazine solution to seek evidence of radical driven reactions under field desorption conditions. The protonated adduct of the two radicals was observed and the formula of this radical cation was confirmed using exact mass measurements (measured mass 265.2144; expected mass for molecular formula $C_{15}H_{26}N_3O$ 265.2154, error 4 ppm). This radical cation fragments readily upon collision and its MS/MS spectrum showed fragments of *m/z* 158 (50%), *m/z* 157 (100%) and *m/z* 109 (10%). The competitive formation of *m/z* 157 and 109 points to a proton bound dimer of phenyl hydrazine and TEMPO. The proton affinity of TEMPO is 882.3 kJ/mol [24] and that of phenyl hydrazine is estimated (see Experimental) as 882 kJ/mol. This suggests, based on the kinetic method[25] of determining thermochemical data, that the relatively strong peaks for proton bound dimer should be observed for both ions. The data are consistent with this expectation in showing *m/z* 157 and 109. However, the fragment ion observed at m/z 158 suggests the presence of a second dimeric structure and the MS^3 spectrum (*m/z* 265 → 158 → products) supports this by showing a fragment *(m/z* 125) corresponding to loss of H_2O and a methyl radical.

Phenyl hydrazine and indoline-2,3-dione mixtures in acidic methanol solution were then added to a commercial field emitter positioned at various distances from the vacuum inlet to the MS to explore the effect of distance on the nature of the molecular ion and on the progress of the dehydration reaction leading to the phenyl hydrazone (*m/z* 238). (Figure 3.1) The radical cation of phenyl hydrazine, generated at small distances, is replaced by the protonated molecule at longer distances and the ratio of the product ion (*m/z* 238) compared to the protonated reagent (*m/z* 109) increases as the distance increases. This is in accordance with the findings of previous distance dependence studies[13] where the result was suggested to be due to more solvent evaporation over longer distances resulting in decreased droplet size, increased surface to volume ratios and hence increased reaction rates. Acceleration has been suggested to be due to increased numbers of charged reagents at the surface and their partial solvation leading to decreased activation energies.[5, 13] The data in Figure 3.1 are consistent with hydrazone formation by acid-catalyzed nucleophilic attack by the hydrazine at the carbonyl with subsequent elimination of water. The fact that the radical cation (*m/z* 108) is replaced as the base peak by protonated phenyl hydrazine *(m/z* 109) at the longer distances at which hydrazone product formation begins is consistent with this mechanism. The radical cation (*m/z* 108) itself shows no reaction other than hydrogen abstraction to produce *m/z* 109, except that it produces the small signal seen at *m/z* 110 at short distances for which exact mass measurement (mass 110.0599) gives a formula $C_6H_8NO^+$ (expected 110.0600). Labeling data could not be obtained on this ion but collision-induced dissociation occurs with loss of a fragment with mass 18 Da, which suggests loss of water from a hydroxylamine group. The unusual hydrazine to hydroxylamine conversion is almost certainly associated with the radical cation.

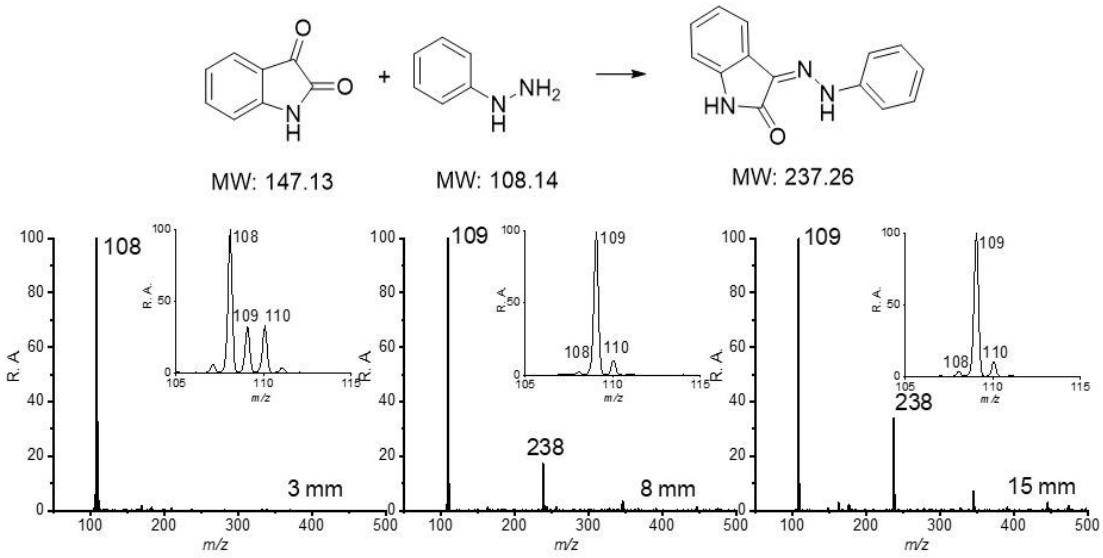

Figure 3.1 Mass spectra showing hydrazone formation from the indicated reaction mixture applied to a field emitter and positioned in air at various distances (3 mm, 8 mm and 15 mm) from the mass spectrometer inlet. Note the increased abundance of the product hydrazone *m/z* 238 relative to the hydrazine reagent as the distance is increased. Note, too, the fact that hydrazine appears as either *m/z* 108 or *m/z* 109, depending on distance. Total intensity fell by a factor of 100 moving from 3 mm to 15 mm.

The distance effect on reaction acceleration was investigated further by applying an orthogonal gas flow to the spray plume (Figure 3.2). With a 0.2 µL/min gas flow, the ratio of product ion vs. starting reagent dropped three-fold from the no-flow case. This effect can be accounted for by the selective removal of the smaller droplets created by field emission by the gas flow and the fact that smaller droplets have a dominant effect on reaction acceleration as shown above and in previous studies.[13, 23] These data are therefore consistent with earlier evidence [22] on droplet size effects on reaction acceleration.

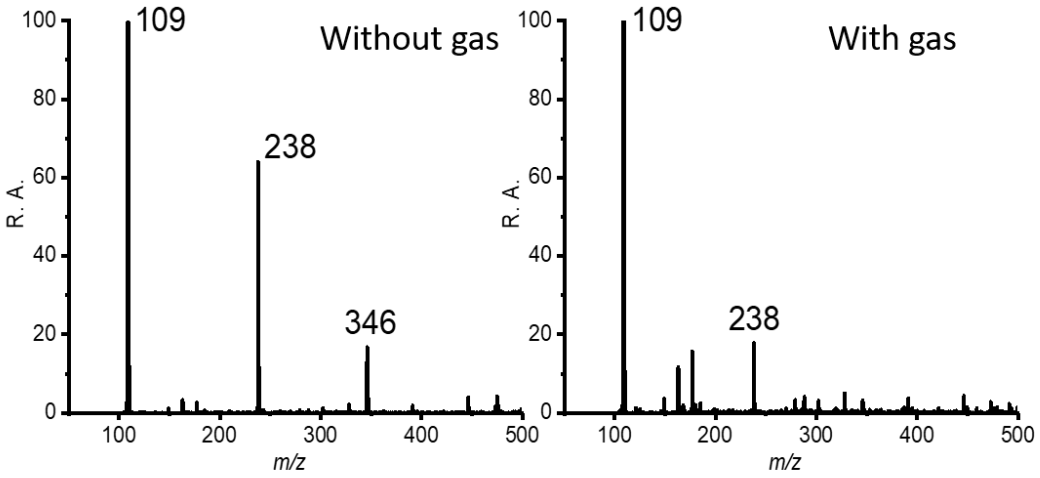

Figure 3.2 Mass spectra of hydrazone formation reaction with and without an orthogonal gas flow with the field emitter positioned at 15 mm. Total product ion intensity fell by a factor of 10 when adding the gas flow. Note that the ion at *m/z* 346 is the proton-bound dimer of the reagent hydrazine, *m/z* 109, and the product hydrazone, *m/z* 238.

3.3.2 Katritzky reaction

The Katritzky reaction of a triphenylpyrylium salt with *p*-methoxyaniline in acetonitrile to yield the corresponding pyridinium salt is very slow in the bulk phase where significant product is not seen until after 30 min. reaction time. In ambient field desorption, the signal due to the product ion was generated immediately, and it increased dramatically within 30 s. This observation is comparable to the acceleration phenomenon observed in reactive paper spray [15] where reagents are transferred onto a triangle paper surface and a spray occurs under the influence of a high electric field while products are examined online by mass spectrometry. The intensity of product signal in the reported paper spray experiment maximized after 10 min after which no reagent ion signal was seen. The acceleration has been attributed to increased concentrations, changed pH and enhanced intermolecular interactions in the thin film on the paper prior to the formation of microdroplets. The structure of the field emitter allows it to hold a small amount of reaction mixture. With rapid solvent evaporation, reagent concentrations are greatly increased and interfacial reactivity is enhanced. The combined effect of evaporation and high electric field causes rapid reaction which apparently occurs in the thin film liquid state on the emitter surface.

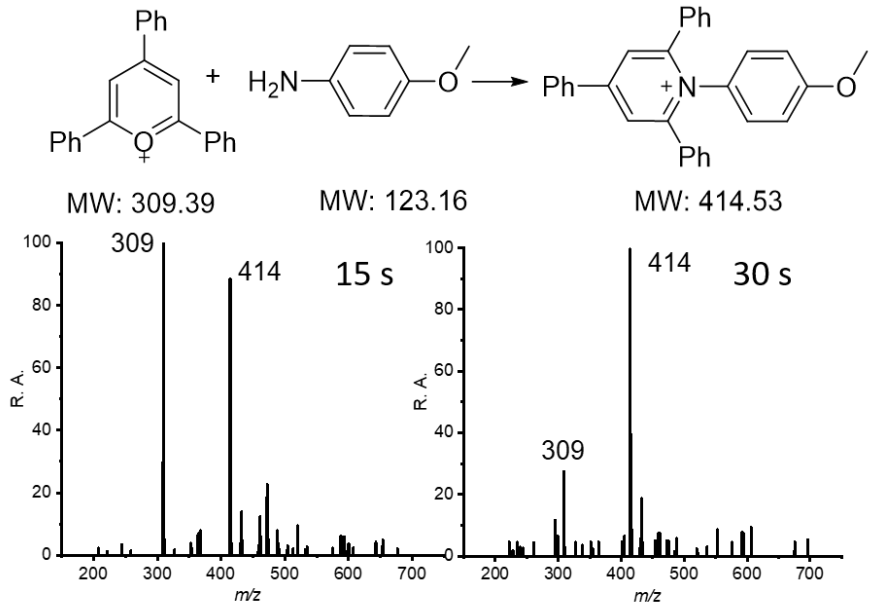

Figure 3.3 Mass spectra recorded as a function of time (15 s and 30 s after dipping the field emitter and positioning it 15 mm in front of the MS inlet). Total intensity is approximately the same in the two spectra. Note the increase in the pyridinium product ion (*m/z* 414) relative to the pyrylium reagent ion (*m/z* 309).

3.3.3 Hantzsch reaction

The Hantzsch synthesis of symmetric 1,4-dihydropyridine (DHP) is a complex multistep reaction involving three reagents and multiple intermediates. This reaction was previously found to be accelerated in electrospray droplets and the distance between the spray source and ion transfer capillary was found to have a significant effect on the progress of the reaction.[13] By extending the distance from 4 cm to 100 cm (approximate flight time 200 microseconds to 5 milliseconds), starting material **2** is gradually transferred to the Knoevenagel product **4** and to the Michael addition product **7** and eventually to DHP **9** and the pyridine **10** (significant dehydrogenation converting **9** to **10** occurs at high temperature). Under FD conditions, the starting materials **1** and **2,** the early stage intermediate **4** and the late stage intermediate **7** were all observed immediately, suggesting that reaction is occurring in droplets of a variety of sizes. The Michael addition product **7** was not seen in nano electrospray experiments if the distance between the source and mass inlet was not significant (ca. 0.5 m). By contrast, in the FD experiment the major peaks in the spectra did not shift when increasing the distance from 3 mm to 15 mm and the dehydration product has not been observed. As observed in the hydrazone reaction, a radical cation is generated in the FD

experiment (**1**, *m/z* 106) and its condensation product **4**, *m/z* 218, is seen as the radical cation. The ion at *m/z* 194 is the dimeric radical cation of benzaldehyde. Again, this radical cation chemistry appears to occur in FD in competition with and parallel to the more usual closed shell ion/molecule chemistry which is associated with amine protonation and which accounts for the major products including the condensation product **7**.

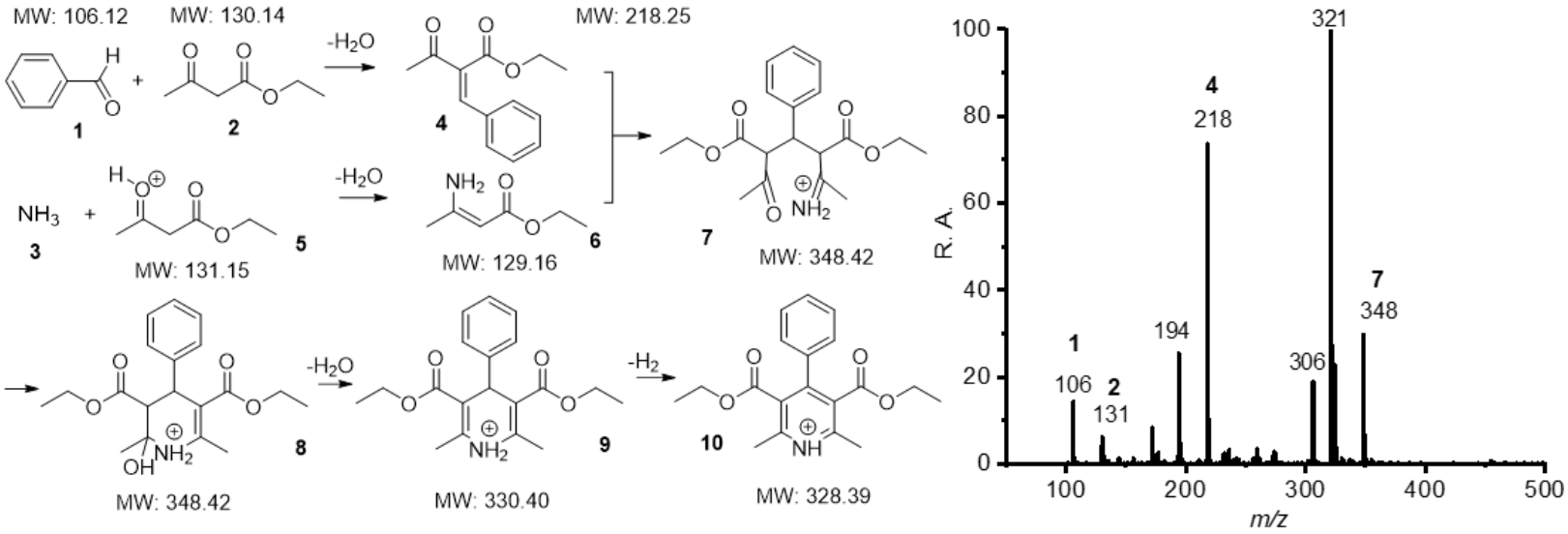

Figure 3.4 Schematic of Hantzsch reaction and mass spectrum of reaction mixture applied to a field emitter and positioned 7 mm from mass spectrometer inlet. Numbers on the spectrum correspond to intermediates in the reaction scheme. Note that **1** and **4** are radical cations.

3.4 Conclusions

Field desorption is studied, probably for the first time, under atmospheric pressure and used to study organic reactions in small volumes of solution. Three reactions: hydrazone formation, the Katritzky transamination and the Hantzsch dihydropyridine synthesis, were observed to occur and to follow the steps seen previously in electrospray and in paper spray, where even-electron reactions dominate. These parallels constitute evidence that reactions take place in solution rather than in the vapor phase. However, in parallel with the closed shell ion chemistry, radical cation reactions were also observed, notably, the formation of adducts of free radical TEMPO and phenyl hydrazine, the condensation of benzaldehyde to generate the dimeric radical cation and first step condensation in the Hantzsch, to form the radical cation. Reaction acceleration relative to the bulk experiments was evident in all three reactions as judged by the time taken for product ions to dominate the spectra; this was especially notable in the Katritzky reaction for which a thin film route is suggested. The increase of product signal in hydrazone formation is attributed to reaction in microdroplets generated by the field emitter. Those droplets could be removed by external gas flow and result in decreased product yield. The increased concentration due to evaporation of solution from the emitter surface and from the released microdroplets as well as the enhanced interfacial reaction rates are proposed to be the underlying reasons for reaction acceleration.

3.5 References

(1) Badu-Tawiah, A. K.; Campbell, D. I.; Cooks, R. G. Accelerated C-N bond formation in dropcast thin films on ambient surfaces. *J. Am. Soc. Mass Spectrom.* **2012**, *23* (9), 1461-1468.

(2) Fallah-Araghi, A.; Meguellati, K.; Baret, J. C.; El Harrak, A.; Mangeat, T.; Karplus, M.; Ladame, S.; Marques, C. M.; Griffiths, A. D. Enhanced Chemical Synthesis at Soft Interfaces: A Universal Reaction-Adsorption Mechanism in Microcompartments. *Phys. Rev. Lett.* **2014**, *112* (2).

(3) Lee, J. K.; Banerjee, S.; Nam, H. G.; Zare, R. N. Acceleration of reaction in charged microdroplets. *Q. Rev. Biophys.* **2015**, *48* (4), 437-444.

(4) Lee, J. K.; Kim, S.; Nam, H. G.; Zare, R. N. Microdroplet fusion mass spectrometry for fast reaction kinetics. *P. Natl. Acad. Sci. USA.* **2015**, *112* (13), 3898-3903.

(5) Yan, X.; Bain, R. M.; Cooks, R. G. Organic Reactions in Microdroplets: Reaction Acceleration Revealed by Mass Spectrometry. *Angew. Chem. Int. Ed.* **2016**, *55* (42), 12960-12972.

(6) Bain, R. M.; Sathyamoorthi, S.; Zare, R. N. "On-Droplet" Chemistry: The Cycloaddition of Diethyl Azodicarboxylate and Quadricyclane. *Angew. Chem. Int. Ed.* **2017**, *56* (47), 15083-15087.

(7) Jacobs, M. I.; Davies, J. F.; Lee, L.; Davis, R. D.; Houle, F.; Wilson, K. R. Exploring Chemistry in Microcompartments Using Guided Droplet Collisions in a Branched Quadrupole Trap Coupled to a Single Droplet, Paper Spray Mass Spectrometer. *Anal. Chem.* **2017**, *89* (22), 12511-12519.

(8) Houle, F. A.; Wiegel, A. A.; Wilson, K. R. Changes in Reactivity as Chemistry Becomes Confined to an Interface. The Case of Free Radical Oxidation of C30H62 Alkane by OH. *J. Phys. Chem. Lett.* **2018**, *9* (5), 1053-1057.

(9) Harris, G. A.; Galhena, A. S.; Fernández, F. M. Ambient Sampling/Ionization Mass Spectrometry: Applications and Current Trends. *Anal. Chem.* **2011**, *83* (12), 4508-4538.

(10) Muller, T.; Badu-Tawiah, A.; Cooks, R. G. Accelerated Carbon-Carbon Bond-Forming Reactions in Preparative Electrospray. *Angew. Chem. Int. Ed.* **2012**, *51* (47), 11832-11835.

(11) Bain, R. M.; Pulliam, C. J.; Thery, F.; Cooks, R. G. Accelerated Chemical Reactions and Organic Synthesis in Leidenfrost Droplets. *Angew. Chem. Int. Ed.* **2016**, *55* (35), 10478-10482.

(12) Girod, M.; Moyano, E.; Campbell, D. I.; Cooks, R. G. Accelerated bimolecular reactions in microdroplets studied by desorption electrospray ionization mass spectrometry. *Chem. Sci.* **2011**, *2* (3), 501-510.

(13) Bain, R. M.; Pulliam, C. J.; Cooks, R. G. Accelerated Hantzsch electrospray synthesis with temporal control of reaction intermediates. *Chem. Sci.* **2015**, *6* (1), 397-401.

(14) Banerjee, S.; Zare, R. N. Syntheses of Isoquinoline and Substituted Quinolines in Charged Microdroplets. *Angew. Chem. Int. Ed.* **2015**, *54* (49), 14795-14799.

(15) Yan, X.; Augusti, R.; Li, X.; Cooks, R. G. Chemical Reactivity Assessment Using Reactive Paper Spray Ionization Mass Spectrometry: The Katritzky Reaction. *ChemPlusChem* **2013**, *78* (9), 1142-1148.

(16) Bain, R. M.; Pulliam, C. J.; Raab, S. A.; Cooks, G. Chemical Synthesis Accelerated by Paper Spray: The Haloform Reaction. *J. Chem. Educ.* **2016**, *93* (2), 340-344.

(17) Li, Y. F.; Yan, X.; Cooks, R. G. The Role of the Interface in Thin Film and Droplet Accelerated Reactions Studied by Competitive Substituent Effects. *Angew. Chem. Int. Ed.* **2016**, *55* (10), 3433-3437.

(18) Beckey, H. D. *Principles of Field Ionization and Field Desorption Mass Spectrometry*; 1 ed., Pergamon, 1977.

(19) Beckey, H. Field desorption mass spectrometry: A technique for the study of thermally unstable substances of low volatility. *Int. J. Mass Spectrom. Ion Phys.* **1969**, *2* (6), 500-502.

(20) Holland, J.; Soltmann, B.; Sweeley, C. A model for ionization mechanisms in field desorption mass spectrometry. *Biomed. Mass Spectrom.* **1976**, *3* (6), 340-345.

(21) Wei, Z. W.; Wleklinski, M.; Ferreira, C.; Cooks, R. G. Reaction Acceleration in Thin Films with Continuous Product Deposition for Organic Synthesis. *Angew. Chem. Int. Ed.* **2017**, *56* (32), 9386-9390.

(22) Li, Y.; Liu, Y.; Gao, H.; Helmy, R.; Wuelfing, W. P.; Welch, C.; Cooks, R. G. Accelerated Forced Degradation of Pharmaceuticals in Levitated Microdroplet Reactors. *Chem. – A Eur. J.* **2018**, *24* (29), 7349–7353.

(23) Bain, R. M.; Pulliam, C. J.; Ayrton, S. T.; Bain, K.; Cooks, R. G. Accelerated hydrazone formation in charged microdroplets. *Rapid Commun. Mass Sp.* **2016**, *30* (16), 1875-1878.

(24) Hunter, E. P.; Lias, S. G. Evaluated gas phase basicities and proton affinities of molecules: an update. *J.Phys. Chem. Ref. Data* **1998**, *27* (3), 413-656.

(25) Cooks, R. G.; Wong, P. S. H. Kinetic Method of Making Thermochemical Determinations: Advances and Applications. *Acc. Chem. Res.* **1998**, *31* (7), 379-386.

CHAPTER 4. QUANTUM MECHANICAL MODELING OF REACTION RATE ACCELERATION IN MICRODROPLETS

Portions of this chapter have been published in the journal: Journal of Physical Chemistry A as article: "Narendra, N.; **Chen, X.**; Wang, J.; Charles, J.; Cooks, R. G.; Kubis, T. Quantum Mechanical Modeling of Reaction Rate Acceleration in Microdroplets. *J. Phys. Chem. A* **2020**, 124 (24), 4984–4989."

4.1 Introduction

Recent studies show that for a number of organic reactions, the rate in the bulk solution phase is often much smaller than that in microdroplets.[1,2] This phenomenon, known as reaction rate acceleration, is associated with increased reaction rates near the surface, evidenced by the fact that acceleration increases strongly in smaller droplets with larger surface/volume ratios.[3,4] Droplets of interest have usually been formed by spray-based mass spectrometry (MS) ionization methods such as electrospray ionization (ESI), [5,6] desorption electrospray ionization (DESI),[7] paper spray (PS)[8] and field desorption (FD)[9]. Alternatively, droplets have been generated by thermal[4,10] or electromagnetic levitation.[11,12] The typical diameters of the droplets generated by nESI are in the hundreds of nanometers range.[13] Rate acceleration has also been reported in other confined volume systems, such as thin films (2D variants of microdroplets)[10] as well as at interfaces between two phases.[14] The large magnitude of the rate accelerations reported for microdroplets (orders of magnitude in microdroplets) has aroused interest since they offer potential for the development of high-throughput methods of selecting optimum reaction conditions and synthesizing compounds on a small scale.[15]

The underlying reason of the large rate acceleration in microdroplets is being explored through a variety of experiments.[1,2,3] These show clearly that confined volume systems differ from their bulk counterpart in reaction rates which parallel the dramatically increased surface area/volume ratios. This implies that interfacial reactions play a key role in reaction acceleration. In particular circumstances, contributions to rate acceleration can be made by increased reagent concentration associated with solvent evaporation.[7,8] Most interesting are the intrinsic effects that increase rate constants. Among those suggested are the reduced collision times of reagents in small compartments,[16] the high electric field at the interface in the case of aqueous microdroplets,[17] and

the decreased solvation energy of reagent molecules at the droplet (or thin film) interface.[1] This computational study explores the possibility that solvation energy differences at the interface and in the bulk are responsible for the increase in intrinsic rate constants. Unlike the situation in bulk solvents, where reagents must overcome large solvation barriers to form the activated complex, reagents near the interface may be less solvated and so have a lower activation energy.[1,16,18,19] (Note that transition states are less affected by solvation than reagents as they have a measure of internal solvation, represented by charge dispersal.)

To explore the mechanism of reaction acceleration in droplets computationally, one needs a method that explicitly considers solvent molecules when calculating the energies and structures of the reagents and the transition state. Density functional tight binding (DFTB) methods are used to provide the energies of solution phase reagents and intermediates in the bulk and at various distances from the interface. Note that the computation does not consider entropic factors affecting reaction rate constants, just energies without any computation of reaction dynamics which would not be computationally possible at the scale used here.

The particular chemical reaction chosen for modeling is hydrazone formation by reaction of phenyl hydrazine and indoline-2-3-dione in HCl/methanol. This reaction has been reported to be accelerated by a factor of 10^4 when the initially generated nESI droplets are allowed to undergo extensive evaporation.[20] The degree to which the rate constant is increased by this concentration effect is not known. In this study we use ab initio computations to estimate the activation energy at the surface and in the bulk to elucidate the cause of the rate acceleration in microdroplets.

4.2 Results and discussion

4.2.1 Reaction pathway

Acid-catalyzed hydrazone formation from phenylhydrazine and indoline-2,3-dione in microdroplets was selected to investigate the activation energy difference between reactions at the interface and in the bulk. The proposed reaction pathway, shown in Figure 4.1, is taken to be that of the gas phase reaction of hydrazine itself with simple carbonyl compounds as studied by flowing afterglow.[21] This is a complex process with many states potentially involved and a mechanism

like that in Figure 4.1 has been proposed for the aqueous phase reaction[22]. The first transition state, TSA, corresponds to formation of a C−N bond through nucleophilic attack by the phenyl hydrazine while the second, TSB, corresponds to loss of water; these states are exactly analogous to those suggested by Bierbaum and coworkers.[21] Calculations show that formation of TSB has the highest energy barrier along the potential energy surface in the gas phase reaction pathway and is thus the rate limiting step. The energy difference between the reactants and TSB is used to estimate the activation energy in the following discussion. Alternative pathways are possible but are not explored in this paper because of the large computational effort involved and the fact that the key features of solvation-mediated energies are likely to occur in any related mechanism.

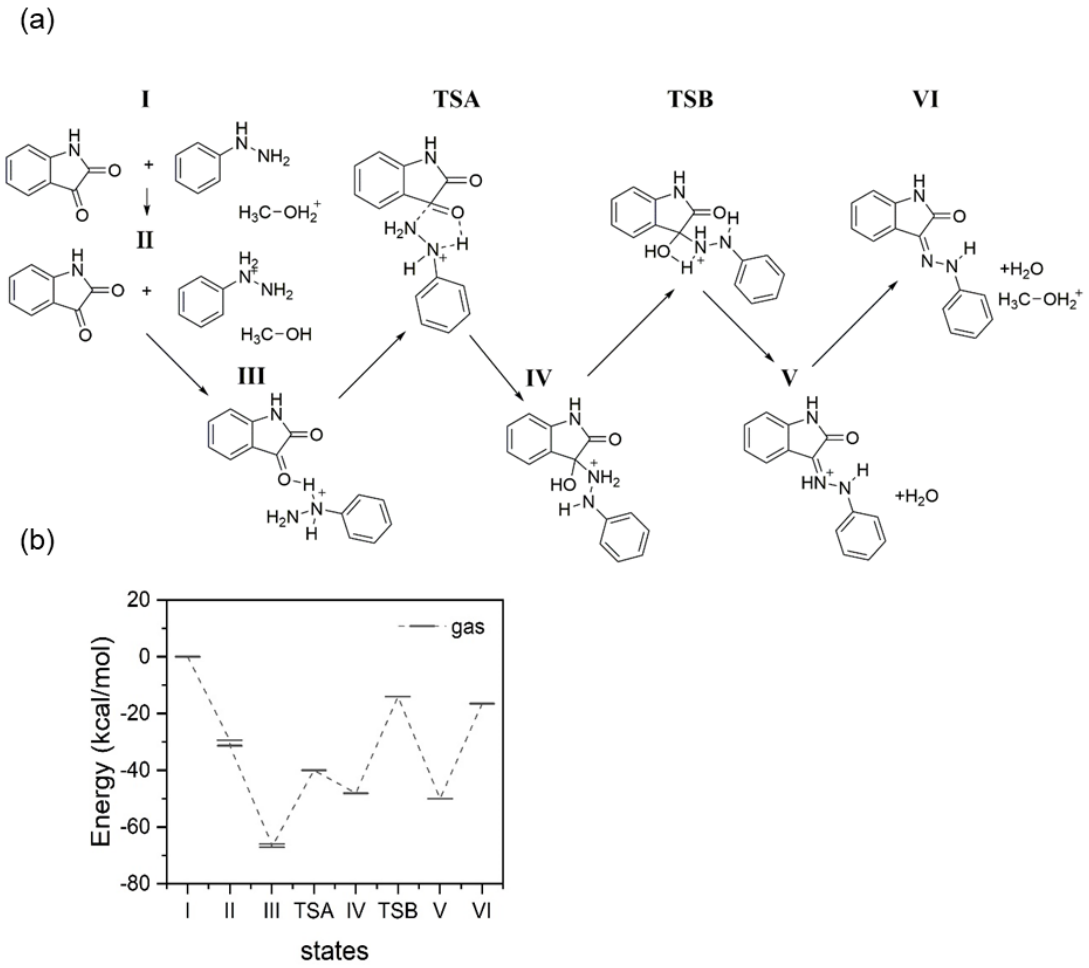

Figure 4.1 (a) Reaction pathway adapted from ref. 21. (b) Energies of all the states along the reaction coordinate for hydrazone formation calculated (this work) using B3LYP density functional theory and 6-31 G(d,p) basis sets. Note the two conformations of structures II and III.

4.2.2 Energetics at the interface

We hypothesize that solvation plays an important role in decreasing the activation energy and that this effect is smaller at the interface than in the bulk. To investigate this, we prepared by methods described in the Methodology section, a set of random configurations of the target molecules in methanol where the distance of the target molecule from the interface is systematically varied. The effect of solvation on the energy of the reagents (indoline-2,3-dione and protonated phenylhydrazine) and the rate limiting intermediate, TSB, was examined by performed 100 simulations of each of these target molecules. This solvent explicit energy calculation was performed using SCC-DFTB at various distance from the methanol/vacuum interface. The results are plotted in Figure 4.2 as the energy difference between the bulk and interface as a function of distance from the interface.

It can be seen that both protonated phenylhydrazine and TSB exhibit a large spread in energy for individual randomly selected orientations at and near the interface. The energy of protonated phenylhydrazine and TSB molecules at the interface can increase by as much as 1.53 eV and 1.65 eV, respectively, relative to bulk; this can be explained by the degree of solvent stabilization of the positive charge site of the molecule. This interfacial effect vanishes some 4 Å from the interface.

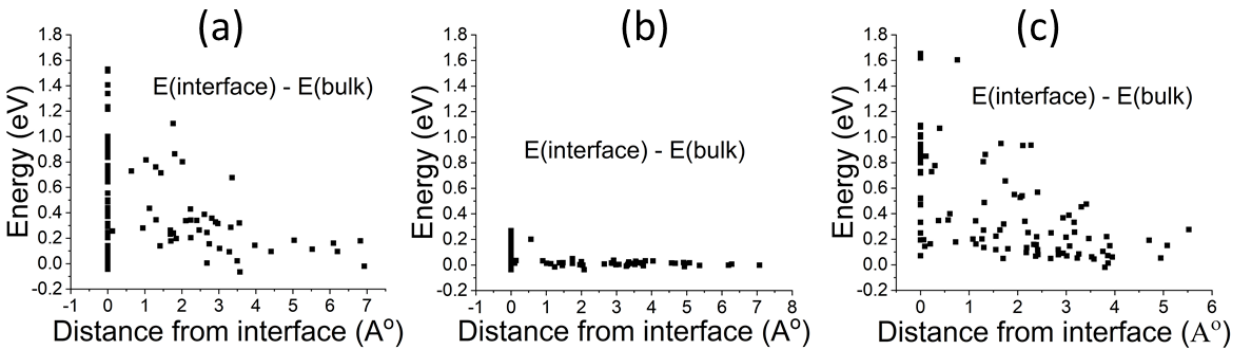

Figure 4.2 Difference in energy between interface and bulk plotted as a function of distance from the interface for target molecules in methanol. One hundred configurations were randomly chosen with the target molecule at the distances shown for (a) Protonated phenylhydrazine (b) Indoline-2,3-dione and (c) TSB. On the other hand, the energy difference for the uncharged indoline-2,3-dione molecule is much smaller and it vanishes above 1 Å.

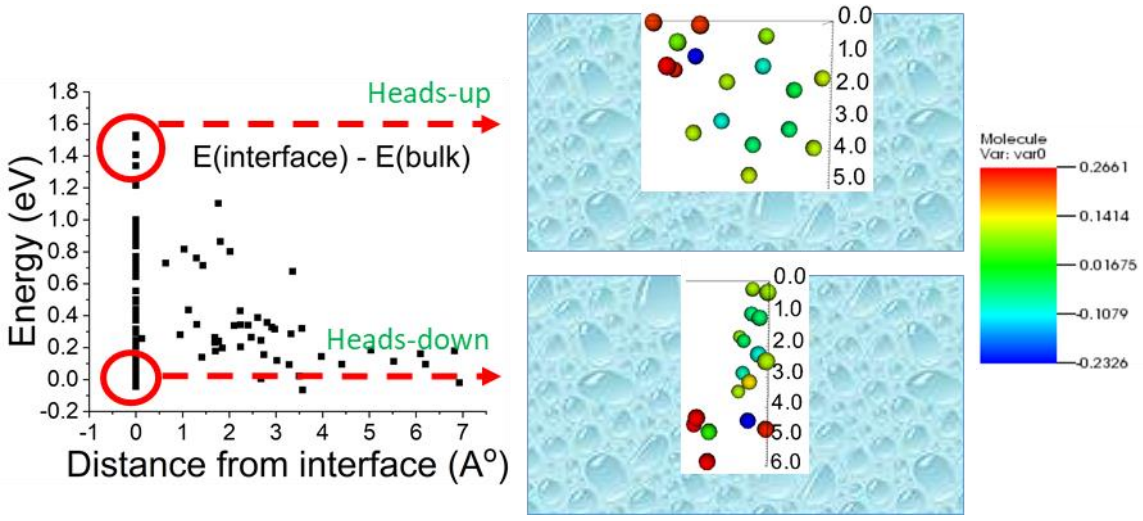

Figure 4.3 (Left) Charge distribution analysis for protonated phenylhydrazine at the interface revealing two categories: heads-up and heads-down. A selected pair of structures is visualized. The z-coordinates are indicated next to the molecular structure in units of Å. The color scale at right represents the charge of the atoms in units of the electron charge. Red indicates high positive charge while blue indicates high negative charge. The three hydrogens on the terminal N carry most positive and the adjacent N the most negative charge.

4.2.3 Molecular orientation at the interface

To gain a better understanding of the large distribution of energies at the interface, the molecular orientation and charge distribution of representative protonated phenylhydrazine molecules with different energies are visualized in Figure 4.3. (The tendency for ions to be located near the interface of droplets is an established assumption in studies of accelerated reactions in microdroplets.[23]) The most energetic molecules at the interface are found to correspond to 'heads-up' configurations, namely those with the positive charge center at or near the interface. Heads-up configurations of the reactants are least solvated by methanol and thus represent the most reactive configurations. Therefore, we hypothesize that the greatly enhanced reaction rate in microdroplets is attributed reaction sequences that start from 'heads-up' configurations. By contrast, the least energetic molecules correspond to 'heads-down' configurations whose positive charge centers are far from the surface. These 'heads-down' configurations, with their charge centers solvated by methanol, resemble bulk-phase target molecules and are of less interest. Similar observations were made for the charged TSB molecules. There is a wide energy distribution among molecules due to different orientations of positive charge center, with the 'heads-up' configurations as the most energetic form and 'heads-down' configurations the less energetic forms. If the formation of TSB

from the heads-up reactants is accompanied by rotation the forming reaction complex energy will be released to form the most stable configuration, i.e., the heads-down configuration. So, we further conclude that heads-up reagent ions correlating with heads-down TSB represents the energetically most favorable pathway.

To systematically classify target molecule configurations as heads-up or heads-down, the angle of the dipole moment of the target molecule with respect to the plane of the interface is considered, as shown in Figure 4.4. Both charged target molecules show a strong correlation of high energy/positive dipole vs. low energy/negative dipole. Configurations with zero dipole moment angle lie in the plane of the interface; configurations with positive dipole moment angle are classified as heads up-configurations while those more negative are classified as heads-down. This clearly establishes a high energy/heads up relationship for the charged target molecules while the uncharged indoline-2,3-dione show no such configurational preference.

4.2.4 Rate acceleration calculation

In order to assess the rate acceleration between interface and bulk, we need to derive reaction rates from the activation energy. Reaction rate R is proportional to reaction rate constant k , where $k \propto e^{-E_a/k_B T}$ (k_B is Boltzmann constant, T is temperature and E_a is activation energy given by $E_a = E_{Transition\ State} - \sum E_{Reactants}$.) The reaction rate acceleration at the interface is given by the ratio of rate constants $k_{interface}/k_{bulk}$ which is equal to $g[e^{-(E_{a_{interface}} - E_{a_{bulk}})/k_B T}]$ Here, g is the ratio of pre-exponential factors of the rate constants for interface and bulk.

The reaction acceleration at the interface is dominated by the least solvated and hence most reactive ‘heads-up’ configurations of protonated phenylhydrazine molecules at the interface. If we assume that there is no change in the molecule configuration along the reaction pathway from the reactant molecules to TSB, then there will be no rate acceleration at the interface. But experiments show that reaction acceleration is observed in microdroplets. From this, it follows that the change in configuration along the reaction pathway is at least an explanation of reaction acceleration at the interface. The upper limit of the rate acceleration is when there is a full change in the configuration from ‘heads-up’ protonated phenylhydrazine to ‘heads-down’ TSB.

To explore this point and gain further insight the energies of the 'heads-up' ('heads-down') configurations of protonated phenylhydrazine (TSB) lying within 0 – 1 Å of the interface were averaged. In the case of the uncharged indoline-2,3-dione, all the configurations within the 0 – 1 Å range were considered given that there is only a slight effect of orientation on energy.

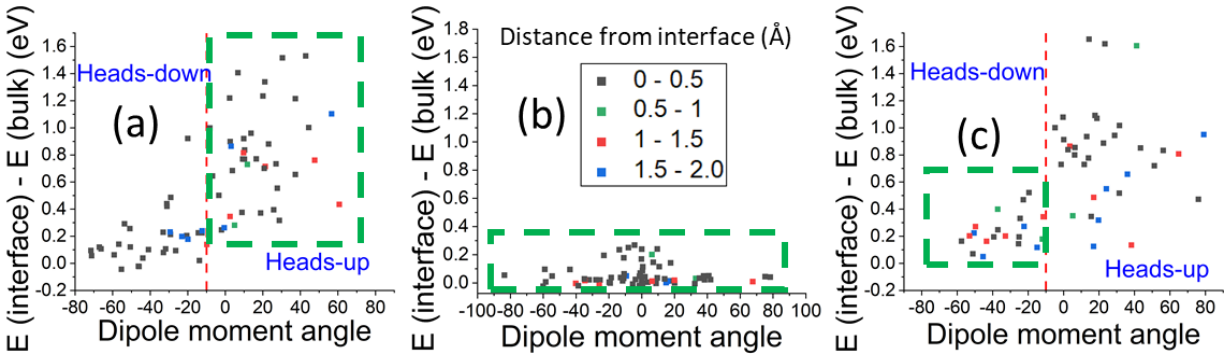

Figure 4.4 Plot of difference in energy between interface and bulk for target molecules as a function of dipole moment angle w.r.t the interface for (a) Protonated phenylhydrazine, (b) Indoline-2,3-dione, and (c) TSB. Green dashed rectangle shows the data points selected for averaging in the activation energy calculation. The color coding shows distance from interface and applies to all three parts of the figure.

By averaging over the selected configurations (within the green dashed boxes in Figure 4.4) and considering only those target molecules within 1 Å distance from the interface, the average difference in energy between interface and bulk for the target molecules is tabulated in Table 4.1. This results in 612 meV decrease in activation energy from bulk to interface. Ignoring the pre-exponential g-factor, this corresponds to an upper bound in reaction rate acceleration of 1.89 x 10^{10} at the methanol/vacuum interface at 300 K.

Table 4.1 Difference in average energies at interface and bulk for reagents involved in hydrazone formation

Target molecule	**Protonated phenylhydrazine**	**Indoline-2,3-dione**	**TSB**
E(interface) – E(bulk) eV	0.821 eV	0.056 eV	0.265 eV

4.2.5 Discussion on methodology

Some aspects of the methodology should now be discussed and will be examined in more detail in the future. They include

(i) The use of solvent correlation between bulk and interfacial target molecules. This was necessary to constraint the computational time required to cover all the possible structural phase space to a practicable limit (even so the total computation time for the results shown in this study was approximately 60,000 core hours). Solvent correlation helps minimize the noise arising from the difference in the solvent molecule orientations surrounding the target molecule between bulk and interface. The process helps to isolate the impact of the interface on the target molecule energy from other factors.

(ii) The effect of relaxation of the solvent at the interface was not considered. Preliminary calculations show that such interface relaxation reduces the average difference in energy between interface and bulk by nearly half compared to unrelaxed interface. Since solvent configuration around the target molecules will change after interface relaxation, it is no longer accurate to compare the interface and bulk target molecule energies on a one-to-one basis. The qualitative analysis described above still holds after interface relaxation.

(iii) From equilibrium statistics, the likelihood of 'heads-up' protonated phenylhydrazine to occur is very low (~10^{-6}). This probability is obtained by the density matrix approach. The statistical weight of each sample is given by $\frac{e^{-E_n/k_BT}}{Z}$ where Z is the partition function $\sum_n e^{-E_n/k_BT}$. If one corrects for this probability, the upper bound of the rate acceleration is 10^4. The bulk rate constant is not known accurately for methanol but a similar case[24] reports a value of ca. 10 M^{-1} s^{-1} which, when

considered with the Bain et al. acceleration factor of 10^4 , gives an approximate interfacial value of 10^5 M^{-1} s^{-1} or, converting units, 2×10^{-16} cm^3 $molecules^{-1}$ s^{-1} . The gas phase reaction rate is ~10^{-9} cm^3 $molecules^{-1}$ s^{-1} which is still orders of magnitude faster than the accelerated interfacial reaction. We note also that rate of acceleration at the microdroplet surface due to 'heads-down' protonated phenylhydrazine is negligible. This leads us to wonder whether the dynamics of evaporation can increase the non-equilibrium probability of occurrence of 'heads-up' configurations. Molecular dynamics would be needed to capture all features of the reaction trajectory and the entropy information which is beyond the scope of the current paper. We note that prior validation tests used only static SCC-DFTB with geometry relaxation and thermodynamic integration methods to calculate the solvation energy of a single molecule in an explicit liquid[25]. Since our results were comparable with literature, this increases confidence in the applicability of static SCC-DFTB to the current application.

4.3 Methodology

Gas phase reaction pathway in calculated with Gaussian[25] using B3LYP density functional theory[26] and 6-31 G(d, p) basis sets. We randomly created 100 different configurations of reagents and transition state near the surface of large number of solvent molecules by slicing solvent box created by PACKMOL.[27] Energetics of target molecules (reactants and transition states) at interface relative to bulk were performed by Self-Consistent Density Functional Tight Binding (SCC-DFTB) quantum mechanical calculations with explicit solvent simulation.

4.4 Conclusions

Explicit solvent calculation of energies shows that protonated phenylhydrazine, when oriented with the charge site at or near the surface, is a partly solvated high energy species. Reagent ions with the opposite orientation have energies that approach values of the bulk species. It is proposed that a l reaction pathway that would result in strong acceleration involves the re-orientation of a 'heads-up' phenylhydrazine to a 'heads-down' TSB. Estimated upper bound value for the rate acceleration for hydrazone formation in microdroplets is about 10^{10} but this factor is offset by the

low statistical probability (ca. 1 in 10^6) of the heads-up configuration. The net result is consistent with the modest rate acceleration factor (one to a few orders of magnitude) seen in the experiment[20]. Some aspects of the methodology should be examined in more detail in the future. They include the use of solvent correlation between bulk and interfacial target molecules and the degree of solvent relaxation allowed. The main problem encountered in this study is that the questions raised can only be answered by a full treatment of reaction dynamics. Because nothing approaching this is possible, we have chosen to explore an extreme reaction trajectory (heads up reagent at interface to heads down transition state, with no other relaxation) and to evaluate its consequences. The results are encouraging in terms of the support they offer for the feasibility of the partial solvation hypothesis which, on the other hand, they do not prove.

4.5 References

(1) Yan, X.; Bain, R. M.; Cooks, R. G. Organic Reactions in Microdroplets: Reaction Acceleration Revealed by Mass Spectrometry. *Angew. Chemie Int. Ed.* **2016**, *55* (42), 12960–12972.

(2) Banerjee, S.; Gnanamani, E.; Yan, X.; Zare, R. N. Can All Bulk-Phase Reactions Be Accelerated in Microdroplets? *Analyst* **2017**, *142* (9), 1399–1402.

(3) Zhou, Z.; Yan, X.; Lai, Y.-H.; Zare, R. N. Fluorescence Polarization Anisotropy in Microdroplets. *J. Phys. Chem. Lett.* **2018**, *9* (11), 2928–2932.

(4) Bain, R. M.; Pulliam, C. J.; Thery, F.; Cooks, R. G. Accelerated Chemical Reactions and Organic Synthesis in Leidenfrost Droplets. *Angew. Chemie Int. Ed.* **2016**, *55* (35), 10478–10482.

(5) Müller, T.; Badu-Tawiah, A.; Cooks, R. G. Accelerated Carbon□Carbon Bond-Forming Reactions in Preparative Electrospray. *Angew. Chemie Int. Ed.* **2012**, *51* (47), 11832–11835.

(6) Banerjee, S.; Zare, R. N. Syntheses of Isoquinoline and Substituted Quinolines in Charged Microdroplets. *Angew. Chemie Int. Ed.* **2015**, *54* (49), 14795–14799.

(7) Girod, M.; Moyano, E.; Campbell, D. I.; Cooks, R. G. Accelerated Bimolecular Reactions in Microdroplets Studied by Desorption Electrospray Ionization Mass Spectrometry. *Chem. Sci.* **2011**, *2* (3), 501–510.

(8) Yan, X.; Augusti, R.; Li, X.; Cooks, R. G. Chemical Reactivity Assessment Using Reactive Paper Spray Ionization Mass Spectrometry: The Katritzky Reaction. *Chempluschem* **2013**, *78* (9), 1142–1148.

(9) Chen, X.; Cooks, R. G. Accelerated Reactions in Field Desorption Mass Spectrometry. *J. Mass Spectrom.* **2018**, *53* (10), 942–946.

(10) Wei, Z.; Wleklinski, M.; Ferreira, C.; Cooks, R. G. Reaction Acceleration in Thin Films with Continuous Product Deposition for Organic Synthesis. *Angew. Chemie Int. Ed.* **2017**, *56* (32), 9386–9390.

(11) Jacobs, M. I.; Davies, J. F.; Lee, L.; Davis, R. D.; Houle, F.; Wilson, K. R. Exploring Chemistry in Microcompartments Using Guided Droplet Collisions in a Branched Quadrupole Trap Coupled to a Single Droplet, Paper Spray Mass Spectrometer. *Anal. Chem.* **2017**, *89* (22), 12511–12519.

(12) Grimm, R. L.; Beauchamp, J. L. Field-Induced Droplet Ionization Mass Spectrometry. *J. Phys. Chem. B* **2003**, *107* (51), 14161–14163.

(13) Xia, Z.; Williams, E. R. Effect of Droplet Lifetime on Where Ions Are Formed in Electrospray Ionization. *Analyst* **2019**, *144* (1), 237–248.

(14) Yan, X.; Cheng, H.; Zare, R. N. Two-Phase Reactions in Microdroplets without the Use of Phase-Transfer Catalysts. *Angew. Chemie Int. Ed.* **2017**, *56* (13), 3562–3565.

(15) Wleklinski, M.; Loren, B. P.; Ferreira, C. R.; Jaman, Z.; Avramova, L.; Sobreira, T. J. P.; Thompson, D. H.; Cooks, R. G. High Throughput Reaction Screening Using Desorption Electrospray Ionization Mass Spectrometry. *Chem. Sci.* **2018**, *9* (6), 1647–1653.

(16) Mondal, S.; Acharya, S.; Biswas, R.; Bagchi, B.; Zare, R. N. Enhancement of Reaction Rate in Small-Sized Droplets: A Combined Analytical and Simulation Study. *J. Chem. Phys.* **2018**, *148* (24), 244704.

(17) Kathmann, S. M.; Kuo, I.-F. W.; Mundy, C. J. Electronic Effects on the Surface Potential at the Vapor−Liquid Interface of Water. *J. Am. Chem. Soc.* **2009**, *131* (47), 17522–17522.

(18) Mortensen, D. N.; Williams, E. R. Ultrafast (1 Ms) Mixing and Fast Protein Folding in Nanodrops Monitored by Mass Spectrometry. *J. Am. Chem. Soc.* **2016**, *138* (10), 3453–3460.

(19) Hagberg, D.; Brdarski, S.; Karlström, G. On the Solvation of Ions in Small Water Droplets. *J. Phys. Chem. B* **2005**, *109* (9), 4111–4117.

(20) Bain, R. M.; Pulliam, C. J.; Ayrton, S. T.; Bain, K.; Cooks, R. G. Accelerated Hydrazone Formation in Charged Microdroplets. *Rapid Commun. Mass Spectrom.* **2016**, *30* (16), 1875–1878.

(21) Custer, T. G.; Kato, S.; Bierbaum, V. M.; Howard, C. J.; Morrison, G. C. Gas-Phase Kinetics and Mechanism of the Reactions of Protonated Hydrazine with Carbonyl Compounds. Gas-Phase Hydrazone Formation: Kinetics and Mechanism. *J. Am. Chem. Soc.* **2004**, *126* (9), 2744–2754.

(22) Sollenberger, P. Y.; Martin, R. B. The Chemistry of the Amino Group. *by S. Patai, Intersci. Publ. London* **1968**, *1*, 349–407.

(23) Wei, Z.; Li, Y.; Cooks, R. G.; Yan, X. Accelerated Reaction Kinetics in Microdroplets: Overview and Recent Developments. *Annu. Rev. Phys. Chem.* **2020**, *71* (1), 31–51.

(24) Kool, E. T.; Park, D.-H.; Crisalli, P. Fast Hydrazone Reactants: Electronic and Acid/Base Effects Strongly Influence Rate at Biological PH. *J. Am. Chem. Soc.* **2013**, *135* (47), 17663–17666.

(25) Frisch, M. J., Trucks, G. W., Schlegel, H. B., Scuseria, G. E., Robb, M. A., Cheeseman, J. R., Scalmani, G., Barone, V., Petersson, G. A. Gaussian 16, Rev. A.03. *Gaussian, Inc., Wallingford, CT* **2016**.

(26) Stephens, P. J.; Devlin, F. J.; Chabalowski, C. F.; Frisch, M. J. Ab Initio Calculation of Vibrational Absorption and Circular Dichroism Spectra Using Density Functional Force Fields. *J. Phys. Chem.* **1994**, *98* (45), 11623–11627.

(27) Allouche, A. Software News and Updates Gabedit — A Graphical User Interface for Computational Chemistry Softwares. *J. Comput. Chem.* **2012**, *32*, 174–182.

CHAPTER 5. GAS PHASE ION CHEMISTRY TO DETERMINE ISOASPARTATE IN A PEPTIDE BACKBONE

Portions of this chapter have been published in the journal: Journal of the American Society for Mass Spectrometry as article "Ayrton, S. T.; **Chen, X.**; Bain, R. M.; Pulliam, C. J.; Achmatowicz, M.; Flick, T. G.; Ren, D.; Cooks, R. G. Gas Phase Ion Chemistry to Determine Isoaspartate in a Peptide Backbone. *J. Am. Soc. Mass Spectrom.* **2018**, 29 (7), 1339–1344."

5.1 Introduction

Isoaspartate (isoAsp) can be generated non-enzymatically by isomerization of aspartate (Asp) or by deamidation of asparagine (Asn) via a succinimide intermediate, so affecting the structures and functions of proteins.[1] Protein L-isoaspartyl methyltransferase (PIMT) is an enzyme produced in vivo to convert isoAsp to Asp.[2] This post-translational modification is also a common degradation reaction. during the production and storage of proteins, which will affect protein drug activity and safety.[3]

Mass spectrometry methods in conjunction with liquid chromatography are often used in determination of this peptide isomerization.[2] Electron transfer dissociation (ETD) and electron capture dissociation (ECD) produce specific fragment ions for isoAsp, which facilitate discrimination of the two isobaric ions.[4,5] Apart from that, enzymatic reactions specific to isoAsp have also been used in separate peptide isomers prior to detection with bioluminescence or MS.[3,6]

5.2 Experimental

Chemicals were purchased from Sigma Aldrich (St. Louis, MO). Ethanol was purchased from Makron Fine Chemicals LTD (Center Valley, PA). The peptide samples were purchased from Anaspec Inc. (Fremont, CA). All reagents and solvents were used directly as received without further purification. The 10 mM stock solution of carbodiimide and 1 mM peptide solution was prepared in 1:1 EtOH: H_2O. Upon analysis, standard solutions containing 500 µM peptide and 1 mM carbodiimide were prepared and 10 µL solution was loaded into a nano electrospray emitter prepare by a micropipette tip puller.

Analysis was performed with a linear ion trap (LTQ, Thermo Scientific, San Jose CA) or an Orbitrap (LTQ-Orbitrap XL, Thermo Scientific, San Jose, CA) The instrumental parameters are capillary voltage 15 V, tube lens 65 V, capillary temperature 150 °C, maximum ion injection time 10 ms, isolation width 5 units, collision energy 25 (manufacturer's arbitrary unit).

5.3 Results and Discussion

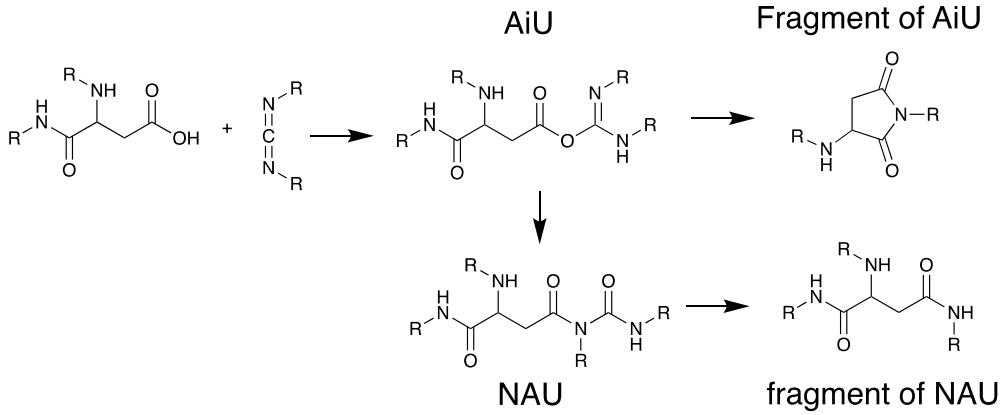

Scheme 5.1 Production of AiU (isourea) from a carboxylate residue and a carbodiimide, the rearrangement of AiU to NAU (an N-acylurea) and the fragment ions yielded by each species

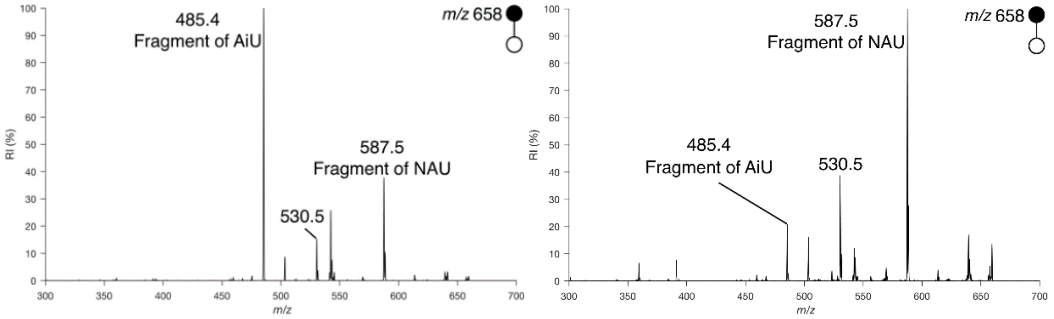

Figure 5.1 Product ion MS/MS spectra due to CID of the protonated peptides (left) Ala-Leu-isoAsp-Gly-Lys (ALDisoGK) and (right) Ala-Leu-Asp-Gly-Lys (ALDGK) giving characteristic ratios of fragment ions (*m/z* 485 & 587)

Carbodiimides are typical carboxylic acid coupling reagents. As illustrated in Scheme 5.1, the binding of carbodiimide to carboxylate residue yields an acylisourea (AiU). AiU can rearrange by 1,3-acyl shift to produce an N-acylurea (NAU). When analyzed by tandem mass spectrometry

(MS/MS), the major fragmentation pathways of these two isobaric ions are quite different: protonated NAU fragments via neutral loss of isocyanate while protonated AiU fragments via loss of urea.

Figure 5.1 shows the MS/MS spectra of the binding product of ALDGK and ALDisoGK (D stands for aspartate, Asp and Diso for isoAspartate, isoAsp) binding with EDC. In ALDGK, the AiU fragment at *m/z* 485 dominates while in ALDisoGK, the NAU fragment at *m/z* 587 dominates. This significant difference in relative abundance of the two fragments thus can be utilized to distinguish the aspartate and isoaspartate residues in peptides. With this method, we generated a semi quantitative calibration curve for the isoAsp ratio in the peptide (Figure 5.2). We attribute the difference in extent of rearrangement (AiU to NAU) for Asp and isoAsp to a steric effect, which is depicted in Scheme 5.2. Peptides with isoAsp residues are more sterically hindered in the rearrangement to NAU. We tested this concept using a group of small peptides bearing Asp and isoAsp residues and the results generally follow the trend (Table 5.1).

We also observed that the extent of rearrangement from AiU to NAU could be affected by gas-phase processes before the collision induced dissociation (CID). The ratio of the AiU and NAU fragments decreased when shorter injection time (residence time) and narrower isolation widths were applied to CID (Figure 5.3). This suggests the rearrangement process occurs in the time scale of the mass spectrometry experiment and is affected by the energy change during ion isolation process.

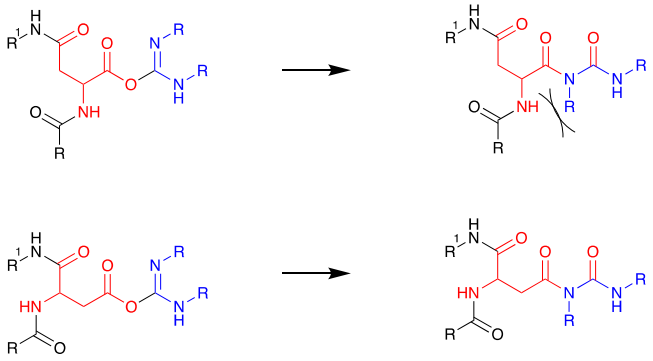

Scheme 5.2 Steric considerations in the rearrangement of AiU to NAU with Asp/isoAsp

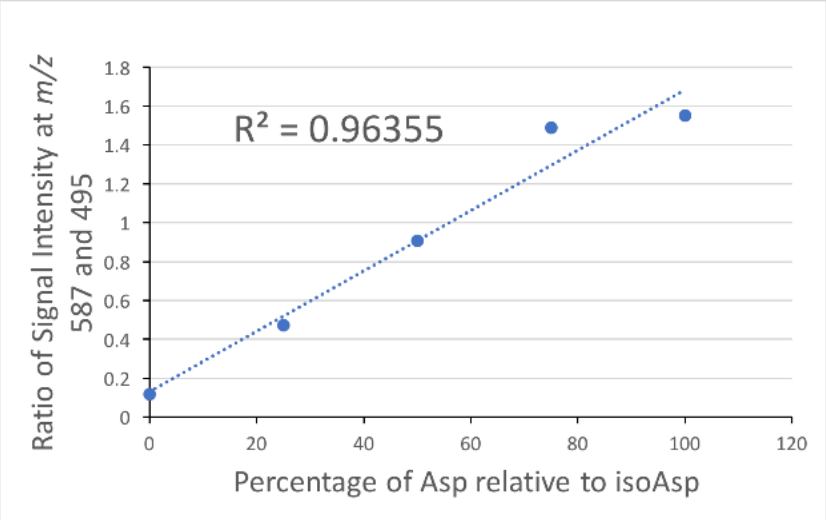

Figure 5.2 semi-quantitative calibration of isoAsp as a percentage of Asp in ALD(iso)GK

Table 5.1 Ratios of characteristic fragment ions for several peptide-diimide ions

Peptide	EDC	DCC	DIC
DL	0:1	-	-
DisoL	1:0	-	-
LDA	1:100	1:5	1:0.2
LDisoA	1:5.88	1:0.1	1:0.01
ALDGK	1:5	1:0.22	1:3.7
ALDisoGK	1:0.5	1:0.03	1:0.43
ALDEK	1:4.0	1:4.9	1:25.5
ALDisoEK	1:2.2	1:1	1:20
ADLGK	1:6.6	1:4.0	1:19
ADisoLGK	1:1.7	1:0.28	1:1
ALDGE	1:4.9	1:1.41	1:0.29
ALDisoGE	1:0.78	1:1.17	1:0.04
GLDLLK	1:2.3	1:19	1:30
GLDisoLLLK	1:0.39	1:3.3	1:4
GDLLLK	1:1.1	1:0.4	1:0.13
GDisoLLLK	1:0.2	1:0.3	1:2.1

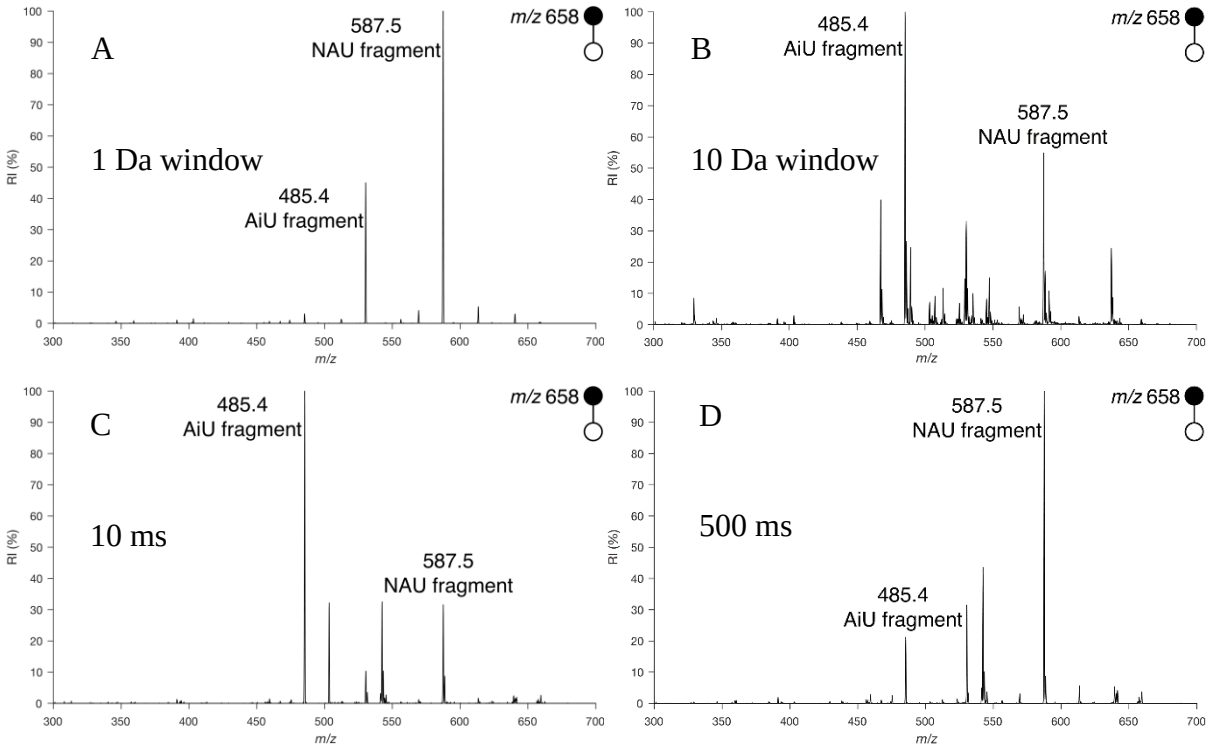

Figure 5.3 Product ion CID mass spectra of ALDisoGK-EDC using; A) narrow isolation width; B) wide isolation width; C) short injection time; D) long injection time

5.4 Conclusions

A fast and simple method to determine isoapsparte and aspartate in peptides gas has been developed. The method is based on differential gas phase rearrangement of diimide-binding peptides bearing Asp/isoAsp residues. It could be a useful new method for study of post-translational modification to isoAsp in the drug industry

5.5 References

(1) Yokoyama, H.; Mizutani, R.; Noguchi, S.; Hayashida, N. Structural and Biochemical Basis of the Formation of Isoaspartate in the Complementarity-Determining Region of Antibody 64M-5 Fab. *Sci. Rep.* **2019**, *9* (1), 1–12.

(2) Galletti, P.; De Bonis, M. L.; Sorrentino, A.; Raimo, M.; D'Angelo, S.; Scala, I.; Andria, G.; D'Aniello, A.; Ingrosso, D.; Zappia, V. Accumulation of Altered Aspartyl Residues in Erythrocyte Proteins from Patients with Down's Syndrome. *FEBS J.* **2007**, *274* (20), 5263–5277.

(3) Hsiao, K.; Alves, J.; Patel, R.; Adams, M.; Nashine, V.; Goueli, S. A High-Throughput Bioluminescent Assay to Monitor the Deamidation of Asparagine and Isomerization of Aspartate Residues in Therapeutic Proteins and Antibodies. *J. Pharm. Sci.* **2017**, *106* (6), 1528–1537.

(4) Syka, J. E. P.; Coon, J. J.; Schroeder, M. J.; Shabanowitz, J.; Hunt, D. F. Peptide and Protein Sequence Analysis by Electron Transfer Dissociation Mass Spectrometry. *Proc. Natl. Acad. Sci. U. S. A.* **2004**, *101* (26), 9528–9533.

(5) Cournoyer, J. J. Deamidation: Differentiation of Aspartyl from Isoaspartyl Products in Peptides by Electron Capture Dissociation. *Protein Sci.* **2005**, *14* (2), 452–463.

(6) Ni, W.; Dai, S.; Karger, B. L.; Zhou, Z. S. Analysis of Isoaspartic Acid by Selective Proteolysis with Asp-N and Electron Transfer Dissociation Mass Spectrometry. *Anal. Chem.* **2010**, *82* (17), 7485–7491.

CHAPTER 6. ANALYSIS OF S-NITROSOGLUTATHIONE IN EXHALED BREATH CONDENSATE SAMPLE

6.1 Introduction

S-nitrosothiols are S-nitrosated products from thiols with the general formula R-S-N=O and are considered to be important in NO-related signal transfer in biological systems.[1] S-nitrosoglutathione (GSNO) is a derivative of glutathione(GSH), which is the most abundant low molecular weight thiol in cells.[2] GSNO is proposed to be an endogenous bronchodilator and its breakdown inhibits smooth muscle relaxation in the airway.[3,4] The study of GSNO thus offer potential therapical benefits to asthma suffers.

Various colorimetric methods have been developed to detect S-nitrosothiols, the most widely used method is based on the Saville assay which involves breaking of S-N bond followed by the Griess reaction[2]. These methods have also been used to quantified GSNO, but they cannot distinguish GSNO with other S-nitrosothiols and nitrite in the sample. Detection of GSNO can be also be achieved by UV in conjunction with HPLC and CE but with less sensitivity, viz. in the μM range.[2] Mass spectrometry based methods allow both selectivity and sensitivity, and usually without chemical labeling. Corpas et al. developed an LC-CE/MS method which allows simultaneous GSNO GSH and GSSG(glutathione disulfide) in pepper plant organs.[5] The UPLC-MS/MS has been developed for quantitative detection of GSNO in human plasma with nM range detection limits for non-endogenous GSNO.[6]

Exhaled breath condensate (EBC) contains aerosols from the airway lining fluid as well as volatiles in breath absorbed by the condensed water. This makes collection of EBC an easy and noninvasive new method of getting samples for disease analysis.[7] In this work, we seek to develop ambient mass spectrometry methods to detect the GSNO in EBC samples.

6.2 Experimental

6.2.1 Chemicals

S-nitrosoglutathione (GSNO) and exhaled breath condensate samples were gifts from Prof. Ben Gaston (Indiana University) and were use as received.

6.2.2 GNSO standard solution

To prepare 1.5 mM stock solution, 5.4 mg GSNO was dissolved in 10.7 mL acetonitrile/water (50:50, v/v, with 1% formic acid). The solution was diluted to 15 µM, 1.5 µM ,150 nM 15 nM in light-resistant Eppendorf tubes and stored in an ice water bath before analysis.

6.2.3 Exhaled breath condensate sample (EBC)

EBC samples were stored in -80°C refrigerator and thawed before use. Analysis of EBC samples was done by first mixing the EBC sample solution with solvent (acetonitrile/water ,50:50, v/v, with 1% formic acid) to make a solution (1:1) and performing nanoESI. Concentrating of the EBC was performed in two ways 1) By nitrogen gas flow.600 µL with the EBC sample placed on ice-water and dry nitrogen gas being used. The whole process took about 5 hours to get rid of all the liquid solution and then the remaining solid was redissolved in 10 µL acetonitrile/H_2O solvent .2) By using a home-built freeze-drying machine with the sample placed in a foam box with dry ice. A vacuum pump is used to remove the liquid overnight.

6.2.4 Analysis

Sample was loaded in nanoESI emitter and analysis by a Thermo LTQ instrument.

NanoESI was performed by adding external voltage of 1.5-1.8 kV. The instrument parameters are capillary voltage 40V, inlet temperature 200°C and tube lens voltage 110 V. In a relay electrospray ionization experiment, the ionization was hand triggered using a piezoelectric discharge gun (Zerostat) The instrument parameters are capillary voltage 35 V, inlet temperature 275°C and tube lens voltage 50 V. Tandem mass analysis was done with isolation width 1 Th with collision induced energy 23 – 25 arbitrary units.

6.3 Results and Discussion

6.3.1 Analysis of GSNO standard solution by nanoESI

The mass spectrum of 1.5 μM GSNO is shown in Figure 6.1. GSNO is readily protonated to form $[GSNO+H]^+$ at *m/z* 337. Since there is interference at the same mass (*m/z* 337), the existence of GSNO was confirmed by selective ion monitoring of mass transition of *m/z* 337 →*m/z* 307 →*m/z* 232 (MS^2 and MS^3). In MS^2, the most abundant fragment peak at *m/z* 307 is formed from homolytic dissociation of the nitroso group to produce $[GS+H]^{+\cdot}$ In MS^3, the fragment of *m/z* 289 is formed by further loss of water and *m/z* 232 is formed by loss of NH_2CH_2COOH. [6] At 150 nM, the *m/z* 307 fragment in MS^2 is not significant and the *m/z* 232 is detectable with signal/noise ratio of about 10 in MS^3 (Figure 6.2). Thus, we conclude that the concentration detection limit in this experiment is 150 nM.

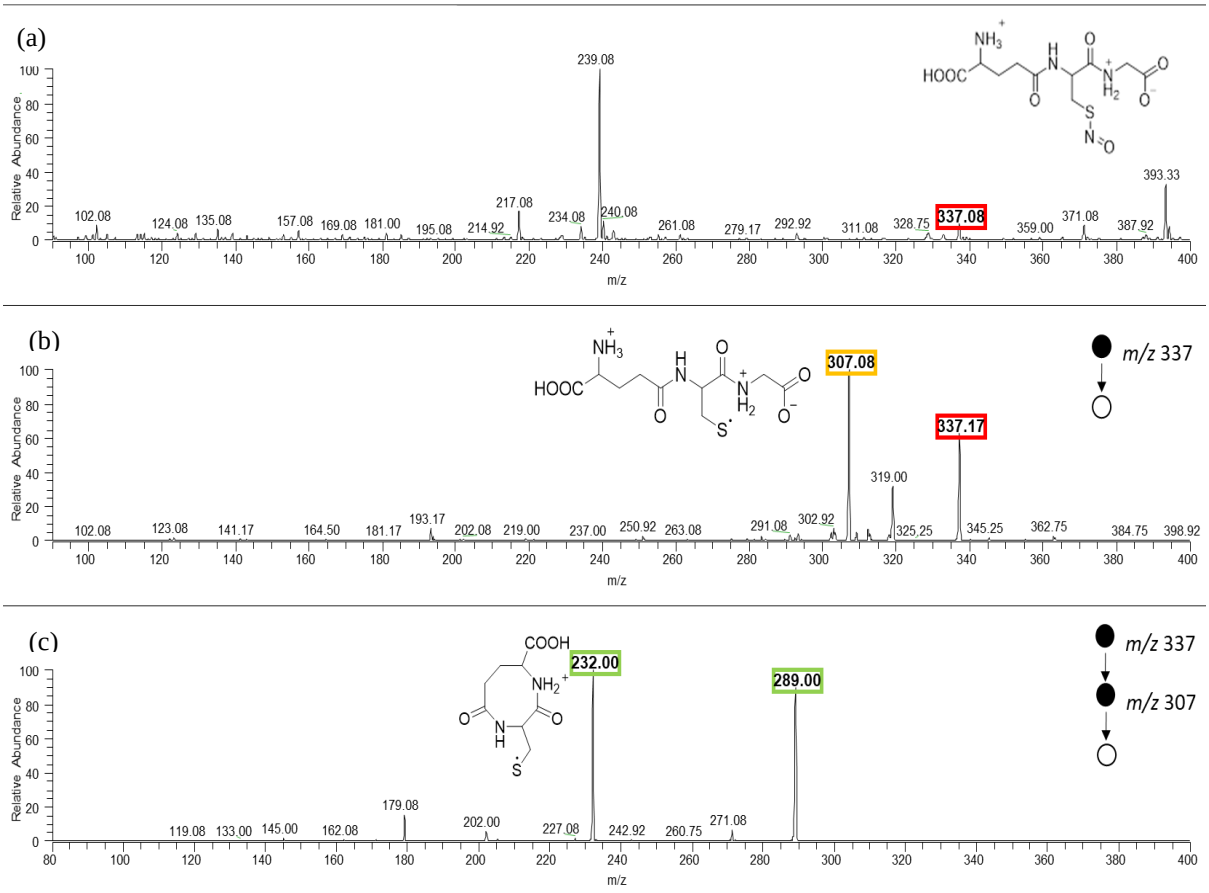

Figure 6.1 Mass spectra of 1.5 µM GSNO standard solution in positive mode (a) product ion scan (b)MS/MS showing collision induced dissociation fragmentation of *m/z* 337 (c) MS^3 showing the collision induced dissociation fragmentation of *m/z* 307

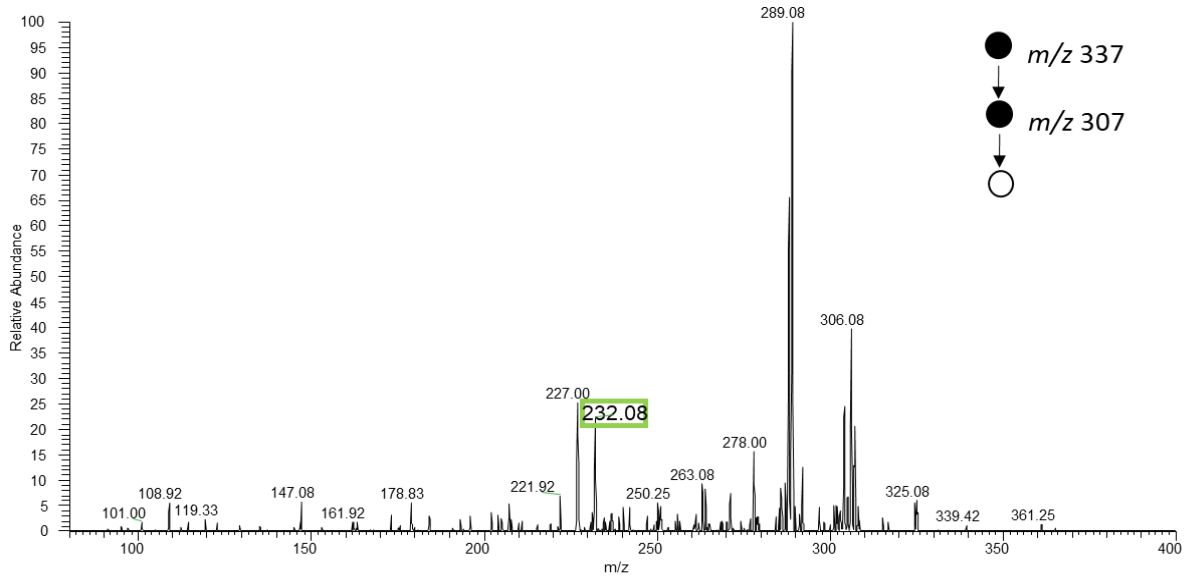

Figure 6.2 MS^3 spectrum of 150 nM GSNO standard solution.

6.3.2 Analysis of GSNO standard solution by relay spray

Relay electrospray ionization(rESI)[8] was reported to have comparable sensitivity with nanoESI but to consume significantly less sample. We challenged this method with GSNO standard solution at about 15 nM, and the characterization fragments (*m/z* 232 and *m/z* 289) were still detectable. The signal of relay spray varied a lot at low concentration with each hand-triggered spray, thus around 10 relay sprays were needed to average the spectrum.

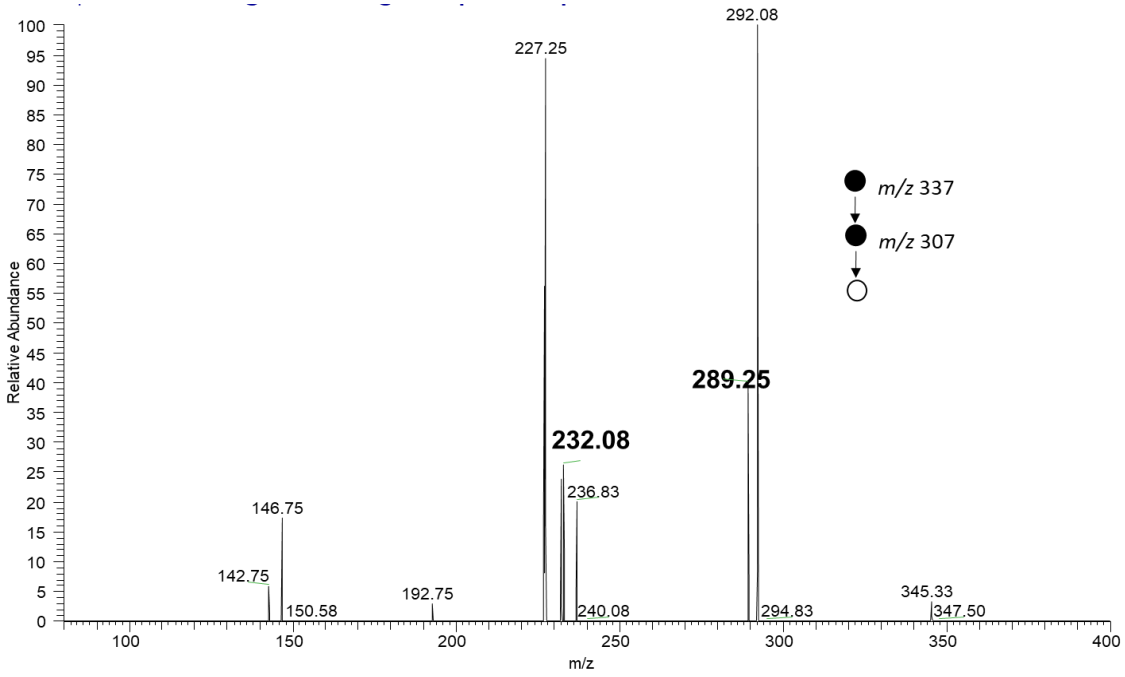

Figure 6.3 MS^3 spectrum of 15 nM GSNO standard solution with relay spray

6.3.3 Analysis of EBC sample

The analysis of real sample of EBC was first done by mixing the EBC solution with solvent(acetonitrile/water, 50:50, v/v, with 1% formic acid) to make a standard solution (1:1) and performing nanoESI. GSNO was not detected. Then we concentrated around 600 µL sample solution with nitrogen gas flow and redissolved the residue in 10 µL acetonitrile/H_2O solvent. In this 60 times concentrated sample, GSNO was still not detectable. This suggests that the concentration of GSNO in EBC sample is less than 3 nM.

We next tried to concentrate 1 mL of sample solution with a home-built freeze drier and redissolved the solid in 3 µL solvent and analyzed again with relay spray. Although both characteristic fragments were detected, the signal to noise ratio was not high enough to confirm the existence of GSNO.

It is possible that the matrix in the sample will affect the detection limit of GSNO. To test the matrix effect, 2 µL of above-mentioned solvent was used to wash the sample tube after preconcentration and the sample was then mixed with 2 µL 150 nM GSNO standard solution. The signal to noise ratio of fragment *m/z* 232 is about three. We could conclude that owing to a strong

matrix effect, the detection limit of the concentrated sample is about 150 nM. The current enrichment is still not adequate to observe a detectable amount of GSNO.

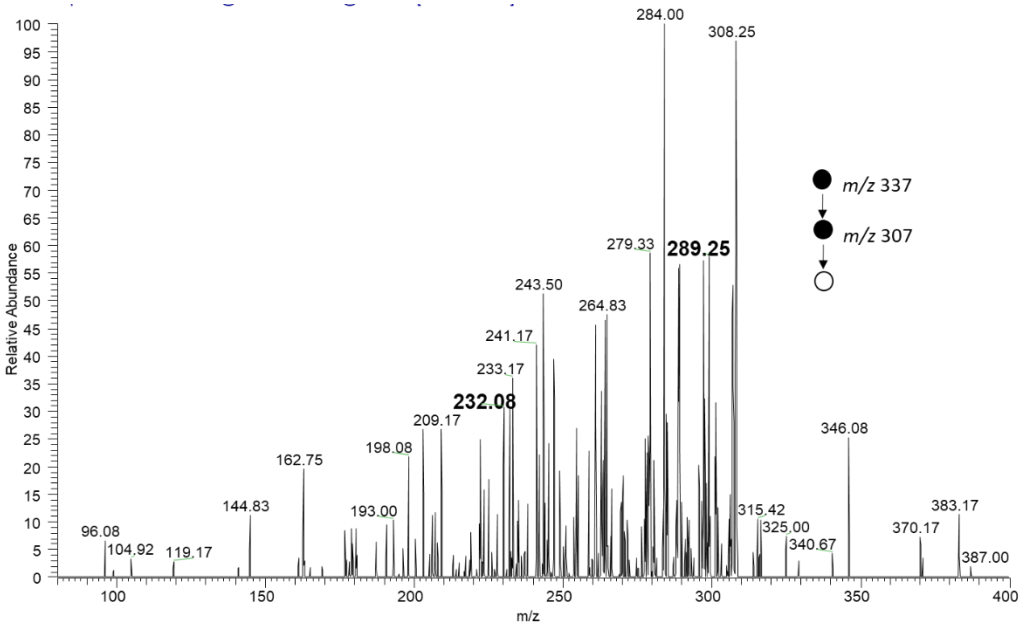

Figure 6.4 MS^3 spectrum of concentrated sample analyzed by relay spray ionization

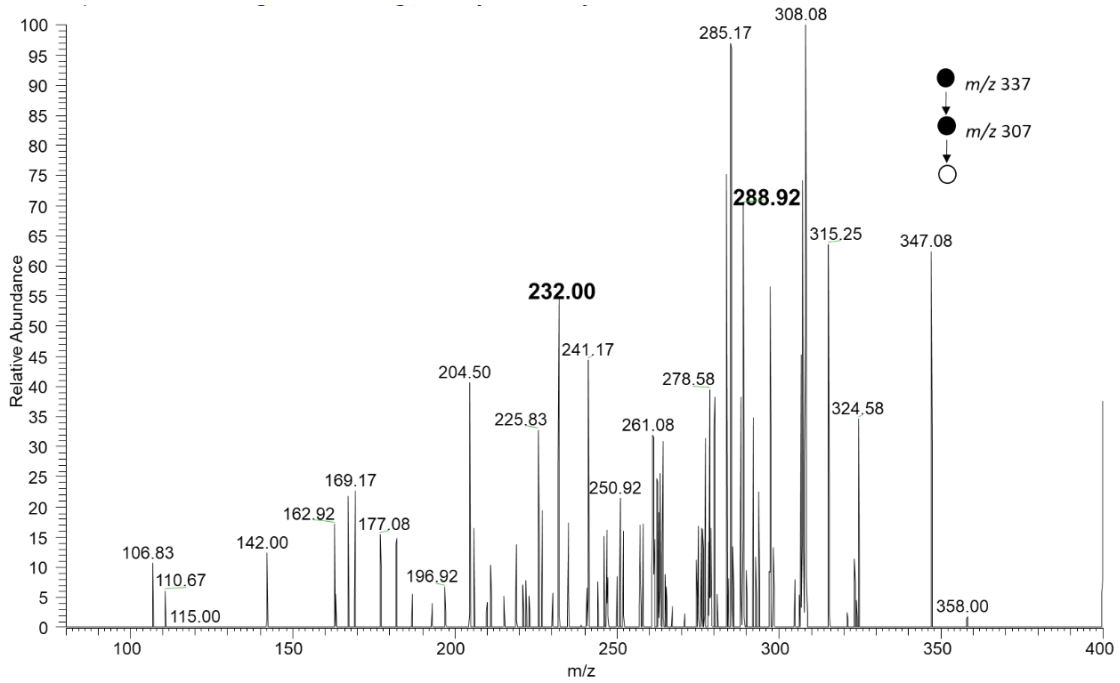

Figure 6.5 MS^3 spectrum of one-to-one mixture of 150 nM standard solution and the concentrated sample

6.4 Conclusions and Outlook

Attempts have been made to develop nanoESI and rESI based methods to detect GSNO in EBC sample. Owing to sample matrix effects, the detection limit of non-endogenous GSNO is about 150 nM in a concentrated EBC sample. A previous study reported the GSNO levels in EBC as about 5 µM, but this measurement was done with a commercial kit based on the non-selective Savilla and Griess reaction.[9] In fact, reported GSNO measurements can be orders of magnitude different: a study using UPLC-MS/MS showed the GSNO in fresh plasma to be lower than 2.8 nM, which is much lower than previously reported values in plasma. The amount of GSNO decreases even when the plasma sample is stored in -80 degree fridge.[10]

We thus suggest that analysis should be perform with freshly prepared EBC samples, and comparison can be made with the currently used frozen EBC samples. It is also worth considering combining nanoESI with capillary electrophoresis as an alternative method to increase the sensitivity of the detection.

6.5 References

(1) Zhang, Y.; Hogg, N. S-Nitrosothiols: Cellular Formation and Transport. *Free Radic. Biol. Med.* **2005**, *38* (7), 831–838.

(2) Broniowska, K. A.; Diers, A. R.; Hogg, N. S-Nitrosoglutathione. *Biochim. Biophys. Acta - Gen. Subj.* **2013**, *1830* (5), 3173–3181.

(3) Fang, K.; Johns, R.; Macdonald, T.; Kinter, M.; Gaston, B. S-Nitrosoglutathione Breakdown Prevents Airway Smooth Muscle Relaxation in the Guinea Pig. *Am. J. Physiol. - Lung Cell. Mol. Physiol.* **2000**, *279* (4 23-4), 716–721.

(4) Que, L. G.; Liu, L.; Yan, Y.; Whitehead, G. S.; Gavett, S. H.; Schwartz, D. A.; Stamler, J. S. Biomedicine: Protection from Experimental Asthma by an Endogenous Bronchodilator. *Science (80-.).* **2005**, *308* (5728), 1618–1621.

(5) Airaki, M.; Sánchez-Moreno, L.; Leterrier, M.; Barroso, J. B.; Palma, J. M.; Corpas, F. J. Detection and Quantification of S-Nitrosoglutathione (GSNO) in Pepper (Capsicum Annuum L.) Plant Organs by LC-ES/MS. *Plant Cell Physiol.* **2011**, *52* (11), 2006–2015.

(6) Tsikas, D.; Schmidt, M.; Böhmer, A.; Zoerner, A. A.; Gutzki, F. M.; Jordan, J. UPLC-MS/MS Measurement of S-Nitrosoglutathione (GSNO) in Human Plasma Solves the S-Nitrosothiol Concentration Enigma. *J. Chromatogr. B Anal. Technol. Biomed. Life Sci.* **2013**, *927*, 147–157.

(7) Hunt, J. Exhaled Breath Condensate—an Overview John. *Immunol Allergy Clin North Am* **2007**, *4* (27), 587–v.

(8) Li, A.; Hollerbach, A.; Luo, Q.; Cooks, R. G. On-Demand Ambient Ionization of Picoliter Samples Using Charge Pulses. *Angew. Chemie.Int. Ed.* **2015**, *54* (23), 6893–6895.

(9) Rundell, K. W.; Slee, J. B.; Caviston, R.; Hollenbach, A. M. Decreased Lung Function after Inhalation of Ultrafine and Fine Particulate Matter during Exercise Is Related to Decreased Total Nitrate in Exhaled Breath Condensate. *Inhal. Toxicol.* **2008**, *20* (1), 1–9.

(10) Tsikas, D.; Hanff, E. Measurement of S -Nitrosoglutathione in Plasma by Liquid Chromatography--Tandem Mass Spectrometry. In *Nitric Oxide: Methods and Protocols*; Mengel, A., Lindermayr, C., Eds.; Springer New York: New York, NY, 2018; pp 113–129.

VITA

Xingshuo was born in Beijing, the capital city in China. She developed her interest in chemistry in high school where she participated in chemistry research activity in the youth research group. In 2012, Xingshuo was admitted to Peking University, College of Yuanpei. She received a Bachler degree of science in Chemistry as well as a dual degree in International Relations and Foreign Affairs. Later Xingshuo attended Purdue University to continue her graduate study in analytical chemistry. In 2016, she joined the Aston labs and conducted doctoral research under the guidance of Professor R. Graham Cooks (Henry B. Hass Distinguished Professor). Her research spreads over reaction monitoring, reaction acceleration in confined volume systems as well as analytical methods for small molecules. She also got training in various ambient mass spectrometry techniques, multiple reaction monitoring profiling (MRM-profiling) workflow for metabolite analysis, statistical data analysis and machine learning. Xingshuo is the author of several publications and gave presentations in conferences including the Annual American Society for Mass Spectrometry (ASMS) conference and Merck-Purdue Center for Measurement Sciences 2021 Symposium. Xingshuo is a member of the Phi Lamba Upsilon (PLU) honor society and Women in Science Programs (WISP). She served as the outreach coordinator of PLU and organized events promoting popular science in the community.

PUBLICATIONS

1. **Chen, X.**; Cooks, R. G. Accelerated Reactions in Field Desorption Mass Spectrometry. *J. Mass Spectrom.* **2018**, 53 (10), 942–946.

2. Ayrton, S. T.; **Chen, X.**; Bain, R. M.; Pulliam, C. J.; Achmatowicz, M.; Flick, T. G.; Ren, D.; Cooks, R. G. Gas Phase Ion Chemistry to Determine Isoaspartate in a Peptide Backbone. *J. Am. Soc. Mass Spectrom.* **2018**, 29 (7), 1339–1344.

3. Narendra, N.; **Chen, X.**; Wang, J.; Charles, J.; Cooks, R. G.; Kubis, T. Quantum Mechanical Modeling of Reaction Rate Acceleration in Microdroplets. *J. Phys. Chem. A* **2020**, 124 (24), 4984–4989.

4. Nie, H.; Wei, Z.; Qiu, L.; **Chen, X.**; Holden, D. T.; Cooks, R. G. High-Yield Gram-Scale Organic Synthesis Using Accelerated Microdroplet/Thin Film Reactions with Solvent Recycling. *Chem. Sci.* **2020**, 11 (9), 2356–2361.

5. Liu, Y.; Zheng, W.; Zhang, W.; Chen, N.; Liu, Y.; Chen, L.; Zhou, X.; **Chen, X.**; Zheng, H.; Li, X. Photoaffinity Labeling of Transcription Factors by DNA-Templated Crosslinking. *Chem. Sci.* **2015**, 6 (1), 745–751.